Clinical and functional characterization of a new muscular dystrophy caused by novel recessive *SNUPN* pathogenic variants

by

Marvan Nashabat

A Dissertation Submitted to the

Graduate School of Health Sciences in Partial Fulfillment of the Requirements for the Degree of

Doctor of Philosophy

in

Cellular and Molecular Medicine

KOÇ ÜNİVERSİTESİ

April 09, 2025

Clinical and functional characterization of a new muscular dystrophy caused by novel recessive *SNUPN* pathogenic variants

Koc University

Graduate School of Health Sciences

This is to certify that I have examined this copy of a doctoral dissertation by

Marvan Nashabat

and have found that it is complete and satisfactory in all respects,
and that any and all revisions required by the final
examining committee have been made.

Committee Members:

Assist. Prof. Nathalie Escande Beillard (Advisor)

Prof. Hülya Kayserili [Co-Advisor]

Prof. Piraye Oflazer

Prof. Devrim Gözüaçık

Prof. Bruno Reversade

Dr. Frederique Magdinier

Date: 09-04-2025

To my beloved parents, whose unwavering love and guidance have shaped every step of my journey.

To my father, whose presence I deeply miss, yet whose wisdom, strength, and dreams continue to inspire me every day. This work is a tribute to your endless sacrifices and the values you instilled in me.

To my dear brother, Mazen, whose memory is forever etched in my heart. Your absence is deeply felt, but your spirit lives on in every achievement and challenge I overcome.

To my parents-in-law, for their constant support, care, and prayers. Your kindness and encouragement have been a source of strength throughout this journey.

And to my wife, Alaa, the greatest blessing of my life. Your unwavering support, patience, and sacrifices have been my anchor through every challenge. This journey would not have been possible without your love and belief in me.

To my wonderful kids Ahmad, Ibraheem, Yahya and Serah. Together to the next adventure.

ABSTRACT

Clinical and functional characterization of a new muscular dystrophy caused by novel recessive *SNUPN* pathogenic variants

Marvan Nashabat

Doctor of Philosophy in Cellular and Molecular Medicine

April 09, 2025

Muscular dystrophies (MDs) are a heterogeneous group of inherited disorders characterized by progressive muscle weakness and degeneration. This study presents a comprehensive investigation of a novel muscular dystrophy phenotype associated to germline recessive mutations in the *SNUPN* gene, identified in 21 patients from 18 unrelated families. Clinically, the affected individuals exhibited progressive muscle weakness with a broad spectrum of severity, ranging from mild symptoms and retained ambulation to severe early-onset muscular dystrophy leading to premature death from respiratory complications. Beyond muscular dystrophy, several patients displayed extra-muscular manifestations, notably neurological deficits, including cerebellar atrophy and congenital cataracts, reflecting broader systemic implications of *SNUPN* mutations.

SNUPN encodes the SNURPORTIN-1 (SPN1) protein, which plays a critical role in the nuclear import of uridine-rich small nuclear ribonucleoproteins (UsnRNPs), crucial components of the spliceosome machinery. Most identified mutations clustered at the C-terminus of the SPN1 protein, highlighting its critical functional role and suggesting it as a potential mutational hotspot. Functional analyses demonstrated that defective SPN1 impairs the nuclear import of UsnRNPs, causing aberrant alternative splicing of numerous genes implicated in muscle structure and function. This aberrant splicing affected critical muscle-related proteins, including extracellular matrix components, sarcolemmal proteins, and cytoskeletal elements, likely contributing to muscle fiber degeneration, fibrosis, and functional impairment.

Furthermore, this study uncovered novel insights into SPN1 protein biology, particularly its self-oligomerization and interaction with the survival motor neuron (SMN) protein complex. Disrupted SPN1-SMN interaction and autophagic dysregulation were observed, potentially suggesting these pathways may play a key role in the muscular dystrophy pathogenesis. Aberrant accumulation of autophagy markers (LC3-II and p62) in patient muscle tissues and cell lines further underscored this dysregulation. Comparative analysis with concurrently published data from independent cohorts supported our findings, reinforcing the genotype-phenotype correlations and highlighting novel disease mechanisms.

Collectively, this research significantly expands the genetic landscape of muscular dystrophies by characterizing *SNUPN*-related muscular dystrophy at clinical, molecular, and functional levels. Future studies employing animal models and extended patient cohorts are essential to further deepen the understanding of *SNUPN* pathology, unravel the intricate molecular mechanisms, and facilitate the development of targeted therapeutic strategies.

OZETCE

Yeni tanımlanmış resesif *SNUPN* patojenik varyantlarının neden olduğu kas distrofisinin klinik ve fonksiyonel karakterizasyonu

Marvan Nashabat
Hücresel ve Moleküler Tıp Doktora
April 09, 2025

Kas distrofileri (MD'ler), ilerleyici kas güçsüzlüğü ve dejenerasyonu ile karakterize edilen heterojen bir kalıtsal hastalık grubudur. Bu çalışma, *SNUPN* genindeki mutasyonlara bağlı olarak gelişen yeni bir kas distrofisi fenotipinin kapsamlı klinik ve fonksiyonel karakterizasyonunu sunmaktadır. Toplamda 18 farklı aileden 21 hastada tanımlanan bu fenotipte, klinik olarak geniş bir şiddet yelpazesinde ilerleyici kas güçsüzlüğü gözlemlenmiş olup, hastaların klinik seyri hafif belirtilerle birlikte yürüyüş yetisinin korunmasından, solunum komplikasyonları nedeniyle erken yaşta ölüme yol açan ağır erken başlangıçlı kas distrofisine kadar değişkenlik göstermiştir. Kas tutulumu dışındaki ekstra-müsküler bulgular arasında serebellar atrofi ve konjenital katarakt gibi nörolojik defisitler tespit edilmesi, *SNUPN* mutasyonlarının daha geniş sistemik etkileri olduğunu ortaya koymaktadır.

Fonksiyonel açıdan *SNUPN* geni, spliceozom kompleksinin önemli bileşenleri olan uridin açısından zengin küçük nükleer ribonükleoproteinlerin (UsnRNP'ler) çekirdeğe taşınmasında kritik görev üstlenen SNURPORTIN-1 (SPN1) proteinini kodlamaktadır. Tanımlanan mutasyonların çoğunluğunun SPN1 proteininin C-terminal bölgesinde kümelenmiş olması, bu bölgenin fonksiyonel olarak kritik olduğunu ve potansiyel bir mutasyonel sıcak nokta teşkil ettiğini düşündürmektedir. Yapılan fonksiyonel analizlerde, mutasyona uğramış SPN1 proteininin UsnRNP'lerin çekirdek içine taşınmasını bozduğu ve bunun sonucu olarak kas yapısı ve fonksiyonlarında rol oynayan birçok genin alternatif ekzon birleşimlerinin (splicing) anormal hale geldiği gösterilmiştir. Bu durumun özellikle hücre dışı matriks proteinleri, sarkolemmal proteinler ve hücre iskeleti bileşenlerini etkilemesi, kas liflerinde dejenerasyon, fibrozis ve fonksiyon kaybına yol açmaktadır.

Ayrıca bu çalışma kapsamında, SPN1 proteininin kendiliğinden oligomerleşmesi ve Survival Motor Neuron (SMN) protein kompleksiyle etkileşimi gibi biyolojik fonksiyonlarına dair yeni bulgular elde edilmiştir. SPN1-SMN etkileşimindeki bozukluklar ve otofaji mekanizmasındaki düzensizlikler gözlenmiş, bu yolların hastalık patogenezine katkıda bulunabileceği öne sürülmüştür. Hasta kas dokularında ve hücre hatlarında otofaji belirteçleri olan LC3-II ve p62 proteinlerinin anormal birikimi, bu düzensizlikleri destekler nitelikte bulunmuştur. Bağımsız hasta kohortlarından elde edilen verilerle yapılan karşılaştırmalı analizler, elde edilen bulguları destekleyerek genotip-fenotip korelasyonlarını güçlendirmiş ve yeni hastalık mekanizmalarını ortaya koymuştur.

Bu çalışma, *SNUPN* ilişkili kas distrofisini klinik, moleküler ve fonksiyonel düzeyde tanımlayarak kas distrofilerinin genetik spektrumunu önemli ölçüde genişletmiştir. İleride hayvan modelleri ve daha geniş hasta kohortları kullanılarak yürütülecek araştırmalar, *SNUPN* gen patolojisinin daha derinlemesine anlaşılmasına, karmaşık moleküler mekanizmaların aydınlatılmasına ve hedefe yönelik tedavi stratejilerinin geliştirilmesine katkı sağlayacaktır.

ACKNOWLEDGMENTS

I would like to express my deepest gratitude to my advisor, Dr. Nathalie Escande Beillard, for her invaluable guidance, patience, and kindness throughout this journey. Her mentorship has not only reshaped my scientific mindset but has also instilled in me the persistence and dedication necessary for research and discovery. She has been the finest example of teamwork and collaboration in science, and I am truly grateful for the opportunity to have learned under her guidance.

I am also profoundly thankful to Prof. Hülya Kayserili for her unwavering support and mentorship. Her wisdom, dedication, and exceptional work ethic have been a great model to follow. Her encouragement and insightful advice have been instrumental in shaping both my research and my academic growth.

I would like to extend my sincere appreciation to Prof. Piraye Oflazer and Prof. Devrim Gözüaçık, whose invaluable guidance throughout the journey of my proposal development significantly shaped my research. Their constructive feedback and insightful advice greatly improved my work. The impact of their mentorship goes beyond this dissertation, as their guidance in planning my future career is deeply appreciated and truly unforgettable.

I would also like to thank all my colleagues in the lab. In particular, Dr. Nasrinsadat Nabavizadeh, the key person in our lab and the reference for all members. Her professional guidance, support, and patience have been invaluable. She was always there during difficult times, providing both expertise and encouragement, and her presence kept the lab running smoothly with her dedication and willingness to help.

A special thank you to Burak Sarıbaş, an active colleague and a true brother. His meticulous approach in the lab was both inspiring and tremendously helpful. I deeply appreciate his dedication and the energy he brings to scientific discussions.

I am also grateful to Seyide Ecesu Uygur for her unwavering support and respectful dedication, which made the lab a better place for everyone.

A heartfelt special thanks to my PhD colleague Hilal Pırıl Saraçoğlu, who made tremendous efforts in supporting me throughout this research. Her exceptional organizational skills and lab approach have been truly inspiring, and I have learned so much from her dedication and precision.

I would like to express my gratitude to all my lab mates and friends, Şeymanur Tur, Mert Kaya, and Ece Çepni, for offering support both at the bench and throughout our daily lives. Their friendship and encouragement have been an essential part of this journey.

A special thanks to Dr. Umut Altunoğlu, whose guidance, support, and dedication were deeply appreciated.

I am also grateful to Prof. Devrim Gözüaçık's lab members for their generous support and assistance, particularly Dr. Yunus Akkoç, whose honest help and collaboration were highly valuable during my research.

Finally, I would like to thank all the Cytogenetics Laboratory members (Dr. Gül Leyla Kılıç, Dicle, Fatma, and Esra) and Molecular Laboratory members (Dr. Serpil Erarslan, Merve, Maltam, Buse, and Selda) for their continuous support, patience, and guidance. Their expertise and generosity have played a crucial role in my academic and scientific development.

TABLE OF CONTENTS

LIST OF TABLES

LIST OF FIGURES

ABBREVIATIONS

ACMG	American College of Medical Genetics
ATG	Autophagy-related genes
CBC	Cap Binding Complex
CBs	Cajal Bodies
CK	Creatine Kinase
CMD	Congenital Muscular Dystrophy
CRM1	Exportin 1 Protein
CRISPR	Clustered Regularly Interspaced Short Palindromic Repeats
DAG1	Dystroglycan 1
DTT	Dithiothreitol
ER	Endoplasmic Reticulum
EMG	Electromyography
FIP200	Focal Adhesion Kinase Family-Interacting Protein of 200 kDa
FKRP	Fukutin-Related Protein
GAPDH	Glyceraldehyde-3-Phosphate Dehydrogenase
gDNA	Genomic DNA
GMPPB	GDP-Mannose Pyrophosphorylase B
H&E	Hematoxylin and Eosin (Staining)
HRP	Horseradish Peroxidase
IBB	Importin Beta Binding
INPP5K	Inositol Polyphosphate-5-Phosphatase K
ISPD	Isoprenoid Synthase Domain-Containing Protein
ITGB2	Integrin Beta-2
LAMA2	Laminin Subunit Alpha-2
LAMA5	Laminin Subunit Alpha-5
LC3	Microtubule-Associated Protein 1A/1B-Light Chain 3
LGMD	Limb-Girdle Muscular Dystrophy
m_3G	2,2,7-Trimethylguanosine
m^7G	7-methylguanosine
MAPK	Mitogen-Activated Protein Kinase

MD	Muscular Dystrophy
mRNA	Messenger RNA
MTORC1	Mechanistic Target of Rapamycin Complex 1
NMD	Nonsense-Mediated Decay
PBS	Phosphate Buffered Saline
PFA	Paraformaldehyde
P62	Sequestosome 1 (SQSTM1)
PLEC	Plectin
PVDF	Polyvinylidene Fluoride
qPCR	Quantitative Polymerase Chain Reaction
RNA-seq	RNA Sequencing
RT-qPCR	Reverse Transcription Quantitative Polymerase Chain Reaction
SGCA	Sarcoglycan Alpha
SGCB	Sarcoglycan Beta
SGCG	Sarcoglycan Gamma
SGCD	Sarcoglycan Delta
SMN	Survival Motor Neuron
SMN2	Survival Motor Neuron 2
SNUPN	SNURPORTIN-1 Gene
SPN1	SNURPORTIN-1 Protein
TBST	Tris-Buffered Saline with Tween
TGS1	Trimethylguanosine Synthase 1
TMEM41B	Transmembrane Protein 41B
UsnRNPs	Uridine-Rich Small Nuclear Ribonucleoproteins
WES	Whole Exome Sequencing
WT	Wild-Type
XPO1	Exportin-1

Chapter 1: **INTRODUCTION**

1.1 Skeletal muscles

Skeletal muscle is a highly dynamic and adaptable tissue, comprising approximately 40% of total body weight and playing critical roles in both mechanical and metabolic functions. It accounts for a significant portion of the body's protein content and turnover, with its mass determined by the balance between protein synthesis and degradation, which is influenced by factors such as nutrition, hormones, physical activity, and disease. Mechanically, skeletal muscle generates force and movement, supports posture, and enables participation in physical and social activities, contributing to overall health and functional independence (Frontera & Ochala, 2015). Metabolically, it serves as a key reservoir for amino acids and carbohydrates, supports basal energy metabolism, regulates body temperature through heat production, and consumes the majority of oxygen and fuel during exercise (Myers, 2024).

Additionally, skeletal muscle plays a crucial role in maintaining systemic health. It provides amino acids for other organs like the skin, brain, and heart, supports blood glucose levels during starvation, and enhances the body's capacity to respond to stress and illness. Reduced muscle mass can impair these vital functions, underscoring the importance of muscle maintenance in health promotion and disease prevention (Wolfe, 2006).

1.1.1 Origin and structure

In humans, there are three distinct muscle tissue types; skeletal, smooth, and cardiac muscles, each exhibiting unique structural and functional characteristics. During embryonic development, skeletal muscles originate from the paraxial mesoderm (PM), specifically within the dermomyotome of the dorsal somite. The PM progenitors express early mesoderm marker, brachyury (T) and the differentiation continue form here being controlled by signaling molecules like WNT, FGF2 and BMP. This intricate process relies on the coordinated activity of various differentiating and transcription factors to accurately

localize and differentiate myoblasts into the precursor cells of skeletal muscles (Figure 1.1) (Buckingham et al., 2003; Iberite, Gruppioni, & Ricotti, 2022). Subsequently, myoblasts undergo fusion, resulting in the formation of single, multinucleated muscle cells (Figure 1.1).

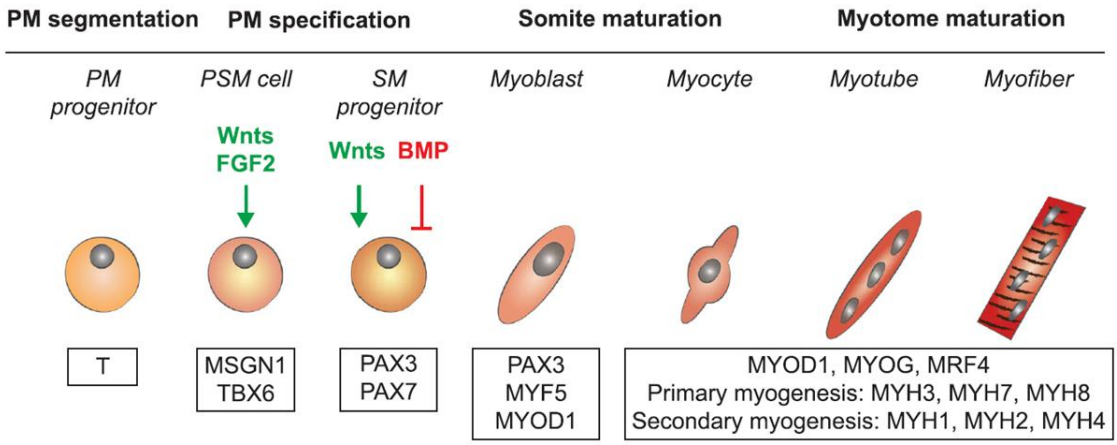

Figure 1.1: Differentiation stages of skeletal muscle cells: Differentiation stages of skeletal muscle cells: The differentiation of skeletal muscle cells begins with the segmentation of the paraxial mesoderm (PM), which gives rise to PM progenitor cells expressing the early mesodermal marker, brachyury (T). As differentiation progresses, the PM undergoes specification, leading to the formation of the presomitic mesoderm (PSM) and subsequently, skeletal muscle (SM) progenitors. This highly regulated process is governed by a network of key signaling molecules, which either promote differentiation (pro-differentiative factors, highlighted in green) or inhibit differentiation (inhibitory factors, highlighted in red). The specific molecular markers expressed at each stage of differentiation are indicated in the boxes below each cell. (Adapted from (Iberite et al., 2022))

The sarcoplasm, which constitutes the cytoplasm of myofibers, is densely packed with myofibrils arranged in a linear fashion that extend along the entire length of the myofiber. This structural organization forms the fundamental functional and contractile units of skeletal muscle, known as sarcomeres (Figure 1.2). Sarcomeres consist of myosin filaments sliding along actin filaments, leading to sarcomere shortening and ultimately enabling muscle contraction (Sieck, Ferreira, Reid, & Mantilla, 2013). The A-band refers to the region of overlap between myosin and actin filaments within the sarcomere, playing

a crucial role in muscle contraction. In contrast, the I-band, which is positioned laterally to the A-band, is composed predominantly of actin filaments and appears lighter under a microscope due to the absence of myosin filaments (Figure 1.3). The Z-line marks the boundary between two adjacent sarcomeres, serving as the structural anchor for the actin filaments and playing a critical role in maintaining sarcomere integrity and alignment during contraction. (D. J. Lowrie, 2020; Iberite et al., 2022). This highly organized structure facilitates the formation of myofibrils, which run longitudinally within the sarcoplasm, thereby displacing the multiple nuclei toward the periphery of the muscle cell. Given their elongated morphology, these specialized muscle cells are commonly referred to as muscle fibers (Iberite et al., 2022).

The sarcolemma, plasma membrane enveloping the muscle cell, encapsulates the sarcoplasm, including the myofibrils and various organelles such as peripheral nuclei, mitochondria, and the sarcoplasmic reticulum (the specialized endoplasmic reticulum (ER) found in muscle fibers). Externally, the sarcolemma is enveloped by a delicate connective tissue layer known as endomysium, providing electrical insulation between neighboring muscle fibers.

Clusters of muscle fibers are further bundled together to form fascicles, which are encased by a thicker connective tissue layer known as the perimysium. Ultimately, the entire muscle is surrounded by the outermost thick layer called epimysium (Figure 1.2(a)). These three interlocking layers converge at the muscle's extremities, culminating in the formation of tendons, which serve as integral connectors, attaching the muscles to bones (D. J. Lowrie, 2020).

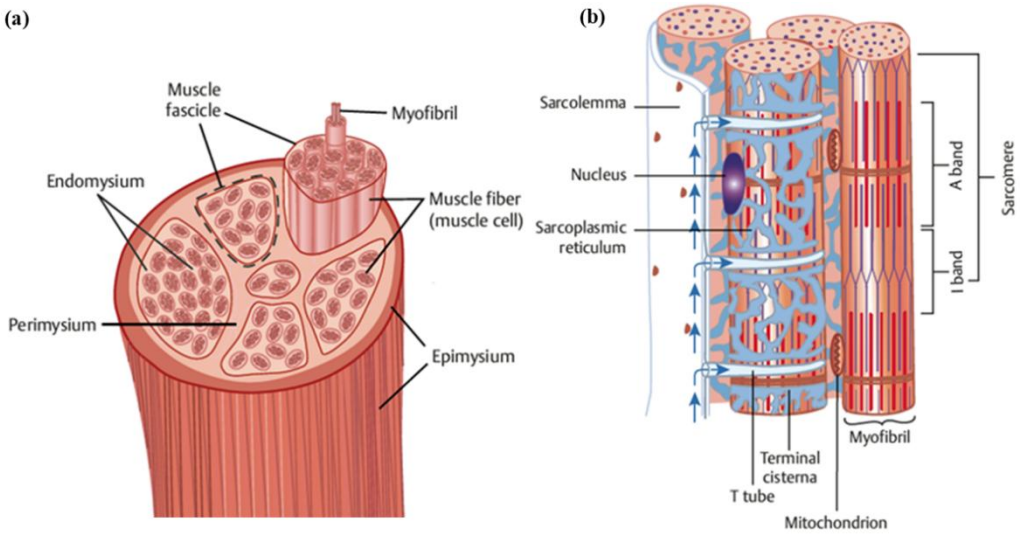

Figure 1.2**1**: Structures of skeletal muscle: (a) Diagram of a skeletal muscle cross-section. Connective tissue elements lie between muscle fibers (endomysium), bundle cells into fascicles (perimysium), and surround the entire muscle (epimysium). (b) Diagram of a longitudinal section of a skeletal muscle fiber (muscle cell), showing four myofibrils and other organelles. The blue arrows represent the path of an action potential along the surface of the muscle fiber and into the T tubule system. Adapted from Lowrie, J.R. (2020) (D. J. Lowrie, 2020).

1.1.2 Extracellular matrix composition and function in skeletal muscles

The extracellular matrix (ECM) is a complex network of structural proteins that surrounds skeletal muscles, providing mechanical support and facilitating contractile mobility. In addition to these structural roles, the ECM is crucial for biochemical signaling, regulating cellular proliferation, differentiation, and regeneration (Bonnans, Chou, & Werb, 2014). Furthermore, the ECM supports and anchors blood vessels, which provide nutrients, immune cells, and other essential components required for skeletal muscle fiber homeostasis (Theocharis, Skandalis, Gialeli, & Karamanos, 2016). The ECM primarily consists of collagens, fibronectins, laminins, and other proteins (Ahmad, Shaikh, Ahmad, Lee, & Choi, 2020). It is estimated that the ECM contains approximately 300 proteins, including numerous types of collagens and proteoglycans (Hynes & Naba, 2012). These components are organized to work in a harmony, ensuring cellular function, communication, and coordination (Cox & Erler, 2011). ECM proteins interact with specific

receptors on the sarcolemma, such as integrins and dystroglycans, thereby supporting the development and maintenance of skeletal muscles (Thorsteinsdottir, Deries, Cachaco, & Bajanca, 2011). Figure 1.3 shows the key components of the ECM with their interaction of sarcolemma and sarcoplasmic components.

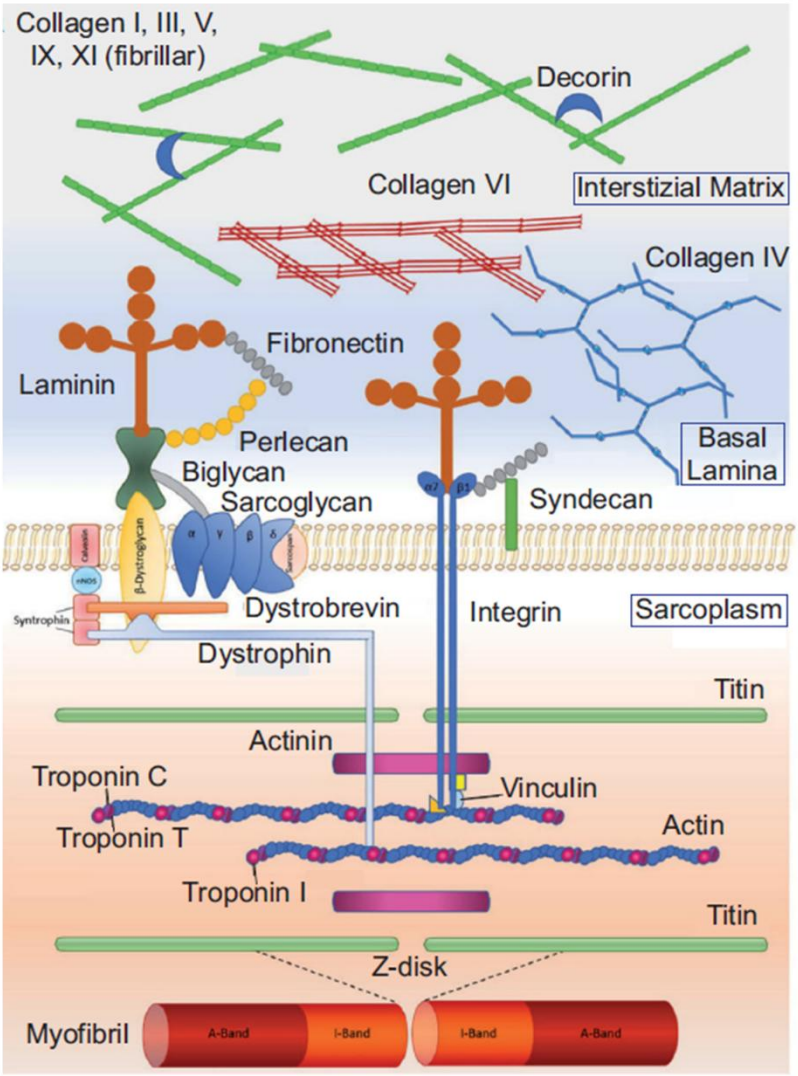

Figure 1.3: key components of the extracellular matrix and their interaction with myofiber sarcolemma and sarcoplasmic structures, extending to the contractile unit, the sarcomere. (Adapted from: (Csapo, Gumpenberger, & Wessner, 2020)).

Collagens are the most abundant components of the ECM, with type IV and type VI being predominant. Other important collagens include type I, type III, and type V, which contribute to forming the primary structural network of the ECM (Schuler et al., 2022; W. Zhang, Liu, & Zhang, 2021). Laminins, a group of glycoproteins, are essential components

of the basement membrane. They are composed of various combinations of alpha, beta, and gamma chains, facilitating cell–ECM adhesion (Miner & Yurchenco, 2004; W. Zhang et al., 2021). Another key component is fibronectins, which tether muscle fibers to the ECM by interacting with integrin receptors on the sarcolemma (P. Singh, Carraher, & Schwarzbauer, 2010). Additionally, sarcolemmal proteins serve as essential mediators that link ECM proteins to the dystrophin-associated protein complex (DPC), ensuring structural integrity and mechanical stability of muscle fibers. These include titin (TTN), actinin (ACTN), and desmin (DES), which collectively maintain muscle fiber resilience during forceful contractions and protect against mechanical stress (Iberite et al., 2022).

The ECM is organized into three distinct layers: the epimysium, perimysium, and endomysium. The innermost layer, the endomysium (or basal lamina), surrounds individual muscle fibers. Groups of adjacent muscle fibers form muscle bundles, which are encased by the perimysium. The outermost layer, the epimysium, encloses the entire muscle (Sleboda, Stover, & Roberts, 2020) (Figure 1.2(b)). Each of these layers has a unique composition of ECM components, reflecting their specific functional roles (W. Zhang et al., 2021).

The loss of function of certain ECM components has been linked to various myopathies and muscular dystrophies. These include, but are not limited to, collagen-related dystrophies and laminin-related dystrophies, such as collagen VI-related muscular dystrophy and LAMA2-related dystrophies (Mohassel, Foley, & Bonnemann, 2018).

1.1.3 Physiological functions

The principal role of skeletal muscle lies in the generation of contractile forces, a vital function that underpins locomotion, respiration, blood circulation, and a range of other physiological processes. This contractile power is generated by the sarcomeres, where the dynamic interaction between actin and myosin filaments occurs, governed by the precise orientation changes of myosin globular heads in the presence of adenosine triphosphate (ATP) and calcium ions (Figure 1.4). The specialized sarcoplasmic reticulum plays a pivotal role by serving as the reservoir for the required calcium ions essential for the

contraction process. This storage and controlled release of calcium enable the rapid and efficient execution of muscle contractions (Luther, 2009).

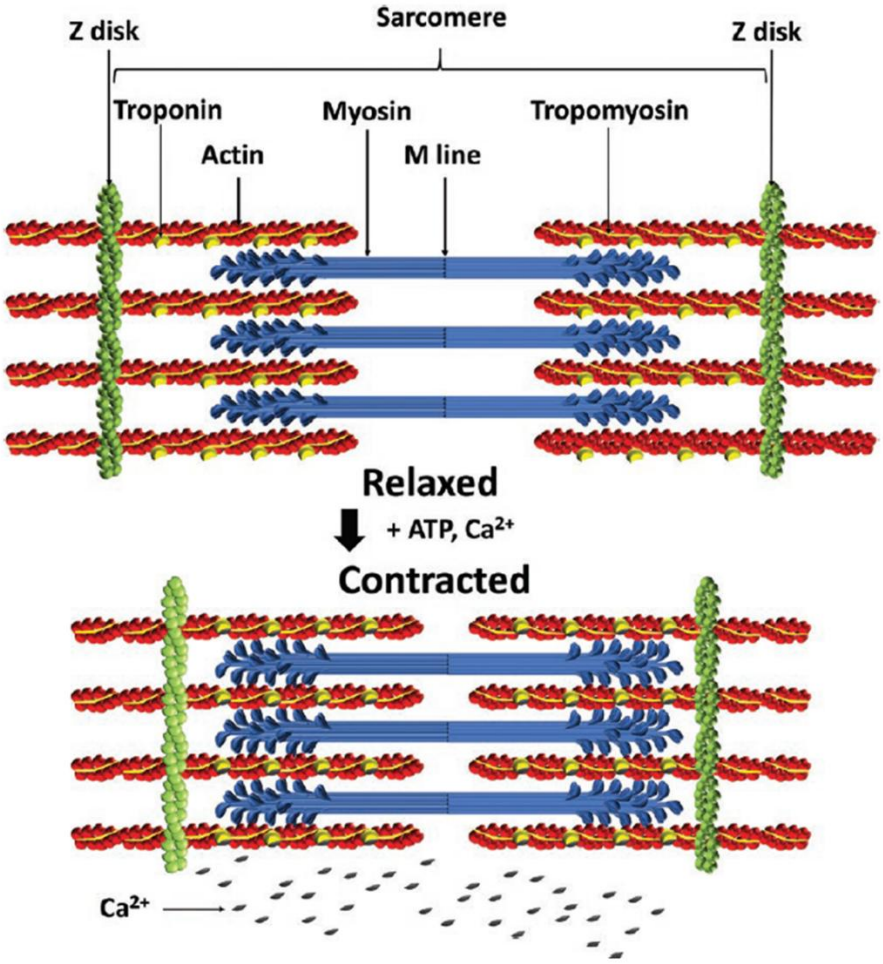

Figure 1.4: The contraction mechanism of skeletal muscles: This schematic representation illustrates the mechanism of skeletal muscle contraction, highlighting the structural changes in the sarcomere during relaxation and contraction. In the relaxed state (upper part of the schematic), the sarcomere is extended, with actin and myosin filaments positioned apart, maintaining the muscle in a resting condition. Upon muscle contraction, an action potential triggers the release of calcium ions (Ca^{2+}) from the sarcoplasmic reticulum. In the presence of adenosine triphosphate (ATP), the globular head of the myosin filaments undergoes a conformational change, shifting its orientation from 45 degrees relative to its own filament to 90 degrees. This movement propels actin filaments to slide over the myosin filaments, leading to the shortening of the sarcomere. The coordinated contraction of all sarcomeres within a muscle fiber results in the overall contraction of the muscle, enabling force generation and movement. (Adapted from (Calik, 2021)).

Skeletal or striated muscles are broadly categorized into two primary groups: type 1 and type 2. Type 1 fibers, generally considered slow-twitch muscle fibers, rely more on aerobic energy production. They exhibit larger mitochondria and a greater resistance to fatigue. In contrast, type 2 fibers, recognized as fast-twitch muscle fibers, depend more on anaerobic respiration. They possess smaller and fewer mitochondria and are more susceptible to fatigue. Typically, skeletal muscles are composed of a combination of both fiber types in varying proportions, a composition dictated by the specific functional demands of the muscle (Seidman, 2017).

Mitochondria are essential organelles in skeletal muscle, a metabolically active tissue that must rapidly adapt to various physiological challenges. To ensure optimal mitochondrial function, the mitochondrial network remains in a continuous dynamic state, allowing for the proper distribution of mitochondrial DNA (mtDNA) and metabolites within the organelle. This dynamic balance is governed by two fundamental processes:

1- Mitochondrial fission, a process in which damaged or dysfunctional mitochondria are split and subsequently removed through mitophagy.
2- Mitochondrial fusion, where two or more mitochondria merge, facilitating the exchange of mitochondrial content and enhancing organelle function and resilience.

A precise balance between fission and fusion is critical for maintaining mitochondrial health, preserving muscle homeostasis, and preventing skeletal muscle degeneration.
The primary protein regulating mitochondrial fission is dynamin-related protein 1 (Drp1), a cytosolic guanosine triphosphatase (GTPase) that facilitates membrane constriction and division (Smirnova, Griparic, Shurland, & van der Bliek, 2001). Conversely, mitochondrial fusion is mediated by Mitofusin 1 (MFN1) and Mitofusin 2 (MFN2), which regulate the fusion of the outer mitochondrial membrane (OMM), while OPA1 controls the fusion of the inner mitochondrial membrane (IMM) (Pernas & Scorrano, 2016). The loss of function of any of these key mitochondrial regulators results in mitochondrial dysfunction, leading to structural damage in muscle fibers and contributing to skeletal muscle pathologies (De Mario, Gherardi, Rizzuto, & Mammucari, 2021). Maintaining mitochondrial dynamics is

therefore essential for skeletal muscle integrity, energy metabolism, and overall cellular function.

1.1.4 Histology of skeletal muscles

Obtaining a muscular biopsy is an essential and definitive diagnostic procedure for patients suffering from neuromuscular disorders. The examination of muscle tissue sections, facilitated by the use of various histological stains, serves the dual purpose of confirming or excluding certain disorders. These stains provide invaluable insights into the structural and, at times, functional status of the muscle tissues under investigation. Cross-sectional frozen biopsies and paraffin-embedded samples are the prevailing choices for muscle biopsy specimens. While the paraffin-embedded samples are better to preserve the slide and muscle section, they cannot take up the antibodies needed for immunohistochemistry studies, making the frozen cross-section, the best choice in this case.

The selection of staining techniques for muscular disease analysis depends on the patient's clinical presentation and the imperative need for a differential diagnosis. The Hematoxylin and Eosin (H&E) stain, for instance, provides visibility into the sarcoplasm, the sarcolemma, and nuclei (Figure 1.5(a)). In contrast, the modified Gomori Trichrome (mGT) stain extends its diagnostic utility by revealing the details of the sarcoplasm, sarcolemma in addition to the nuclei and mitochondria (Figure 1.5(b)). Additional staining methods, such as the Nicotinamide Adenine Dinucleotide Tetrazolium Reductase stain (NADH-tr), offer selective visualization of mitochondria, making it particularly useful in distinguishing between type 1 and type 2 muscle fibers, with the former, enriched in mitochondria, appearing darker in color (Figure 1.5(c)) (Seidman, 2017).

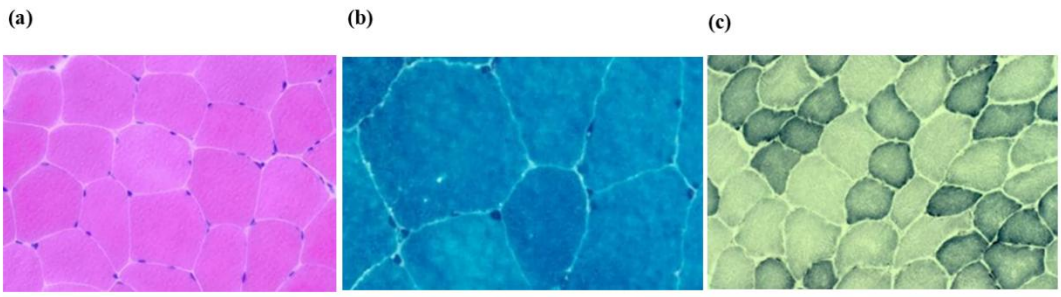

Figure 1.5: Histological staining of normal muscle: (a) Normal muscle. High power hematoxylin and eosin (H&E) cross-section. All muscle fibers are homogeneously stained

and have comparable sizes. The endomysium appears very thin, and all the nuclei (purple) are peripherally located. (b) Normal muscle. Modified Gomori trichrome stain cross-section. Homogeneous uptake of the stain with peripherally located nuclei. In this stain, mitochondria could appear red (not shown here). (c) Normal muscle. Nicotinamide adenine dinucleotide tetrazolium reductase (NADH or NADH-tr) stain demonstrates two populations of myofibers. NADH is an oxidative mitochondrial enzyme. Type 1 myofibers stain more darkly than type 2 myofibers due to the greater use of aerobic metabolism by type 1 fibers (Seidman, 2017).

To achieve a comprehensive assessment of muscle tissue, both qualitative and quantitative analyses should be performed on muscle sections. The choice of staining technique is crucial, as it must facilitate these assessments to ensure an accurate diagnosis. Qualitative analysis includes the evaluation of muscle fiber shape and type, the number and localization of nuclei, and the presence of cellular infiltration, fibrosis, or necrosis, which are indicative of pathological conditions. In contrast, quantitative measures focus on the number and size of muscle fibers, as variations in these parameters provide important diagnostic insights (Briguet, Courdier-Fruh, Foster, Meier, & Magyar, 2004). An increased number of large muscle fibers may suggest hypertrophy, a compensatory response to mechanical or metabolic stress, while smaller fibers are typically associated with atrophy, reflecting muscle-wasting conditions (Seidman, 2016).

In a normal muscle cross-section, histological staining reveals muscle fibers of relatively uniform size, arranged in distinct bundles, with peripherally located nuclei, indicative of healthy and functionally mature muscle tissue. Additionally, the sarcoplasm appears homogeneous and unfragmented, reflecting the structural integrity of the muscle fibers. Any deviation from these features, such as fiber size variability, internalized nuclei, disrupted sarcoplasm, or inflammatory infiltrates, may suggest neuromuscular disorders, muscular dystrophies, or metabolic myopathies (Frontera & Ochala, 2015). Therefore, a combined approach using both qualitative and quantitative analyses is essential for a thorough histopathological evaluation of muscle tissue and for reaching a precise diagnosis.

1.1.5 Dysfunction of muscle

The highly ordered structure and functionality of skeletal muscle rely on precise coordination between cellular, extracellular, and molecular components. Any disruption in these tightly regulated processes, whether due to genetic mutations, impaired protein turnover, or defective cellular signaling, can compromise muscle integrity and contribute to pathological conditions (Figure 1.6). Dysfunction in any of the extracellular matrix (ECM), sarcolemmal, or sarcoplasmic components and organelles can disturb the physiological homeostasis of muscle fibers, leading to necrosis, fibrosis, inflammatory infiltration, and ultimately loss of function. Such disturbances may cause muscle fiber degeneration, atrophy, or hypertrophy, depending on the underlying pathogenic mechanism (Mukund & Subramaniam, 2020).

One of the key characteristics of skeletal muscle tissue is its ability to regenerate, a process primarily driven by satellite cells (SCs), a specialized type of unipotent muscle precursor cells. These adult stem cells, which originate from embryonic progenitor cells, play a crucial role in muscle repair and regeneration (Buckingham, 2007). Satellite cells are strategically positioned between the basal lamina and the sarcolemma, where they typically remain in a quiescent state. They are marked by the expression of PAX7, while lacking MYOD1 and MYOG, which are characteristic markers of myoblasts (Mukund & Subramaniam, 2020).

Upon muscle injury or physiological stress, chemoattractants and cytokines are released (Figure 1.6), triggering the activation of satellite cells through a cascade of well-coordinated signaling pathways (Hindi & Kumar, 2016). This activation serves a dual purpose: to replace damaged muscle fibers and to replenish the satellite cell pool to ensure continuous muscle regeneration. However, in muscular dystrophy (MD), satellite cells exhibit a reduced regenerative capacity, which contributes to progressive muscle degeneration and impaired tissue repair (Heslop, Morgan, & Partridge, 2000).

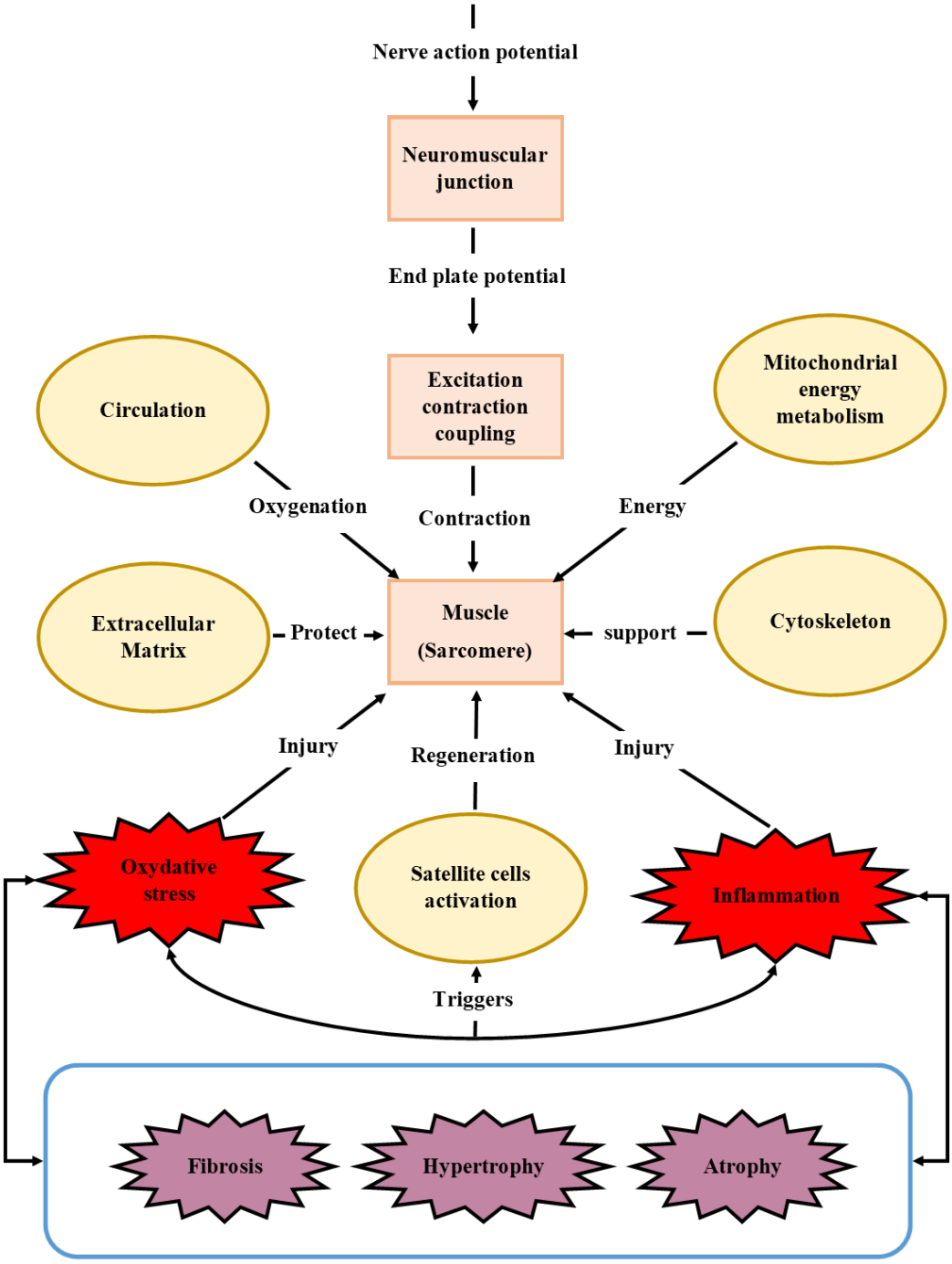

Figure 1.6: Structural and functional components of muscle fibers: This schematic representation summarizes the key elements required to maintain healthy skeletal muscle function and structure. The homeostasis of skeletal muscle fibers depends on the integration of multiple physiological processes, including energy production, oxygenation, structural support, and cellular protection mechanisms. Any disruption in these fundamental aspects can lead to muscle fiber damage that exceeds the regenerative capacity of satellite cells. When this damage becomes irreversible, it results in progressive

muscle fiber degeneration, impaired contractile function, and eventual loss of muscle integrity (Adapted from: (Mukund & Subramaniam, 2020)).

1.2 Muscular dystrophy (MD)

1.2.1 Definition of muscular dystrophies

Muscular dystrophy is a group of genetically and phenotypically heterogeneous inherited diseases characterized primarily by progressive muscle weakness and dystrophic changes. Currently, more than 60 genes have been identified in correlation with a muscular dystrophy diagnosis. The mode of inheritance, age of onset, group of involved muscles, and extra muscular manifestations such as central nervous system (CNS) involvement, provide indication for a definitive diagnosis (Cohen, Bonne, Rivier, & Hamroun, 2021).

To diagnose a patient with muscular dystrophy, a thorough clinical history and physical examination are required, along with biochemical, histological, radiological and genetic investigations. Typically, patients present with difficulty in walking, running and climbing stairs. These nonspecific complaints add to the challenge of diagnosing muscular dystrophies. Careful examination by the physicians to assess the power of various muscle groups and identify extra muscular signs is essential. One of the fundamental biochemical investigations is the creatinine kinase (CK) level, which tends to be elevated in the majority of muscular dystrophies. Muscle biopsy may be indicated to examine muscle fibers and differentiate the cause of the disease. Furthermore, CNS radiological investigations, like brain magnetic resonance imaging (MRI) may be required to exclude neurological causes. Finally, the most important aspect nowadays is the genetic assessment using next generation sequencing, which is recommended as the first-tier investigation for patients with suspected MD (O'Grady et al., 2016). Despite advancements in molecular diagnostics, approximately 40% of patients remain genetically undiagnosed (Mercuri, Bonnemann, & Muntoni, 2019).

The onset of muscular dystrophies range between early infancy to childhood as seen in congenital muscular dystrophy (CMD), to adulthood in mild limb girdle muscular dystrophy (LGMD) types (Zambon & Muntoni, 2021). The pattern of muscles involved

may suggest certain conditions like in LGMD, which primarily involves pelvic and shoulder girdle muscles (Georganopoulou et al., 2021; Mercuri & Muntoni, 2013). Additionally, the progression of the disease and the involvement of other musculoskeletal manifestations such as myotonia, joint contractures and scoliosis might provide clues for definitive diagnosis. Extra-muscular findings are common in MD, such as Duchenne muscular dystrophy (DMD) and some LGMD, which are known to be associated with intellectual dystrophy and / or cardiomyopathy. Some MDs are associated with eye defect such as Muscle-eye-brain disease and Facioscapulohumeral dystrophy (FSHD) (Mercuri & Muntoni, 2013). In most of MDs, muscle biopsies have nonspecific histological findings. Myofiber necrosis, myophagocytosis, regenerating fibers with central nuclei, myopathic rounded atrophic fibers, myofiber hypertrophy and fiber splitting, endomysial fibrosis, increased uptake of some stains (opaque fibers), and increased variability of myofiber sizes (Seidman, 2016) are commonly observed. These nonspecific pathological changes can be observed across various types of MDs and, in many cases, may not be sufficient to establish a definitive diagnosis. H&E staining often reveals similar dystrophic features in muscle biopsies from patients with different MD subtypes, making it challenging to distinguish between them based on histological examination alone (Figure 1.7).

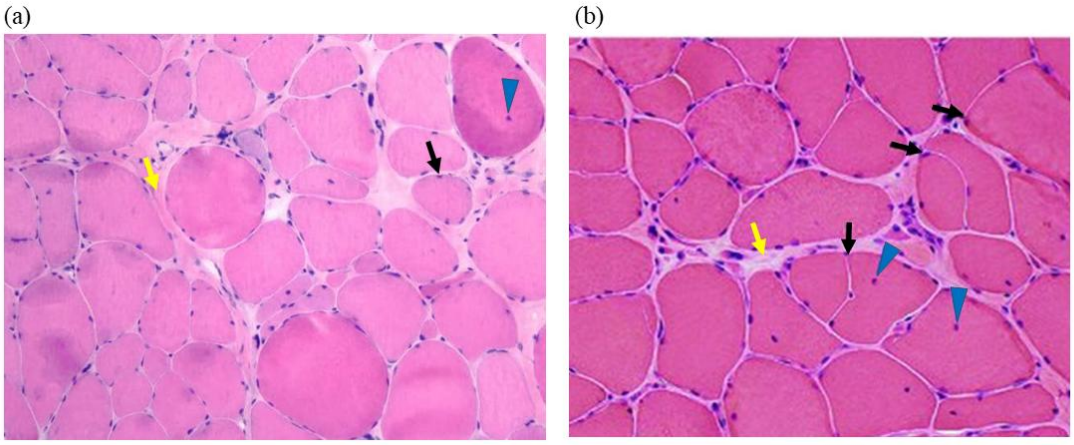

Figure 1.7: H&E stain of cross-sectional muscle biopsy from patients with muscular dystrophy: (a) Muscle biopsy from a patient with Becker muscular dystrophy and (b) from a patient with GDP-Mannose Pyrophosphorylase B (GMPPB) deficiency. The staining reveals marked variability in fiber size and stain uptake, indicative of the coexistence of atrophic and hypertrophic fibers. A central nucleus is marked by the blue arrowhead, while endomysial fibrosis is indicated by the yellow arrow. Myofiber splitting is highlighted by

the black arrow. The images were adapted from. The figures were adapted from (Chompoopong & Milone, 2023; Seidman, 2016).

1.2.2 Types and classification of muscular dystrophies

Muscular dystrophies (MDs) have historically been classified based on clinical phenotypes, including age of onset, the pattern of muscle involvement, and the presence of extra-muscular manifestations. Congenital muscular dystrophies (CMDs) are defined by symptom onset before the age of ambulation, while limb-girdle muscular dystrophies (LGMDs) typically manifest after two years of age, primarily affecting proximal limb muscles. Each group of these diseases has been further subclassified based on their identification sequence and mode of inheritance.

In contrast, some earlier recognized and more prevalent forms of MDs have been classified as distinct entities, such as Duchenne muscular dystrophy (DMD), Becker muscular dystrophy (BMD), Emery-Dreifuss muscular dystrophy (EDMD), and facioscapulohumeral muscular dystrophy (FSHD). However, with the advancement of diagnostic tools and a better understanding of disease pathophysiology, there has been a shift toward a functional classification system. This emerging approach aims to categorize muscular dystrophies based on their underlying molecular mechanisms, genetic defects, and affected cellular pathways, rather than relying solely on clinical presentation and inheritance patterns. (Mercuri et al., 2019).

1.2.3 Functional and molecular pathophysiology of muscular dystrophies

Understanding the normal physiology of skeletal muscles is essential for identifying causative genes responsible for muscular dystrophy phenotypes. Advances in diagnostic tools, particularly next-generation sequencing (NGS), have significantly contributed to the discovery of novel disease-causing genes. Subsequent functional studies have demonstrated that these genes play a critical role in maintaining muscle fiber homeostasis.

For instance, extracellular matrix (ECM) defects are known to cause primary merosin deficiency and Ullrich muscular dystrophy, which result from *LAMA2* and *COL6A* gene mutations, respectively. Mutations in genes encoding external sarcolemmal proteins can also lead to muscular dystrophies, as observed in integrin β-7-related congenital muscular dystrophy (CMD). Furthermore, proteins such as dystroglycan, the dystrophin-associated protein complex, and glycosyltransferase enzymes are essential for maintaining sarcolemmal integrity and linking the ECM to the cytoskeleton. Mutations in these genes are associated with various forms of muscular dystrophy, while other subtypes are linked to nuclear membrane proteins, sarcomeric proteins, or sarcoplasmic reticulum proteins (Mercuri et al., 2019).

To provide a comprehensive understanding of muscular dystrophies, Barton et al. (2020) proposed a functional classification system for limb-girdle muscular dystrophies (LGMDs) (Figure 1.8), grouping them into four major clusters: (1) proteins involved in dystroglycan glycosylation, (2) mechanical signaling proteins, (3) mitochondrial dysfunction-related proteins, and (4) other associated factors (Barton, Pacak, Stoppel, & Kang, 2020).

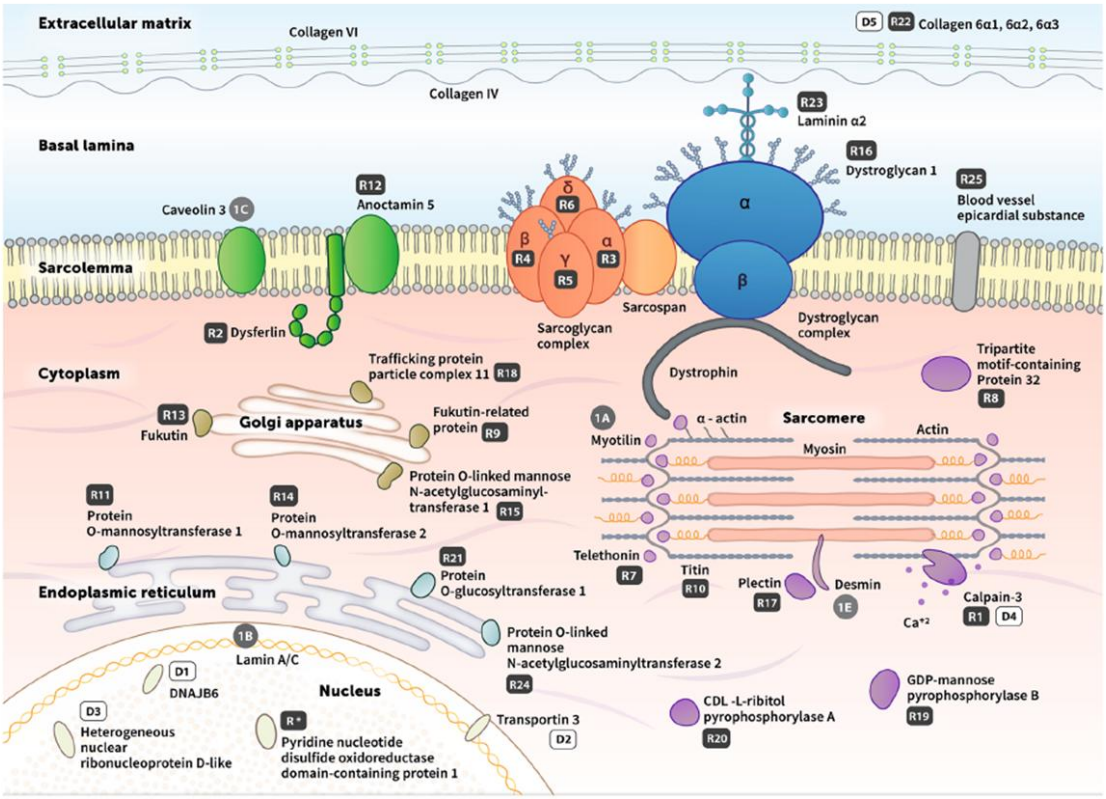

Figure 1.8: Schematic representation of the localization and function of proteins associated with limb-girdle muscular dystrophy (LGMD). R#: Recessive subtype of LGMD; D#

Dominant subtype of LGMD; 1# Old LGMD subtype no longer officially recognized as LGMG. (Adapted from (Georganopoulou et al., 2021)).

Similarly, Zambon and Muntoni (2021) presented a functional classification system for congenital muscular dystrophies (CMDs) (Figure 1.9), categorizing them into six main groups: (1) proteins involved in the basal membrane and extracellular matrix, (2) dystroglycanopathies, (3) endoplasmic reticulum-associated proteins, (4) nuclear envelope proteins, (5) proteins involved in ER-to-Golgi trafficking, and (6) other functionally relevant groups (Zambon & Muntoni, 2021). Table 1 summarizes this classification.

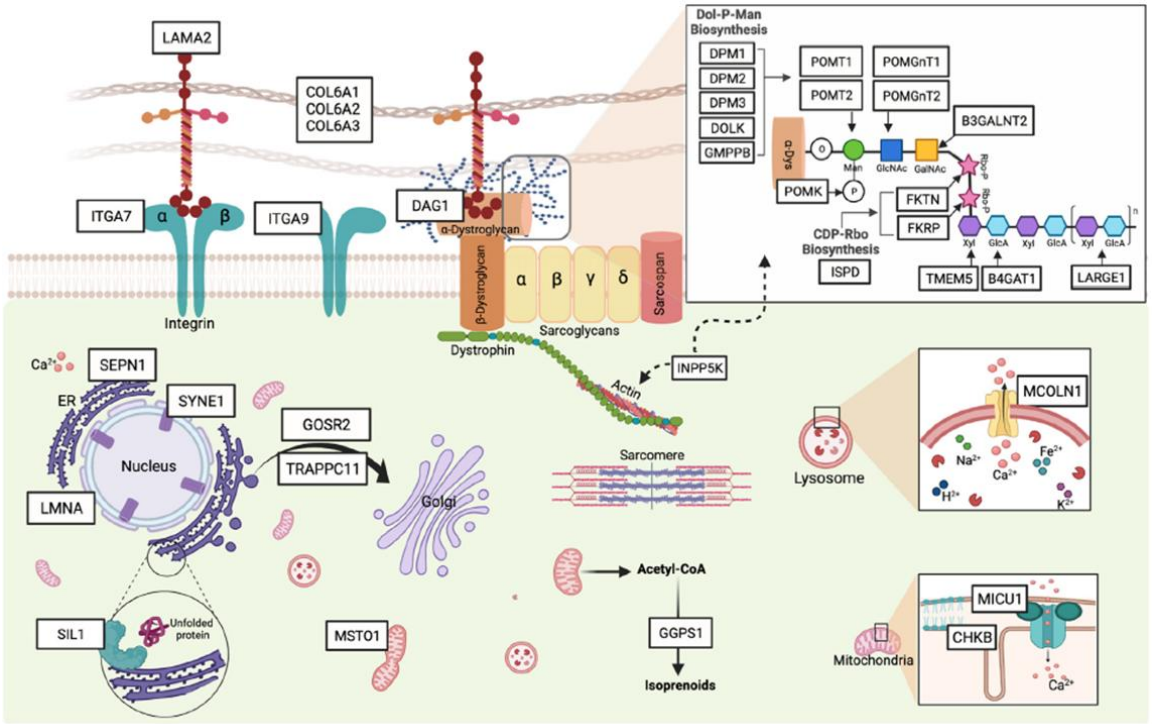

Figure 1.9: Schematic representation of the localization and function of proteins associated with congenital muscular dystrophy (CMD): These proteins are primarily found in the extracellular matrix, sarcolemma, and nucleus, as well as in organelles such as the endoplasmic reticulum, Golgi apparatus, lysosomes, and mitochondria. Additionally, some proteins are linked to cytoskeletal fibers, playing essential roles in structural stability and cellular signaling. (Adapted from (Zambon & Muntoni, 2021)).

Table 1: Summary of LGMD and CMDs functional classification with their causative genes

Functional Classification	**Muscular dystrophy**	**Gene symbol**
Limb-girdle muscular dystrophies		
Glycosylation of Dystroglycan	LGMD R9 (FKRP), LGMD R11 (POMT1), LGMD R13 (FKTN), LGMD R14 (POMT2), LGMD R15 (POMGnT1), LGMD R16 (DAG1), LGMD R19 (GMPPB), LGMD R20 (ISPD), LGMD R24 (POMGNT2)	*FKRP, POMT1, FKTN, POMT2, POMGnT1, DAG1, GMPPB, ISPD, POMGNT2*
Mechanical Signaling Defects	LGMD R3 (SGCA), LGMD R4 (SGCB), LGMD R5 (SGCG), LGMD R6 (SGCD), LGMD R1 (CAPN3), LGMD R2 (DYSF)	*SGCA, SGCB, SGCG, SGCD, CAPN3, DYSF*
Mitochondrial Dysfunction	LGMD R1 (CAPN3), LGMD R3 (SGCA), LGMD R4 (SGCB), LGMD R5 (SGCG), LGMD R6 (SGCD), LGMD R9 (FKRP), LGMD R22 (COL6A1, COL6A2, COL6A3), LGMD R23 (LAMA2)	*CAPN3, SGCA, SGCB, SGCG, SGCD, FKRP, COL6A1, COL6A2, COL6A3, LAMA2*
Other Functional Clusters	LGMD R17 (PLEC), LGMD R18 (TRAPPC11), LGMD R21 (POGLUT1), LGMD R25 (BVES)	*PLEC, TRAPPC11, POGLUT1, BVES*
Congenital muscular dystropies		
Defect in structural proteins of basal membrane and extracellular matrix	LAMA2-RD, COL6-RD (Ulrich CMD), Integrin α-7 deficient CMD, Integrin α-9 deficient CMD	*LAMA2, COL6A1, COL6A3, ITGA7, ITGA9*
Dystroglycanopathies (DGP) / defects of α-DG glycosylation	Primary dystroglycanopathy, Secondary dystroglycanopathies	*DAG1, POMT1, POMT2, POMGnT1, FKTN, FKRP, LARGE1, ISPD, TMEM5*
Endoplasmic reticulum protein	SEPN1-Related Myopathy,	*SEPN1*
Nuclear envelope proteins	LMNA-Related CMD, SYNE1-Related CMD	*LMNA, SYNE1*

Proteins involved in ER to Golgi apparatus trafficking	CMD with fatty liver and infantile-onset cataract	*TRAPCC11, GOSR2*
Other CMDs / CMD spectrum	Mitochondrial CMD (megaconial), MD with cerebellar Involvement, MD with extrapyramidal Signs, CMD with cataracts and intellectual disability	*CHKB, MSTO1, MICU1, INPP5K*

While multiple molecular pathways contribute to the pathogenesis of muscular dystrophies, two mechanisms stand out due to their critical role in muscle maintenance and disease progression: RNA splicing and autophagy. RNA splicing is an essential process that enables the production of functional, tissue-specific protein isoforms, ensuring proper muscle integrity and function. Disruptions in splicing regulation have been implicated in several muscular dystrophies, underscoring the importance of post-transcriptional modifications in muscle homeostasis (Nilsen & Graveley, 2010; Pistoni, Ghigna, & Gabellini, 2010).

Similarly, autophagy, including its specialized form, mitophagy, plays a pivotal role in maintaining cellular homeostasis by eliminating damaged organelles and misfolded proteins, thereby preventing cellular dysfunction and degeneration. Impaired autophagic flux has been reported in various muscular dystrophies, highlighting its contribution to muscle pathology and disease progression

1.2.4 Muscular dystrophy and alternative splicing

Messenger RNA (mRNA) is transcribed by RNA polymerase II in a premature format that requires extensive modifications to become ready for translation. Among these modifications are 5' capping and the generation of the 3' poly-A tail (Gruss, Meduri, Schilling, & Fischer, 2017). One critical maturation process is splicing, which removes noncoding introns and joins exons.

The splicing machinery is a complex and dynamic molecular system that ensures the accurate processing of pre-messenger RNA (pre-mRNA) into mature mRNA. Splicing occurs in two main steps and is catalyzed by a ribonucleoprotein complex known as the spliceosome, which consists of five small nuclear ribonucleoproteins (snRNPs) and

numerous associated proteins. The spliceosome assembly follows a stepwise process where the U1 snRNP initially recognizes the 5' splice site, while U2 snRNP binds to the branch point sequence upstream of the 3' splice site (Will & Luhrmann, 2011). The recruitment of the U4/U6-U5 tri-snRNP complex leads to extensive RNA-RNA rearrangements that allow the spliceosome to adopt its catalytically active conformation. Splicing involves two transesterification reactions: the first reaction generates a lariat intermediate, while the second reaction results in exon ligation and intron removal (Figure 1.10(a)) (Schneider et al., 2010).

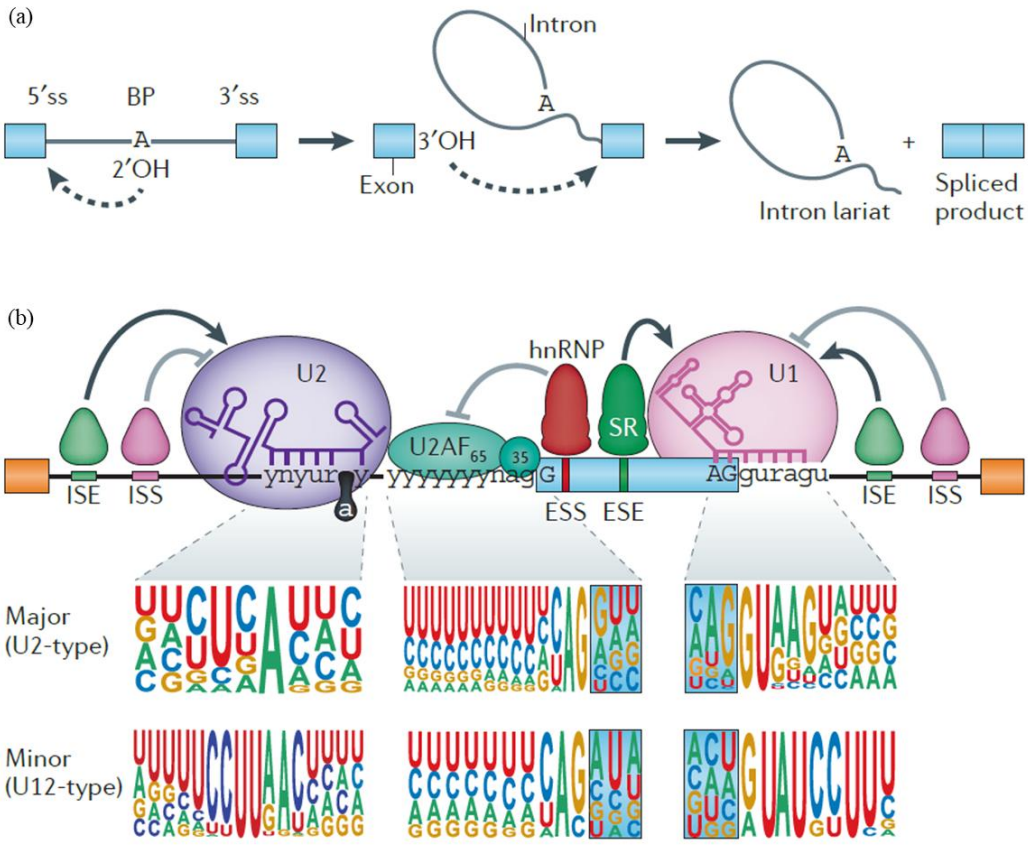

Figure 1.10: mRNA splicing process: (a) Stepwise Mechanism of Splicing: The splicing process is initiated by a transesterification reaction, where the branch point (BP) adenosine within the intron attacks the 5' splice site (5' SS). This results in the formation of an intermediate intron lariat structure, which remains connected to the 3' splice site (3' SS). In a subsequent step, a second transesterification reaction occurs, where the 5' SS attacks the 3' SS, leading to the release of the intron lariat and the precise ligation of adjacent exons, ultimately forming the spliced RNA. (b) Regulation of Splicing and Splice Site Recognition: The regulatory mechanisms governing splicing involve cis-acting splicing

elements that either enhance or suppress exon recognition. Within the intron regions, intron splicing enhancers (ISEs) promote UsnRNP recruitment, thereby facilitating efficient intron removal. Conversely, intron splicing silencers (ISSs) inhibit splicing by preventing spliceosome assembly at the adjacent splice sites. Similarly, exon splicing enhancers (ESEs) and exon splicing silencers (ESSs) regulate exon inclusion or exclusion by interacting with trans-acting splicing factors, such as Ser/Arg-rich (SR) proteins, which act as activators, and heterogeneous nuclear ribonucleoproteins (hnRNPs), which function as repressors. The lower part of the schematic illustrates splice site recognition through consensus sequences within introns, which guide the selection of the correct splice sites. The major splicing machinery, which processes U2-type introns, is guided by U2 snRNPs, whereas the minor splicing pathway, responsible for the removal of U12-type introns, relies on U12 snRNPs. The relative frequency of nucleotide residues at key positions within the consensus sequences is depicted, indicating their importance in splice site selection and recognition efficiency. (Adapted from (Scotti & Swanson, 2016)).

There are two major types of splicing pathways: the major spliceosome pathway, which processes U2-type introns, and the minor spliceosome pathway, which processes the less common U12-type introns (Matera & Wang, 2014). The major pathway, responsible for the vast majority of splicing events, involves U1, U2, U4, U5, and U6 snRNPs, whereas the minor pathway utilizes a distinct set of snRNPs (U11, U12, U4atac, U6atac, and U5) (Verma, Akinyi, Norppa, & Frilander, 2018). Alternative splicing, a key regulatory mechanism, allows for the production of multiple protein isoforms from a single gene by selectively including or excluding exons. This process is tightly regulated by cis-acting splicing regulatory elements and trans-acting splicing factors, which can act as enhancers or silencers to modulate exon recognition (Figure 1.10(b)) (Scotti & Swanson, 2016). Alternative splicing also enables the generation of tissue-specific and developmentally regulated isoforms of proteins through a process known as alternative splicing (Nilsen & Graveley, 2010). This highly regulated process is essential for producing functional proteins, as even minor errors can result in dysfunction (Matera & Wang, 2014; Wilkinson, Charenton, & Nagai, 2020).

There are various types of alternative splicing, as summarized in Figure 1.11. Almost all human cell types undergo alternative splicing for multi-exon coding genes, making this process essential for tissue-specific protein diversity. During development, alternative splicing enables the same gene to produce distinct protein isoforms, ensuring proper cell differentiation and function (Wang et al., 2008).

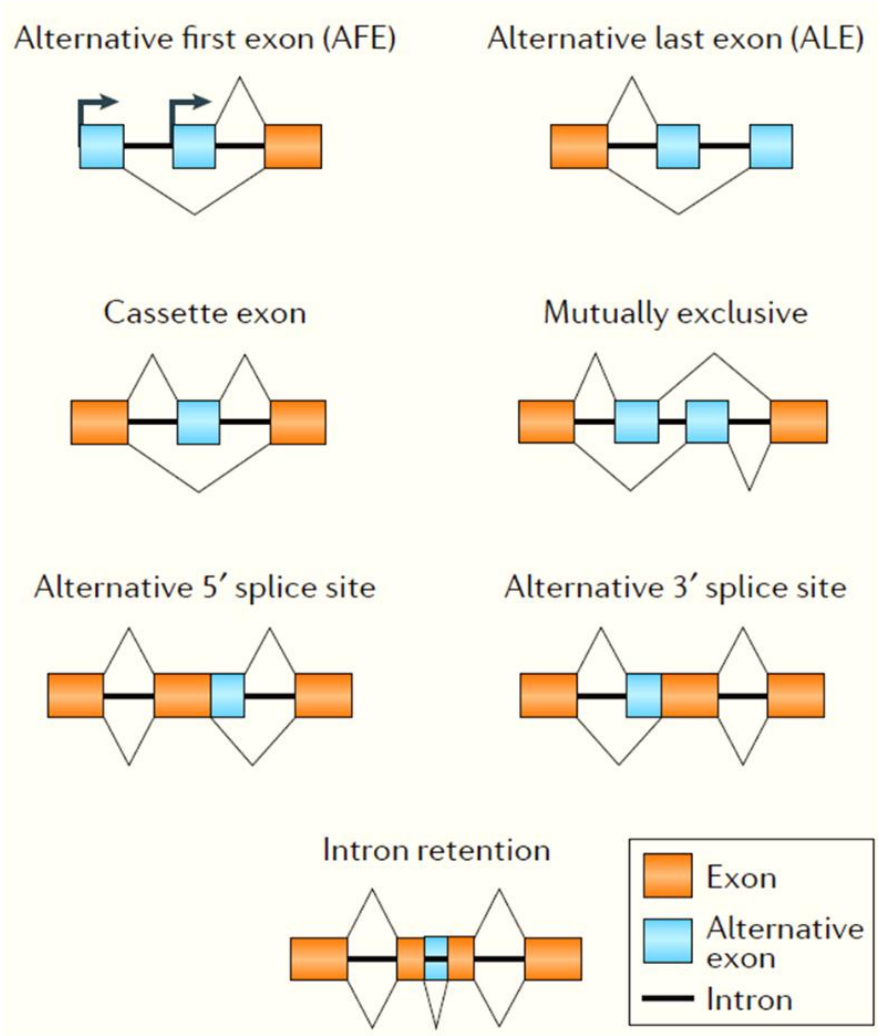

Figure 1.11: Variable types of alternative splicing events (Adapted from (Scotti & Swanson, 2016)).

The most common type of alternative splicing is exon skipping, which occurs in approximately 75% of multi-exon genes. The selection of splice sites and the type of alternative splicing event are regulated by splicing regulatory elements that act in cis or

trans. These splicing codes can predict cell- and tissue-specific alternative splicing patterns, playing a crucial role in developmental processes and adaptive responses to environmental conditions (Scotti & Swanson, 2016).

Skeletal muscle tissues exhibit a high frequency of alternative splicing events, leading to muscle-specific transcripts and diverse protein isoforms essential for muscle fiber function and development (Pistoni et al., 2010). Muscular diseases associated with aberrant splicing can arise through two primary mechanisms. The first involves mutations within splice site sequences, as seen in *LNMA* gene mutations, where the phenotypic variability depends on the mutations' location within the gene. The second mechanism results from mutations affecting the splicing machinery or its regulatory components, leading to widespread disruptions in RNA processing and protein synthesis. Two primary types of muscular dystrophies, myotonic muscular dystrophy (DM) and facioscapulohumeral muscular dystrophy (FSHD), are directly associated with spliceosomal machinery defects. Both disorders are inherited in an autosomal dominant pattern and manifest as progressive muscle weakness in adults.

Myotonic dystrophy (DM) type 1 (OMIM 160900) is caused by an abnormal expansion of CTG repeats in the 3′ UTR of the *DMPK* gene. It presents with both muscular and extramuscular manifestations, including cardiac conduction defects, neurological symptoms, and cataracts. DM type 2 (OMIM 602668) is linked to CCTG repeat expansions in intron 1 of the *ZNF9* gene. Mutations in these genes disrupt the function of two key alternative splicing regulators, *MBNL1* and *CUGBP1*.(Johnson, 2019; Pistoni et al., 2010) FSHD (OMIM 158900) is characterized by atrophy of specific muscle groups, as indicated by the name of the disease, along with extramuscular manifestations such as hearing loss and retinal telangiectasia. FSHD is primarily caused by the loss of D4Z4 repeats in the 4q35 region, leading to the overexpression of the *FRG1* gene. FRG1 is believed to play a role in splicing, as it localizes to the nucleus and Cajal bodies, interacting with spliceosome components and SMN. Mis-splicing events have been identified in FSHD patients and confirmed in models overexpressing *FRG1* (Lemmers et al., 2012; Pistoni et al., 2010; Schatzl, Kaiser, & Deigner, 2021). These findings underscore that defect in the splicing pathway, resulting in mis-splicing, can contribute to the muscular dystrophy phenotype.

1.2.5 Muscular dystrophy and autophagy

Definition and function of autophagy

Autophagy is a fundamental cellular process essential for maintaining homeostasis by degrading and recycling intracellular components, such as damaged organelles, misfolded proteins, and cytoplasmic debris. There are two well conserved pathways of autophagy, the macroautophagy and microautophagy. The macroautophagy process involves the formation of double-membraned vesicles known as autophagosomes, which transport these components to lysosomes for enzymatic degradation. On the other hand, the microautophagy involves invagination of lysosomal membrane ingulfing part of cytoplasm and digest the contents directly (Mejlvang et al., 2018; Schuck, 2020; Yamamoto, Zhang, & Mizushima, 2023). The recycled products are subsequently utilized for biosynthesis and energy production. Autophagy plays a critical role in cellular adaptation to stress conditions, such as nutrient deprivation, by providing essential building blocks necessary for survival. Additionally, it underpins key physiological processes, including development, immune responses, and aging (Mizushima & Komatsu, 2011).

The functional versatility of autophagy is pivotal for cellular health and functionality. By removing damaged organelles and misfolded proteins, autophagy mitigates oxidative stress and preserves intracellular homeostasis (Lamark & Johansen, 2021). Furthermore, it supplies nutrients during periods of starvation by recycling intracellular resources, facilitating cellular remodeling during differentiation and tissue development. Dysregulation of autophagy is implicated in a spectrum of pathological conditions, including neurodegenerative diseases, cancer, and muscular disorders (Klionsky et al., 2021; Mizushima & Levine, 2020). In skeletal muscles, autophagy ensures protein turnover, energy homeostasis, and the clearance of dysfunctional cellular components, thereby safeguarding muscle integrity and function (Grumati & Bonaldo, 2012).

Autophagy pathway

The canonical autophagy pathway is typically initiated under nutrient-deprived conditions through the inhibition of mechanistic target of rapamycin complex 1 (mTORC1) (Figure 1.12). This inhibition activates the ULK1/Atg1 kinase complex, which recruits downstream autophagy-related (ATG) proteins to facilitate the nucleation and elongation

of the isolation membrane or phagophore (Fujioka et al., 2014). Alternatively, ULK1 complex can be activated by cargo-induced assembly driven by the binding of autophagy cargo adaptor, P62 a polyubiquitin-binding protein, to the polyubiquitinated cargos. P62 is then recognized by FIP200, a component of ULK1 complex (Turco et al., 2019). The autophagy vesicle assembly is initiated by the ATG9 complex, which serves as the origin for the autophagy bilayer membrane (Sawa-Makarska et al., 2020). This membrane undergoes elongation through the transport of phospholipids from the endoplasmic reticulum (ER) in a process known as scrambling. A critical component of this machinery is TMEM41B, an ER transmembrane protein that plays a pivotal role in maintaining the structural integrity of autophagosomes. TMEM41B facilitates the mobilization of lipids required for the elongation and closure of the autophagosomal membrane (Huang et al., 2021).

During this elongation process, LC3 (microtubule-associated proteins 1A/1B light chain 3) is activated from its cytoplasmic form, LC3, to its active form, LC3-I, which then undergo lipidation to form LC3-II (Fujita et al., 2008). The lapidated LC3-II becomes embedded in both the inner and outer membranes of the autophagosome. This modification enables LC3 to direct p62-bound cargos, including ubiquitinated proteins and damaged organelles, into the autophagosome for degradation (Sou et al., 2008; Yamamoto et al., 2023).

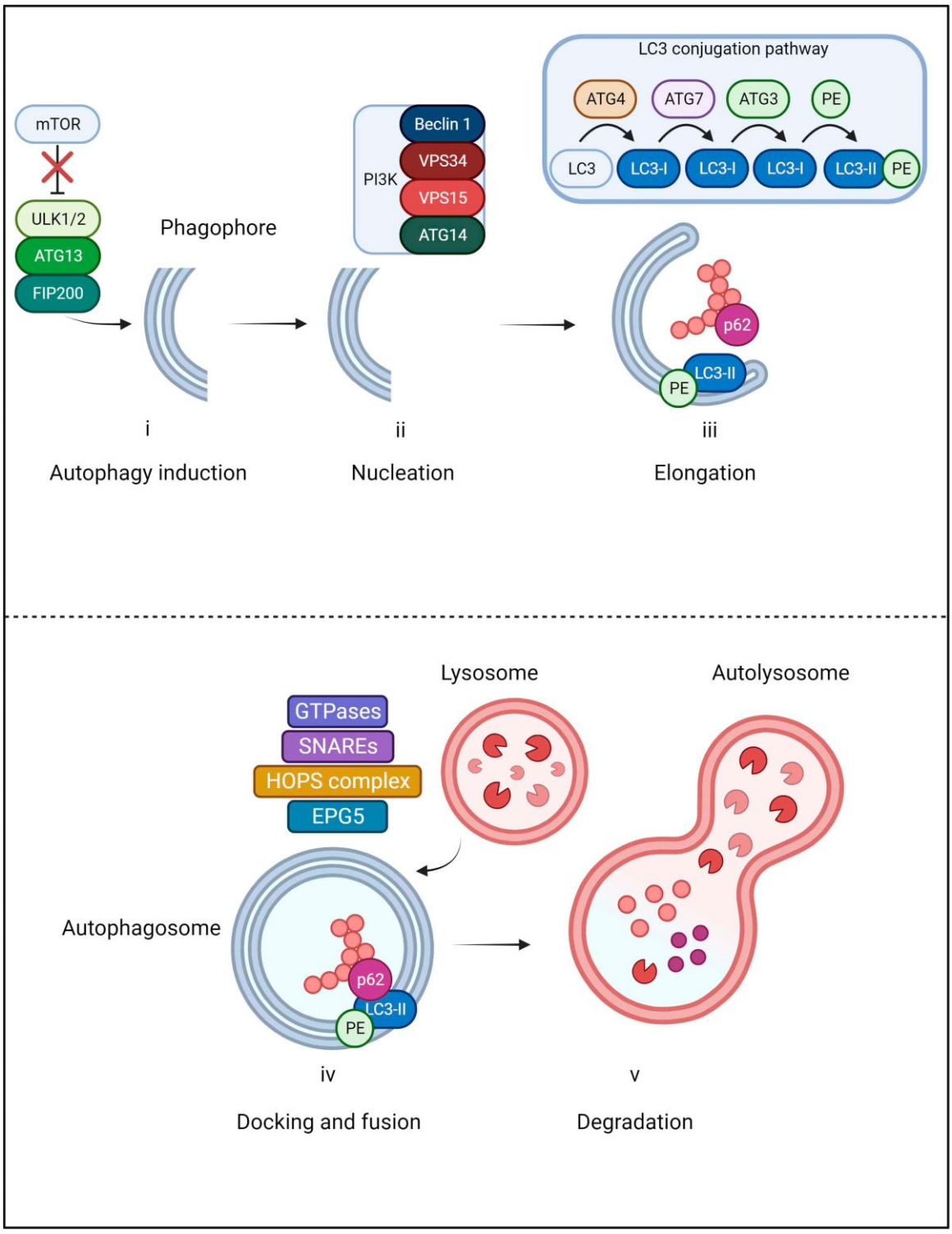

Figure 1.12: Schematic representation of the basic steps of canonical autophagy: Autophagy is a highly regulated catabolic process that ensures cellular homeostasis by degrading and recycling unnecessary or damaged cellular components. The process begins with induction, which activates the autophagic machinery in response to cellular stress or nutrient deprivation. This is followed by nucleation, where an initial membrane structure, the phagophore, begins to form. During the elongation phase, the phagophore expands,

engulfing cytoplasmic material, including damaged organelles and protein aggregates. Once fully enclosed, the mature autophagosome forms and subsequently fuses with a lysosome, creating an autolysosome. This fusion initiates the degradation phase, where lysosomal hydrolases break down the sequestered material, allowing for the recycling of biomolecules to sustain cellular metabolism and energy balance. (Adapted from (Rashid & Dimitriadi, 2023)).

As the autophagosome matures, it detaches from the ER membrane, forming a closed vesicle that is primed for fusion with lysosomes in a process known as autophagic flux. Upon fusion, the autophagosome and lysosome combine to form an autolysosome, where the enclosed contents are enzymatically degraded. The degradation products are then recycled; components of the lysosomal membrane are reused, and the breakdown products of lysed materials are made available for cellular needs. Loss of autophagic flux is associated with many diseases including neurodegenerative diseases, cancers, immune diseases and storage diseases (Zhao & Zhang, 2019).

Role of autophagy in skeletal muscle homeostasis

Autophagy is indispensable in skeletal muscles for the removal of cellular debris and damaged components generated by mechanical and oxidative stress. Skeletal muscle fibers, known for their high metabolic activity, rely on autophagy to prevent the accumulation of dysfunctional organelles and protein aggregates. In addition to its housekeeping role, skeletal muscle, which constitutes approximately 40% of body mass, serves as a critical reservoir of amino acids during periods of starvation. Consequently, autophagy in skeletal muscle remains continuously active, though meticulously regulated to balance protein turnover and energy needs (De Palma, Perrotta, Pellegrino, Clementi, & Cervia, 2014; Neel, Lin, & Pessin, 2013). Studies have demonstrated that constitutive basal autophagy is necessary for normal muscle function, as its inhibition leads to the accumulation of protein aggregates, mitochondrial dysfunction, and muscle degeneration (Jung et al., 2008; Masiero et al., 2009).

Autophagy is also crucial for muscle adaptation to various physiological conditions, including exercise and fasting. Exercise-induced autophagy is essential for maintaining

muscle health, as it facilitates the clearance of damaged proteins and provides energy through the recycling of cellular components (He et al., 2012). Additionally, autophagy plays a pivotal role in muscle regeneration by regulating satellite cell function. Satellite cells, which are muscle stem cells, rely on autophagy for maintaining their quiescence and activation in response to injury or stress (Tang & Rando, 2014). Defective autophagy in satellite cells leads to oxidative stress, mitochondrial dysfunction, and impaired regenerative capacity (Garcia-Prat et al., 2016).

Dysregulation of autophagy in skeletal muscle has been strongly associated with pathological outcomes, including muscle atrophy, weakness, and impaired regenerative capacity. Reduced autophagic activity has been linked to the progression of muscular dystrophies, exacerbating cellular damage and functional decline. Conversely, enhancing autophagic flux in skeletal muscle has shown promise in mitigating disease progression and improving muscle function by restoring cellular homeostasis and reducing the accumulation of harmful components (Grumati & Bonaldo, 2012).

Autophagy-related genes mutations cause muscular dystrophy

Mutations in autophagy-related genes have been implicated in various forms of muscular dystrophy and other pathological conditions. For instance, mutations in *LAMP2* disrupt lysosomal function, as observed in X-linked dominant Danon disease. This condition is characterized by defective lysosomal degradation, leading to the accumulation of cellular waste. Danon disease primarily affects cardiac and skeletal muscles and is often accompanied by intellectual disability and other clinical manifestations (Lobrinus et al., 2005; Roos, Daniels, Morris, Hyry, & Cox, 2018). Similarly, abnormalities in *ATG5*, a gene critical for autophagosome formation, exacerbate muscle degeneration by impairing autophagic activity. Mutations in ATG5 have been linked to spinocerebellar ataxia, highlighting the gene's role in maintaining cellular integrity (Kim et al., 2016). Truncating mutations in *ATG7*, a gene essential for the activation of ATG5 and the lipidation of LC3-I to LC3-II, have been associated with a neurodevelopmental disorder characterized by myopathic changes and endocrine hypofunction (Collier et al., 2021). Furthermore, defects in P62/SQSTM1, an autophagy receptor, contribute to a wide range of diseases, including cancer, neurodegenerative disorders, metabolic syndromes, and musculoskeletal diseases.

Notably, mutations in *P62/SQSTM1* are associated with adult-onset autosomal dominant myopathy, where the impaired function of this receptor leads to the accumulation of toxic protein aggregates, exacerbating disease progression (Bucelli et al., 2015; Sanchez-Martin & Komatsu, 2018).

Dysregulated autophagy pathways in muscular dystrophy

Dysregulation of autophagy is a hallmark of several muscular dystrophies. In Duchenne muscular dystrophy (DMD), impaired autophagic flux results in the accumulation of damaged proteins and organelles, disrupting cellular homeostasis. Furthermore, autophagy dysfunction negatively affects the function of satellite cells, the primary drivers of muscle regeneration. This impairment exacerbates the degradation of muscle fibers, contributing to the progressive muscle degeneration characteristic of DMD (De Palma, Morisi, et al., 2014; Fiacco et al., 2016). Furthermore, limb-girdle muscular dystrophy type R9 (LGMDR9), caused by mutations in the fukutin-related protein gene (*FKRP*) encoding a glycosyltransferase involved in α-dystroglycan modification, has been associated with dysregulation of the autophagy pathway. Studies have demonstrated that in LGMDR9, levels of LC3-II and Atg5 are elevated in patient samples, while P62 and mTORC1 are decreased. These findings suggest that altered autophagic activity plays a significant role in the pathophysiology of the disease (Franekova, Storjord, Leivseth, & Nilssen, 2021). Similarly, in merosin-deficient congenital muscular dystrophy (MDC1A), mutations in the *LAMA2* gene affected muscle fibers showed hyperexpression of LC3, however the P62 was increased as well (Mastrapasqua et al., 2023). Interestingly, treating MDC1A mouse model with autophagy inhibitors ameliorated the mice phenotype and increased the life span of the affected mice (Carmignac et al., 2011). Other conditions such as Ullrich congenital muscular dystrophy (UCMD), caused by collagen type IV (COL61A) exhibit defect in autophagic flux leading to the accumulation of defective mitochondria and accelerating apoptosis and muscle atrophy (Grumati et al., 2010). Studies targeting the activation of autophagy in UCMD mouse models or patients improved their condition and decreased the muscle fiber apoptosis (Castagnaro et al., 2016). These findings underscore the importance of maintaining tightly regulated autophagy including mitophagy to preserve muscle structure and function.

1.2.6 Mitophagy and skeletal muscles

Mitophagy, a specialized form of macroautophagy, selectively degrades damaged mitochondria, thereby preserving mitochondrial quality and cellular energy balance (Ashrafi & Schwarz, 2013). This process is particularly vital in skeletal muscles, where mitochondria play a central role in energy production, reactive oxygen species (ROS) regulation, and apoptosis. Mitophagy ensures the removal of dysfunctional mitochondria, safeguarding muscle function by mitigating oxidative stress and maintaining metabolic efficiency. Dysregulation of mitophagy in skeletal muscles is associated with aging-related sarcopenia and muscular dystrophies, where impaired mitochondrial clearance exacerbates muscle degeneration (Leduc-Gaudet, Hussain, Barreiro, & Gouspillou, 2021).

Mitophagy pathway

The PINK1/Parkin pathway is the most well-characterized mechanism of mitophagy (Figure 1.13). In physiological conditions, the mitochondrial membrane potential is maintained high, preventing the attachment of phosphatase and tensin homolog (PTEN)-induced kinase 1 (PINK1) to the outer mitochondrial membrane (Figure 1.13(a)). Upon mitochondrial damage, a reduction in transmembrane potential inhibits the translocation of PINK1 to TIM23 in the inner mitochondrial membrane. This prevents its degradation by mitochondrial processing peptidase (MPP) (PARL) (Figure 1.13(b)) (Greene et al., 2012), leading to the accumulation of PINK1 on the outer mitochondrial membrane (OMM). On the OMM, PINK1 phosphorylates ubiquitin and activates Parkin, an E3 ubiquitin ligase, which amplifies the ubiquitination of several outer mitochondrial membrane proteins (Kane et al., 2014; Narendra et al., 2010).

Key ubiquitinated proteins in this process include Mitofusin 1 (MFN1), Mitofusin 2 (MFN2), translocase of the outer membrane 20 (TOM20), and voltage-dependent anion channel (VDAC), among others (Leduc-Gaudet et al., 2021). These ubiquitinated proteins act as docking sites for autophagy receptors, such as P62, which tether damaged mitochondria to LC3-II on autophagosomes (Figure 1.13(c)). This interaction facilitates the selective degradation of damaged mitochondria within lysosomes. The PINK1/Parkin pathway is critical for maintaining cellular homeostasis, preventing oxidative stress, and avoiding metabolic imbalances (Johansen & Lamark, 2020; Matsumoto, Wada, Okuno, Kurosawa, & Nukina, 2011).

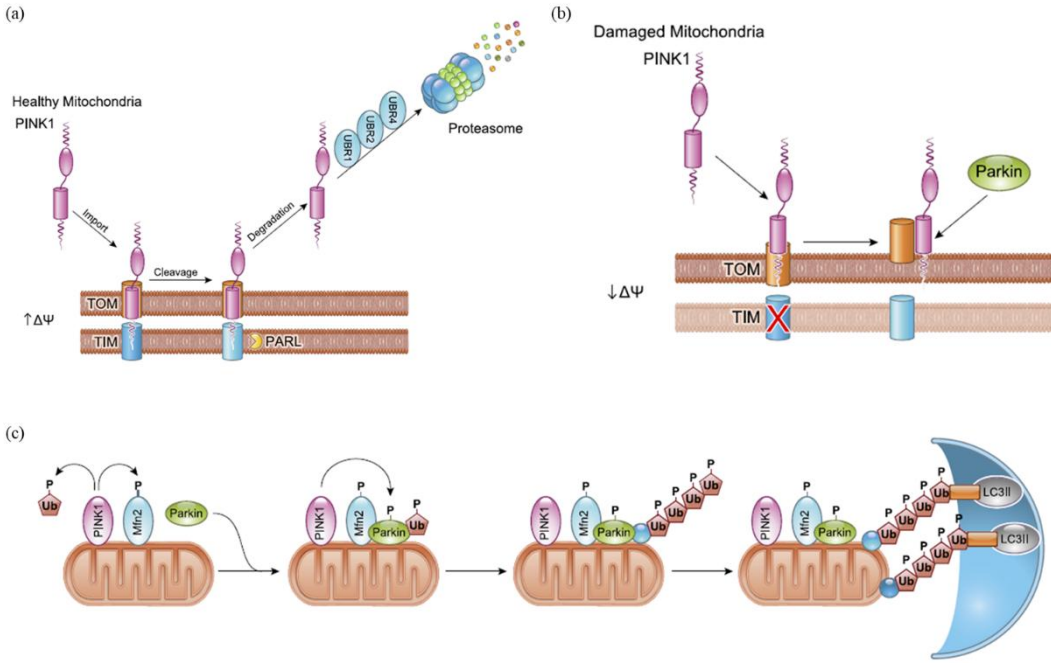

Figure 1.13: The canonical mitophagy pathway: (a) In healthy mitochondria, the membrane potential (ΔΨ) is maintained, allowing PINK1 to be imported into the inner mitochondrial membrane (IMM) via the translocase of the inner membrane (TIM). Once inside, PINK1 undergoes proteolytic cleavage and is subsequently ubiquitinated and degraded by the proteasome, preventing mitophagy initiation. (b) When mitochondria become damaged, the membrane potential (ΔΨ) decreases, preventing the cleavage of PINK1. As a result, PINK1 accumulates on the outer mitochondrial membrane (OMM), where it serves as a recruitment signal for PARKIN, an E3 ubiquitin ligase. (c) As a kinase, PINK1 phosphorylates PARKIN, ubiquitin (Ub), and various OMM proteins, activating PARKIN's ubiquitin ligase activity. PARKIN then ubiquitinates OMM proteins, serving as a recognition signal for autophagy adaptor proteins such as P62, which facilitate the binding of damaged mitochondria to LC3-II on the growing phagophore membrane. This process leads to mitochondrial engulfment by the autophagosome, which ultimately fuses with the lysosome, resulting in the degradation and recycling of damaged mitochondria. (Adapted from (Gustafsson & Dorn, 2019))

In addition to the PINK1/Parkin pathway, four alternative mitophagy mechanisms have been identified. These include alternative autophagy, the endosomal pathway, microautophagy, and mitochondrial-derived vesicles, which provide additional layers of

regulation and ensure mitochondrial quality control under diverse conditions (Gustafsson & Dorn, 2019).

Mitophagy in muscular dystrophy and spinal muscular atrophy

Mitophagy is crucial for maintaining mitochondrial health, particularly in energy-intensive tissues like skeletal muscles. Dysregulated mitophagy is a key contributor to the pathogenesis of various muscular dystrophies. In DMD, for instance, the under-expression of mitophagy mediators such as Parkin results in the accumulation of dysfunctional mitochondria. This dysfunction amplifies oxidative stress, promotes ROS generation, and accelerates muscle fiber degeneration through inflammatory and apoptotic pathways (Kang, Badr, Kyrychenko, Eskelinen, & Shirokova, 2018; Reid & Alexander, 2021).

In Ullrich congenital muscular dystrophy (UCMD), caused by mutations in collagen VI, a critical component of the extracellular matrix forming the network fibers of the skeletal muscle endomysium, dysfunction in autophagy has been identified as a key pathological feature. Mutations in the *COL6A1* gene lead to the destabilization of mitochondrial integrity, triggering apoptosis and contributing to progressive muscle wasting (Bernardi & Bonaldo, 2013). Studies have demonstrated an excessive accumulation of defective organelles, including dysfunctional mitochondria, due to impaired autophagy machinery. This impairment is characterized by a loss of key autophagy markers such as Beclin1, LC3, and Bnip3. Bnip3, a mitophagy receptor anchored to the outer mitochondrial membrane (OMM), plays a critical role in the selective clearance of damaged mitochondria. The loss of these components disrupts autophagic flux and mitophagy, further exacerbating mitochondrial dysfunction and cellular degeneration in UCMD (Grumati, Coletto, Sandri, & Bonaldo, 2011; Gustafsson & Dorn, 2019). Restoring autophagic function through starvation, low-protein diets, or pharmacological treatments has been shown to reduce the accumulation of dysfunctional organelles and alleviate the disease phenotype, highlighting the therapeutic potential of targeting autophagy pathways (Grumati et al., 2010; Grumati et al., 2011).

1.2.7 Expanding the genetic and molecular landscape of muscular dystrophies

Despite significant advancements and developments in molecular diagnostic technologies, a substantial number of patients with muscular dystrophy remain without a genetic diagnosis (Mercuri et al., 2019). This indicates that numerous genes responsible for the disease have yet to be discovered, highlighting the substantial gaps in current knowledge about the genetics of muscular dystrophies. The continuous expansion of the muscular dystrophy research field reflects the ongoing efforts to identify new genes associated with these disorders, leading to a better understanding of their diverse phenotypes. Review articles regularly incorporate information on newly discovered disease-causing genes and the related phenotypes, providing valuable insights into the genetic basis of these new conditions (Zambon & Muntoni, 2021). However, for real-time updates on these developments, online databases like the GeneTable (https://www.musclegenetable.fr/) of Neuromuscular Disorders serves as an essential resource. This database is regularly updated, detailing the latest genetic findings and expanding on the phenotypic spectrum of neuromuscular disorders including congenital muscular dystrophy and LGMD (Benarroch, Bonne, Rivier, & Hamroun, 2023). It underscores the increasing complexity of muscular dystrophies and the necessity of deeply characterizing newly identified causative genes to unravel the pathophysiology of these intricate conditions, thereby informing the development of targeted therapeutic strategies.

While significant progress has been made in identifying genes and pathways associated with muscular dystrophies, many molecular mechanisms underlying these conditions remain unknown.

1.2.8 Prognosis and available treatments

Muscular dystrophies are devastating diseases that are often fatal and significantly affect the patients' and families' quality of life. The severity of the phenotype and prognosis varies based on the underlying cause. In the most studied disease, DMD, affected boys experience significant deterioration after the age of 7 years. Without appropriate treatment, they will lose their ability to walk by the age of 13 years (Mazzone et al., 2011).

Thus far, two main approaches have been investigated for treating MD. The first is to target the mutated gene, aiming to correct the mutation or improve the expression of the defective

proteins. The second is to target the secondary consequences of the gene's deficiency, which can alleviate the patients' phenotype and improve the prognosis. Both strategies have their pros and cons. Currently, there is no approved treatment modality for MDs. Numerous clinical trials are currently underway, exploring various approaches such as antisense oligonucleotides, gene therapy, corticosteroids, anti-inflammatory, anti-fibrotic, and more. These studies are being conducted on various types of MD, with a particular emphasis on the most prevalent form, DMD (Mercuri et al., 2019).

The therapeutic approaches for DMD have evolved significantly, focusing on both genetic correction and symptomatic management. Gene therapies, particularly exon skipping strategies, utilize antisense oligonucleotides (AONs) to restore dystrophin expression. Eteplirsen, Golodirsen, and Casimersen target specific exons (51, 53, and 45, respectively) to bypass mutations and generate a functional, albeit truncated, dystrophin protein. Another genetic approach, CRISPR-Cas9 genome editing, aims to correct the dystrophin gene at the DNA level by removing duplicate exons or repairing mutations via homology-directed repair (Krishna et al., 2024).

Stop codon readthrough therapies, such as Gentamicin and Ataluren, allow the ribosome to bypass premature termination codons, enabling the production of functional dystrophin in patients with nonsense mutations (Sheikh & Yokota, 2021). Additionally, AAV-mediated gene therapy is being explored for delivering mini-dystrophins via viral vectors, with ongoing clinical trials assessing its efficacy (Crone & Mah, 2018).
Beyond genetic interventions, secondary therapies include glucocorticoids like prednisone and deflazacort, which delay muscle degeneration. Supportive treatments address calcium dysregulation, histone deacetylase inhibition, and oxidative stress to preserve muscle function and improve quality of life (Krishna et al., 2024).

Understanding the functional similarities of the disease mechanisms might pave the way for new therapeutic targets that could benefit in variable types of MDs (Barton et al., 2020).

1.3 SNURPORTIN-1

1.3.1 SNUPN gene

The Snurportin-1 gene (*SNUPN*) (OMIM 607902) spans 28,387 bases on the minus strand and is located on the long arm of chromosome 15 (15q24.2) and is composed of nine exons (Figure 1.14).

The *SNUPN* gene exhibits notable conservation across diverse species, as indicated in various conservation databases such as PhyloP and Multiz Alignments. Figure 1.14 illustrates the similarity observed in nearly all exons of the human *SNUPN* gene compared to those in other species. This representation was sourced from the University of California Santa Cruz (UCSC) Genome Browser website (Group, 2023).

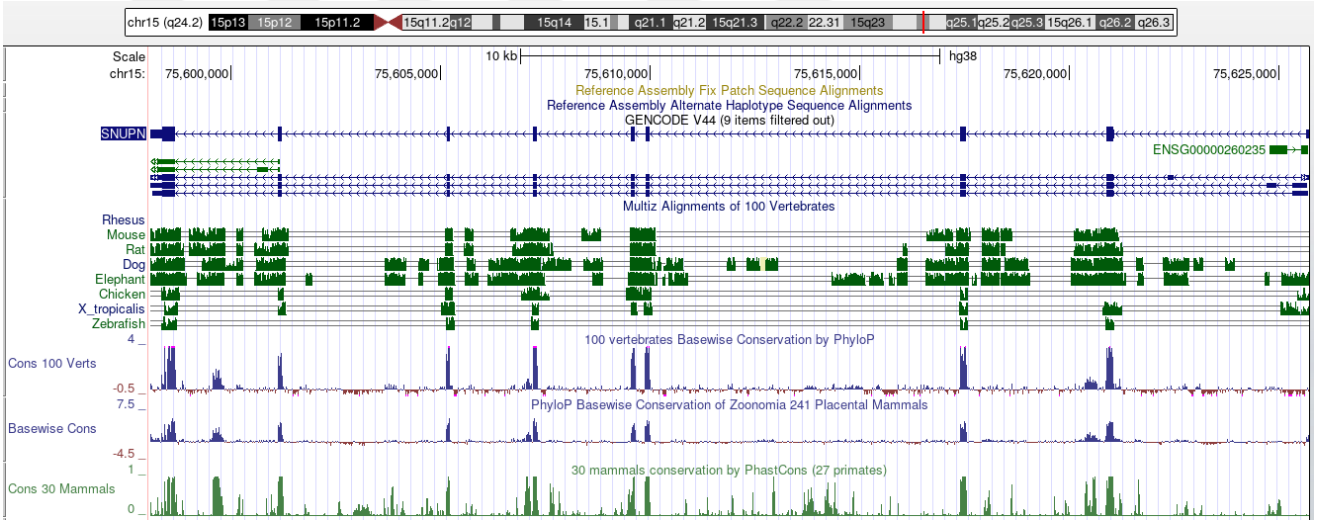

Figure 1.14: Genomic location and conservation of *SNUPN*: Genomic location of *SNUPN* on chromosome 15, including a schematic representation of the exons in the human *SNUPN* gene, followed by the conservation of these exons across various species (Group, 2023).

SNUPN is ubiquitously expressed across various tissues, exhibiting low tissue specificity. However, its expression levels are notably higher in neurological tissues and skeletal muscles, suggesting a potential role in these systems (Figure 1.15).

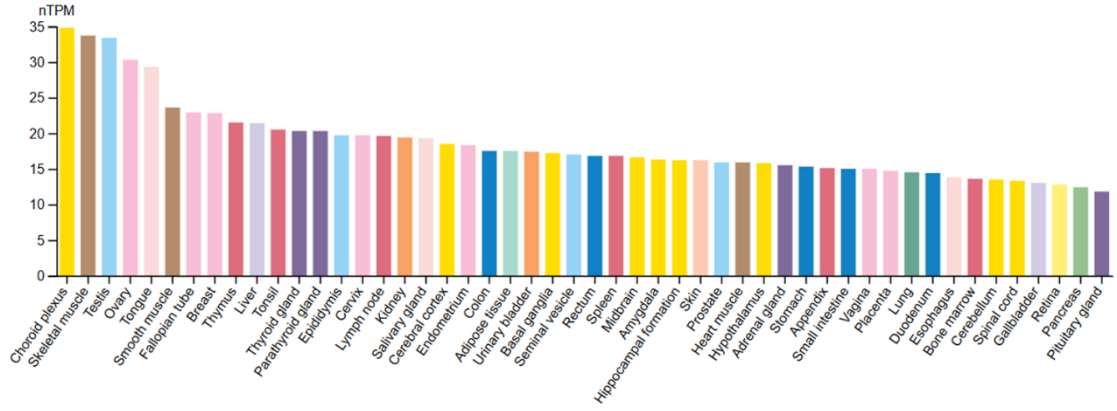

Figure 1.15: Relative expression of *SNUPN* gene in variable tissues. nTPM: number of Transcripts per million (The Human Protein Atlas).

1.3.2 SNURPORTIN-1 function

The isolation and cloning of complementary DNA (cDNA) of SNURPORTIN-1 (SPN1) were first performed by Huber et al. (1998), revealing a 45 kDa protein with a specific affinity for the 5-prime-2,2,7-terminal trimethyl guanosine (m_3G or TMG) cap structure of uridine-rich small nuclear RNA (UsnRNA) (Huber et al., 1998). The human SPN1 protein consists of 360 amino acids, with a molecular weight of 41,143 Da, and contains two primary domains. The N-terminal Importin β binding (IBB) domain, spanning amino acids 1–65, facilitates interaction with Importin β1 (Imp-β1), while the m_3G/TMG cap-binding domain, located closer to the C-terminus (approximately amino acids 100–300), enables recognition of the trimethylguanosine cap of UsnRNAs (Figure 1.16).

SPN1 is known to interact with Importin subunit beta-1 (Imp-β1) and Exportin-1 (CRM1), in addition to binding its ligand, the m_3G cap and its associated complex. Furthermore, intramolecular interactions between the N- and C-termini play a regulatory role by sequestering the IBB domain, preventing the nuclear import of cargo-less SPN1 (Ospina et al., 2005). SPN1 is predominantly localized in the cytoplasm, and its function, interactions, and localization have been investigated through *in vitro* and overexpression studies.

Figure 1.16: Schematic representation of the SPN1 protein: The SPN1 protein consists of two primary functional domains: the N-terminal Importin β Binding (IBB) domain, which facilitates interaction with Importin β1 for nuclear import, and the C-terminal Trimethylguanosine (TMG) binding site, which is essential for recognizing and binding TMG-capped UsnRNPs. These domains are crucial for SPN1's role in nucleocytoplasmic transport and RNA splicing regulation.

1.3.3 UsnRNPs complex biogenesis and splicing machinery

The primary function of SPN1 is its role as a specialized adaptor for the nuclear import of uridine-rich small nuclear ribonucleoproteins (UsnRNPs). The N-terminal Importin β1 binding (IBB) domain of SPN1 directly interacts with Importin subunit β1 (Imp-β1), a karyopherin responsible for transporting the SPN1-loaded import complex into the nucleus (Figure 1.17) (Mitrousis, Olia, Walker-Kopp, & Cingolani, 2008; Wing, Fung, & Chook, 2022).

The assembly of the import complex begins with the nuclear export of 7-methylguanosine (m^7G)-capped UsnRNA to the cytoplasm, where it undergoes processing with the survival motor neuron (SMN) complex. The SMN complex facilitates the association of UsnRNA with cytoplasmic Sm proteins, forming a UsnRNP particle. Seven known Sm proteins bind to the Sm-binding site of UsnRNA, a process crucial for the stabilization and function of the splicing machinery. Following this interaction, the m^7G cap undergoes hypermethylation, converting it into the trimethylguanosine (m_3G) cap, a hallmark of mature UsnRNPs (Massenet, Pellizzoni, Paushkin, Mattaj, & Dreyfuss, 2002).

At this stage, SPN1 binds specifically to the m_3G cap via its C-terminal m_3G cap-binding site, directing the import complex toward the nucleus through Imp-β1-mediated transport. Once inside the nucleus, the import complex dissociates, releasing UsnRNPs and the SMN complex into Cajal bodies, which are non-membranous nuclear subdomains involved in UsnRNP maturation. Within Cajal bodies, UsnRNPs undergo additional modifications, enabling them to participate in the spliceosome assembly, a process essential for mRNA processing and maturation (Matera & Wang, 2014; Strasser, Dickmanns, Luhrmann, &

Ficner, 2005). Following this process, SPN1 is unloaded from the UsnRNP complex and rapidly binds to Exportin-1 (CRM1), facilitating its recycling to the cytoplasm for another round of nuclear import (Paraskeva et al., 1999).

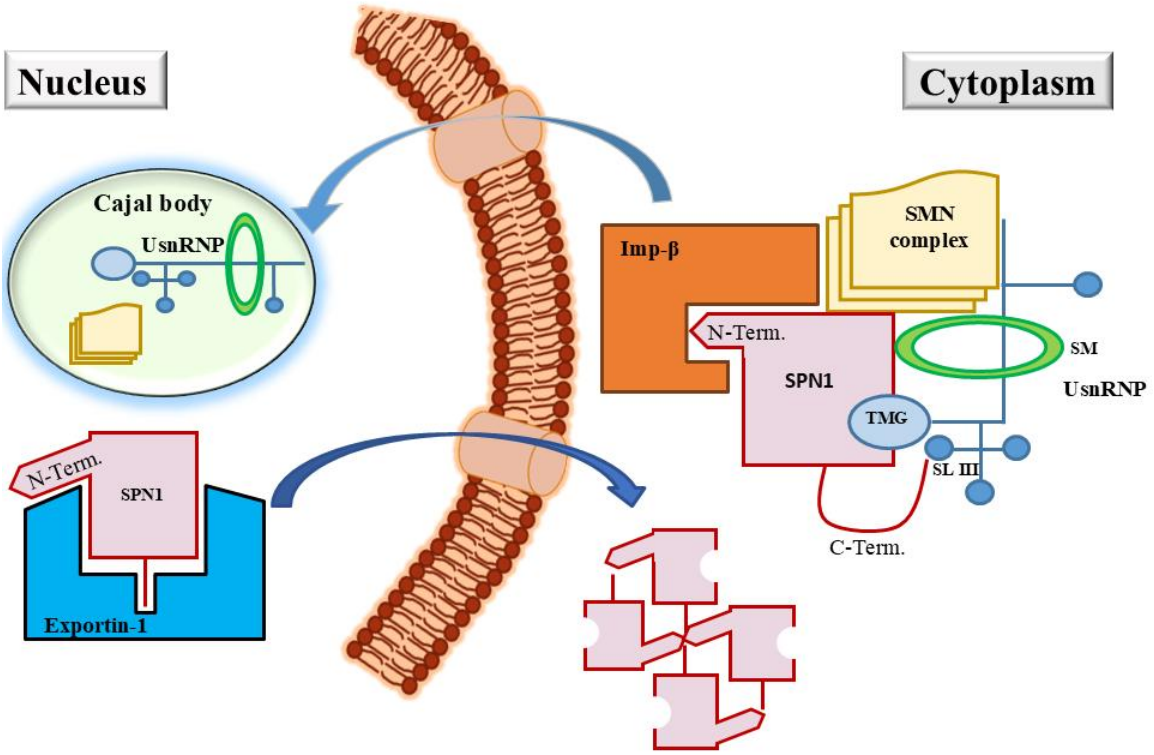

Figure 1.17: Schematic representation of the SPN1 protein cycle**:** The SPN1 cycle begins with the formation of the import complex, where SPN1 binds UsnRNP via the trimethylguanosine (TMG) cap at its C-terminal m_3G cap-binding site, while its N-terminal IBB domain interacts with Importin-β1 (Imp-β1). Additionally, the C-terminal domain of SPN1 directly interacts with stem loop III (SL III) of UsnRNP, a crucial structural region for nuclear transport (Kuhn-Holsken et al., 2010). The Sm proteins, which are integral components of the UsnRNP complex, also establish direct interactions with SPN1 near the TMG-binding site. The Survival Motor Neuron (SMN) complex, essential for the assembly of UsnRNPs, further interacts with SPN1 (Kuhn-Holsken et al., 2010). Once inside the nucleus, the import complex dissociates, directing UsnRNPs and SMN to Cajal bodies for maturation and subsequent integration into the spliceosomal machinery. Meanwhile, SPN1 is exported back to the cytoplasm by CRM1, where it undergoes conformational rearrangement, preventing premature re-association with Imp-β1 until a new UsnRNP complex is available for transport.

1.4 Import complex components

1.4.1 UsnRNPs

Uridine-rich small nuclear ribonucleoproteins (UsnRNPs) are a specialized class of RNA-protein complexes that form the core components of the spliceosomal machinery. They are classified into major spliceosome-associated UsnRNPs (U1, U2, U4/U6, and U5) and minor spliceosome-associated UsnRNPs (U11, U12, U4atac/U6atac, and U5) (Matera & Wang, 2014).

The biogenesis of UsnRNPs begins in the nucleus, where their RNA components (UsnRNAs) are synthesized by RNA polymerase II and RNA polymerase III. Following transcription, UsnRNAs are directed to Cajal bodies, where they undergo initial processing. This includes post-transcriptional modifications such as trimming of the 3′ end and addition of a 7-methylguanosine (m^7G) cap at the 5′ end, which interacts with the Cap Binding Complex (CBC), facilitating nuclear export. Once processed, the UsnRNAs assemble into a nuclear export complex composed of PHAX, CRM1 (XPO1), and RAN-GTP, which mediates their temporary export to the cytoplasm for further maturation (Fischer, Englbrecht, & Chari, 2011).

In the cytoplasm, UsnRNAs undergo a crucial maturation step by associating with Sm proteins, a highly conserved set of seven proteins (B/B′, D1, D2, D3, E, F, and G) that assemble into a ring-like structure around the Sm-binding site of the UsnRNAs. This assembly process is facilitated by the Survival of Motor Neuron (SMN) complex, which plays a pivotal role in ensuring the proper formation and stability of UsnRNPs. The SMN complex acts as a chaperone, mediating the ordered binding of Sm proteins to the UsnRNAs and preventing the formation of nonfunctional intermediates. (Fischer et al., 2011). At this stage, trimethylguanosine synthase 1 (TGS1) catalyzes the hypermethylation of the 7-methylguanosine (m^7G) cap at the 5′ end of UsnRNAs, converting it into a 2,2,7-trimethylguanosine (m_3G) cap. This modification is critical for the recognition and binding of SNURPORTIN-1 (SPN1), which specifically interacts with the m_3G cap to facilitate the nuclear import of mature UsnRNPs (Gruss et al., 2017; Piecyk et al., 2015), in conjunction with SMN, back into the nucleus via Importin β1. Within the nucleus, UsnRNPs are actively transported to Cajal bodies for the final maturation of these UsnRNPs. Once fully

matured, UsnRNPs are stored in nuclear speckles, which function as dynamic reservoirs for splicing factors (Mao, Zhang, & Spector, 2011).

Mutations in components of UsnRNPs, including Sm and Sm-like proteins, as well as other spliceosomal machinery elements, are implicated in various diseases affecting the retina, spinal cord, and skeletal system (Griffin & Saint-Jeannet, 2020). Recently, mutations in the *RNU4-2* gene, which encodes U4 snRNA, have been linked to an autosomal dominant neurodevelopmental disorder known as ReNU syndrome (OMIM 620851), characterized by hypotonia, brain anomalies, and developmental delay (Schot, Ferraro, Geeven, Diderich, & Barakat, 2024). Similarly, mutations in the *RNU7-1* gene, encoding U7 snRNA, are associated with autosomal recessive type I interferonopathy, Aicardi-Goutières syndrome 9 (OMIM 619487). This severe neurodevelopmental condition is characterized by cerebral atrophy with white matter disease, developmental delay, and early mortality due to renal and hepatic failure (Uggenti et al., 2020). *RNU12* gene, which encodes U12 snRNA, a component of the minor spliceosome pathway, have been linked to craniosynostosis, anal anomalies, and porokeratosis in CDAGS syndrome (OMIM 603116). Additionally, mutations in *RNU12* have been associated with autosomal recessive spinocerebellar ataxia type 33 (OMIM 620208), as identified in six patients from one family (Elsaid et al., 2017; Mendoza-Londono et al., 2005).

1.4.2 SMN complex

The *SMN* gene is located on chromosome 5 and consists of nine exons: 1, 2a, 2b, 3, 4, 5, 6, 7, and 8. This gene has two paralogues, the telomeric *SMN1* and the centromeric *SMN2* (Figure 1.18). The primary distinction between these copies lies in a single coding nucleotide variant (c.840C>T) in exon 7 of *SMN2*. This variant causes exon 7 to be skipped in approximately 90% of *SMN2* mRNA translation events, resulting in a truncated and unstable SMN protein that is rapidly degraded. Conversely, all nine exons are fully translated in the *SMN1* transcript, producing a complete and stable SMN protein (Lorson, Hahnen, Androphy, & Wirth, 1999).

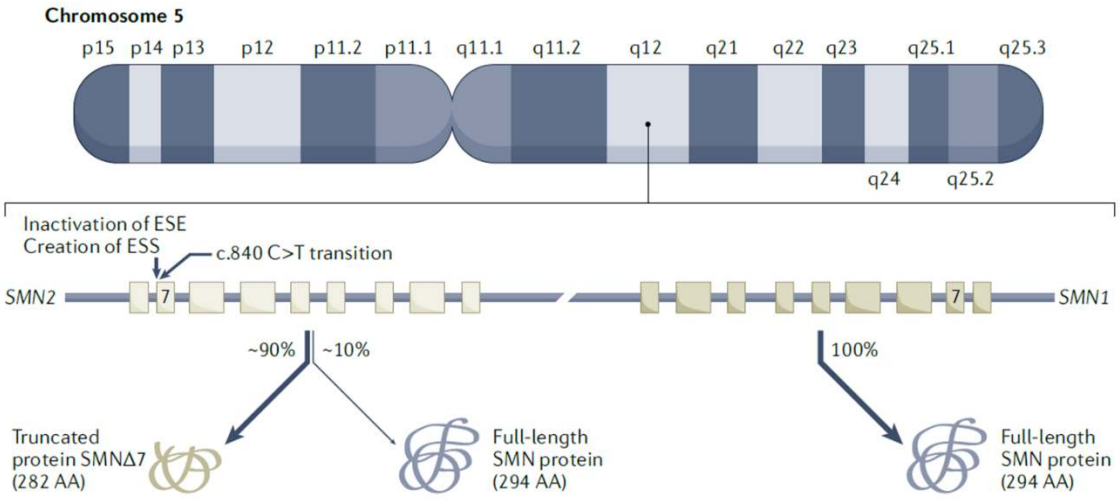

Figure 1.18: The centromeric *SMN2* and telomeric *SMN1* genes are both located on chromosome 5. The *SMN1* gene is fully transcribed and translated into a functional protein. In contrast, *SMN2* contains a single nucleotide variant (c.840C>T), which disrupts an exon splice enhancer (ESE) and generates an exon splice suppressor (ESS). This alteration leads to the predominant skipping of exon 7 during mRNA processing. Consequently, approximately 90% of the SMN2-derived transcripts produce truncated, non-functional proteins, while only 10% result in full-length, functional proteins. (Adapted from (Mercuri, Sumner, Muntoni, Darras, & Finkel, 2022)).

The full-length SMN protein, with a molecular weight of 38 kDa, is expressed ubiquitously and oligomerizes through its C-terminal YG box domain to form self-oligomers. Additionally, SMN interacts with Gemin proteins 2–8 to form a larger functional complex. SMN is essential for several critical cellular functions, including the assembly of spliceosomal components (snRNPs). In this process, it catalyzes the interaction between Sm proteins and the Sm binding site of UsnRNA (Battle et al., 2006). The SMN-UsnRNP complex subsequently interacts with SPN1 to facilitate its nuclear import via importin β1. Once inside the nucleus, SMN, along with UsnRNPs, is directed to Cajal bodies for further maturation (R. N. Singh, Howell, Ottesen, & Singh, 2017).

Mutations in the *SMN1* gene cause autosomal recessive spinal muscular atrophy (SMA), a pediatric neuromuscular disorder with a spectrum of severity ranging from the fatal and severe type I to the milder type IV. The severity of SMA correlates with the number of

functional *SMN2* copies and the amount of protein they express. The disease is characterized by the loss of motor neurons, leading to muscular atrophy (Mercuri et al., 2022; Prior, Leach, & Finanger, 1993). Furthermore, the loss of function in other components of the SMN complex can also result in neurological deficits. For instance, mutations in *GEMIN4* cause an autosomal recessive neurodevelopmental disorder characterized by microcephaly, cataracts, and renal abnormalities (OMIM 617913) (Alazami et al., 2015). Similarly, mutations in *GEMIN5* are associated with a neurodevelopmental disorder featuring cerebellar atrophy and motor dysfunction (OMIM 619333) (Kour et al., 2021).

1.4.3 Importin β1

The *KPNB1* gene is located on chromosome 17q21.32 and encodes Karyopherin Subunit Beta 1, also known as importin β1. Importin β1 functions as a nuclear importer in association with import adaptors such as importin α or SPN1, both of which include an Importin β Binding (IBB) domain (Lott & Cingolani, 2011). The IBB domain of SPN1 is located at the N-terminus and undergoes a conformational change, enabling interaction with importin β1 only when the UsnRNP-SMN import (mature) complex is attached to SPN1. Notably, this import process is RAN-independent (Bhardwaj & Cingolani, 2010; Huber, Dickmanns, & Luhrmann, 2002). Beyond its role in nuclear import, importin β1 has a wide range of additional functions, including the regulation of the cell cycle and the import of various inner nuclear membrane proteins (Wing et al., 2022).

1.4.4 Exportin-1 (XPO1, CRM1)

The *XPO1* gene, located on chromosome 2p15, encodes the Exportin 1 protein, which plays a crucial role in the nuclear export of proteins containing a nuclear export signal (NES) to the cytoplasm. In addition to protein transport, Exportin 1 facilitates the export of various RNAs, including UsnRNA, from the nucleus to the cytoplasm (Fornerod, Ohno, Yoshida, & Mattaj, 1997). This export process is dependent on RAN-GTP, which forms a complex with CRM1 (Exportin 1) and its cargo. Upon reaching the cytoplasm, RAN-GTP undergoes hydrolysis to RAN-GDP, resulting in the dissociation of the cargo from the export complex. Exportin 1 then recycles back to the nucleus to initiate a new export cycle.

Beyond its role in RNA transport, Exportin 1 is also responsible for the nuclear export of unloaded SPN1. Within the nucleus, SPN1 interacts with Exportin 1 with high affinity via its N-terminal and C-terminal regions, ensuring efficient export to the cytoplasm (Monecke et al., 2009; Paraskeva et al., 1999). Mutations in XPO1 have been implicated in various malignancies, including primary mediastinal B-cell lymphoma (Jardin et al., 2016), highlighting its critical role in cellular homeostasis and disease pathogenesis.

1.5 Implications for neuromuscular disorders

Emerging evidence suggests that disruptions in RNA splicing and nucleocytoplasmic transport may contribute significantly to the pathogenesis of neuromuscular disorders. Until 2024, SPN1 had not been linked to any clinical phenotype, and no *in vivo* knockout models had been developed to investigate its function. However, given its critical role in facilitating the nuclear import of UsnRNPs and regulating RNA splicing, recent studies have identified SPN1 as a causative factor in MD with extramuscular manifestations, leading to its classification as Limb-Girdle Muscular Dystrophy Type 29 (LGMD R29) and spinocerebellar atrophy (Iruzubieta et al., 2024; Nashabat et al., 2024; Okubo et al., 2024).

Chapter 2: **MATERIALS AND METHODS**

2.1 Ethical considerations

This study was conducted in full compliance with ethical standards governing human research. Written informed consent was obtained from all participants and/or their legal guardians, authorizing the collection and use of clinical and genetic information, as well as biological samples. The participants and their families were provided with detailed information about the study objectives, procedures, and potential implications. They also reviewed the materials intended for publication, including clinical data and images, and provided their explicit consent for publication.

The ethical framework for this research was established following the ethical review approvals from multiple institutions across different countries, including Turkey, Italy, Switzerland, Iraq, Iran, Macedonia, Colombia, Romania, and Guatemala. Additionally, the study protocol was reviewed and approved by the Koç University Hospital Institutional Review Board (Approval No. 2015.120.IRB2.047). All procedures involving human-derived samples strictly adhered to the principles outlined in the World Medical Association's Declaration of Helsinki and the Belmont Report issued by the U.S. Department of Health and Human Services.

2.2 Patient recruitment and clinical assessment

The recruitment process for this study involved the identification of 21 individuals diagnosed with muscular dystrophy from 18 independent families across various countries. The index case originated from a non-consanguineous Kosovar family (F1) and was diagnosed at Koç University Hospital (Türkiye). Subsequently, 20 additional cases from 17 different families were identified through international clinical collaborations. These included patients diagnosed and evaluated at multiple institutions:

- Italy: Clinical assessments for F2-II:1 were conducted at Unit of Clinical Pediatrics, State Hospital, San Marino Republic, with further consultations at Bambino Gesù

Children's Hospital, IRCCS, and IRCCS Institute of Neurological Sciences of Bologna.

- United States: F3-II:4 was examined at the Division of Neurology, Nationwide Children's Hospital, with additional evaluations performed at the National Institute of Neurological Disorders and Stroke, NIH.
- Switzerland: F4-II:2 was assessed at the Institute of Medical Genetics, University of Zurich, University Children's Hospital Zurich, Division of Sleep Medicine, and the Neuromuscular Center, Department of Pediatric Neurology, University Children's Hospital Zurich.
- Germany: F5-II:4 underwent diagnosis and evaluation at Children's and Youth Hospital Auf der Bult, Hannover Medical School, and Institute of Diagnostic and Interventional Neuroradiology, Hannover Medical School.
- Iran: Patients F6-II:3, F7-II:1, F16-II:1, and F17-II:1 were examined at the Genetics Research Center, USWR, and Kariminejad-Najmabadi Pathology & Genetics Center.
- Colombia: F13-II:1 and F14-II:1 were reported by Corporación Nuevos Rumbos and Hospital Pablo Tobon Uribe, respectively.
- Romania: F9-II:1 was evaluated at Dr. Victor Gomoiu Children's Hospital and University of Medicine and Pharmacy of Craiova.
- United States: F10-II:1 was diagnosed at the Dr. John T. Macdonald Foundation Department of Human Genetics, University of Miami.
- Germany: Patients F11-II:1, F12-II:2, and F15-II:1 were evaluated at Ludwig-Maximilians-University, Technical University Munich School of Medicine, University Medical Center Hamburg-Eppendorf, and Genetikum.
- Türkiye: Patient F18-II:1 was evaluated at Hacettepe University, Ankara.

Each patient's clinical phenotype, disease progression, and genetic profile were meticulously documented for subsequent molecular analyses.

2.3 In silico pathogenicity prediction tools

Variants were assessed using computational prediction tools such as PolyPhen-2, SIFT, MutationTaster, CADD, DANN, FATHMM-MKL, and Mutation Assessor. Conservation was checked by Phylop. Splice site mutations were assessed using Splice AI tool.

2.4 Sanger sequencing

Candidate *SNUPN* variants were subsequently validated by segregation analysis using targeted Sanger sequencing with the BigDye Terminator Cycle Sequencing Kit (Applied Biosystems, Catalog #4337455).

2.5 Cell culture and fibroblast derivation

Primary dermal fibroblasts were established from skin biopsies obtained from five affected individuals (F1-II:1, F3-II:4, F4-II:2, F4-II:3, and F10-II:1) and three unrelated healthy individuals (WT controls). Fibroblast cultures were maintained in high-glucose DMEM (Sigma, Catalog #D6429) supplemented with:

- 10% fetal bovine serum (FBS) (Biowest, Catalog #S1600-500)
- 1% Penicillin/Streptomycin (Biowest, Catalog #L0022-100)

Cells were grown under 5% CO_2 at 37°C in a humidified incubator. Additional cell lines, including HeLa (ECACC #93021013) and HEK293T (ATCC #CRL-3216), were cultured under identical conditions. All cell lines were regularly tested for Mycoplasma contamination using the MycoAlert Mycoplasma Detection Kit (Lonza, Catalog #LT07-118).

2.6 CRISPR/Cas9 gene editing of *SNUPN*

The CRISPR/Cas9 system was employed to generate *SNUPN* mutant cell lines. Two distinct single-guide RNAs (sgRNA#1 and sgRNA#2) were designed to target exon 2 and exon 9 of *SNUPN*. The lentiCRISPRv2 plasmid system was used for gene editing, and lentiviral particles were produced in HEK293T cells. Successfully transduced HeLa cells underwent selection with 0.5 µg/mL puromycin, and individual clones were isolated by serial dilution. Genomic sequencing identified two mutant clones:

- $SPN1^{sgEx2}$: Containing mutations in exon 2.
- $SPN1^{sgEx9}$: Harboring mutations in exon 9.

These cell lines were used for subsequent functional assays.

2.7 Western blotting

Western blot analysis was performed using protein extracts separated on 4–20% gradient gels (Criterion™ TGX™ Precast Midi Protein Gels, Bio-Rad, catalog #5671093). Proteins were transferred onto activated PVDF membranes (Bio-Rad, catalog #1620261) using the semi-dry transfer technique via a Trans-Blot® Turbo™ Transfer System (Bio-Rad, catalog #1704150). The membranes were blocked with 5% skim milk or BSA for 1 hour, followed by incubation with primary antibodies overnight at 4°C. After incubation, the membranes were washed three times and incubated with horseradish peroxidase (HRP)-conjugated secondary antibodies for 1 hour at room temperature. The membranes underwent additional washing steps and were developed using enhanced chemiluminescence (ECL) reagent (Bio-Rad). Protein bands were visualized and documented using the ChemiDoc MP Imaging System (Bio-Rad, catalog #17001395).

2.8 Antibodies and reagents

A comprehensive set of primary and secondary antibodies was used for Western blotting, immunofluorescence, and immunohistochemistry. The details of the antibodies, including their catalog numbers, clone names, dilutions, and manufacturers, are provided below:

2.8.1 Primary antibodies

- SPN1 (SNUPN) Polyclonal Antibody (Proteintech, #15358-1)
  - WB: 1:1000 | IF (Cells): 1:50 | IF (Muscle Sections): 1:100
- SNRPB Monoclonal Antibody (Y12 Clone) (Invitrogen, #MA5-13449)
  - WB: 1:100 | IF: 1:50
- COILIN Monoclonal Antibody (IH10 Clone) (Abcam, #ab87913)
  - WB: 1:500 | IF: 1:100
- SMN Polyclonal Antibody (Proteintech, #11708-1-AP)
  - IF: 1:25
- α-SARCOGLYCAN Monoclonal Antibody (AD1/20A6 Clone) (Leica, #NCL-L-a-SARC)
  - IF: 1:50
- β-DYSTROGLYCAN Monoclonal Antibody (43DAG1/8D5 Clone) (Leica, #NCL-b-DG)

  - WB: 1:1000
- β-TUBULIN Monoclonal Antibody (TUB2.1 Clone) (Sigma, #T5201)
  - IF: 1:100
- GAPDH Monoclonal Antibody (0411 Clone) (Santa Cruz, #47724)
  - WB: 1:500
- FLAG Polyclonal Antibody (Cell Signaling, #2368)
  - WB: 1:1000
- DESMIN Monoclonal Antibody (DE-B-5 Clone) (Millipore, #Mab3430)
  - IHC/IF: 2.5 µg/mL
- ACTIN Monoclonal Antibody (HHF35 Clone) (Dako, #M0635)
  - IF: 1:50
- LC3B Polyclonal Antibody (cell signaling, 2775S)
  - WB: 1:1000
- P62 Polyclonal Antibody (Novus Biologicals NBP1-48320)
  - WBL 1:1000
- P53 Monoclonal Antibody (SantaCruz sc-126)
  - WB: 1:500
- Anti Myc Monoclonal Antibody (Sigma 05-724)
  - WB: 1:1000

2.8.2 Secondary antibodies

- Alexa Fluor 488-conjugated Anti-Rabbit IgG (Invitrogen, #A32766, 1:500)
- Alexa Fluor 594-conjugated Anti-Mouse IgG (Invitrogen, #A32754, 1:500)
- HRP-conjugated Anti-Mouse IgG (Abbkine, #A21010, 1:5000)
- HRP-conjugated Anti-Rabbit IgG (Abbkine, #A21020, 1:5000)

All antibodies were used following the manufacturer's guidelines and optimized for each experimental condition.

2.9 Construct generation and transient transfection

To study the functional consequences of *SNUPN* mutations, wild-type and mutant constructs were generated. Epitope-tagged constructs, FLAG and Myc sequences were inserted at either the N-terminal (after the start codon) or C-terminal (before the stop

codon). Site-directed mutagenesis was performed using the QuickChange II XL Site-Directed Mutagenesis Kit (Agilent, #2005c22) to generate mutant *SNUPN* constructs (*m1*, *m6*, *m7*, *m9*, *m11*, and *m12*). Sequences of all primers used for cloning and mutagenesis are detailed in Supplementary Table 1.

Plasmid transfections were performed using Lipofectamine 2000 (Invitrogen, #11668019) in Opti-MEM Reduced Serum Medium (Gibco, #31985062) according to the manufacturer's protocol.

2.10 Immunofluorescence staining

For fibroblast immunofluorescence, cells were grown on Millicell EZ 8-well chamber slides (Millipore, #PEZGS0896) and processed as follows:

1. Cells were washed with PBS and fixed with 4% paraformaldehyde for 20 minutes at room temperature.
2. Permeabilization was carried out using 0.5% Triton X-100/PBS for 30 minutes.
3. Blocking was performed in 1% BSA/PBS for 1 hour.
4. Cells were incubated overnight at 4°C with primary antibodies in 1% BSA/PBS.
5. The following day, cells were washed and incubated with Alexa Fluor-conjugated secondary antibodies (1:500, Invitrogen) for 2 hours in the dark.
6. Nuclei were counterstained with DAPI (10 µg/mL) for 15 minutes.
7. Slides were mounted using ProLong™ Diamond Antifade Mounting (Invitrogen, #P36965).

For muscle tissue immunostaining, cryosections were air-dried, fixed, blocked, and incubated with primary and secondary antibodies following a similar protocol. All fluorescence images were captured using Leica MD4 B Upright Fluorescent and Leica DMi8 SP8 Inverted Confocal Microscopes.

2.11 Immunohistochemistry (IHC) staining

Human muscle cryosections were subjected to hematoxylin-eosin staining and IHC. For IHC:

1. Sections were incubated overnight with primary antibodies.

2. Biotinylated polyclonal secondary antibodies (Dako) were applied for 1 hour.
3. Sections were treated with a streptavidin-biotin-peroxidase complex (Dako) and developed with DAB substrate.
4. Sections were counterstained with hematoxylin.

2.12 RNA extraction and quantitative PCR (RT-qPCR)

Total RNA was extracted from fibroblasts using the NucleoSpin RNA Kit (Macherey-Nagel, #740955.50), including an rDNase treatment step.

- 1 µg of RNA was reverse transcribed using the iScript™ cDNA Synthesis Kit (Bio-Rad, #1708890).
- Quantitative PCR was performed using the FastStart™ Universal SYBR® Green Master (Roche, #4913914001) on a PikoReal 96 Real-Time PCR System (Thermo Fisher, #TCR0096).
- GAPDH was used as the internal reference gene for normalization.

2.13 Primers for all genes analyzed

Table 2: List of primers

Gene	Primer Category	Primer Name	Primer Sequence (5′–3′)
SNUPN	Genotyping Primers	SNUPN-m1-F	CACCAGCTCCAGCAGAGTATGGAGCACAAGAAG
SNUPN	Genotyping Primers	SNUPN-m1 (926 T>G) R	CTTCTTGTGCTCCATACTCTGCTGGAGCTGGTG
SNUPN	Genotyping Primers	SNUPN- /m3-F	AGCTGCCCTTGTGTGTATAG
SNUPN	Genotyping Primers	SNUPN-m2/m3-R	TCCTTAAGGAGGCTTCTCTC
SNUPN	Genotyping Primers	SNUPN-m9-F	CTCTCCATCCCTGTCCAGTC
SNUPN	Genotyping Primers	SNUPN-m9-R	ACTGCAGAAATCCAAGCAGCTGGATTATGTGAACC
SNUPN	Cloning Primers	SNUPN-ORF-F	ATCGGATCCGGGAAGATGGAAGAGTTGAGTCAGGCCCT
SNUPN	Cloning Primers	SNUPN-ORF-R	TAGCTCGAGTTAATTCTCCATGAGGCATCCAGG
SNUPN	Cloning Primers	SNUPN-ORF-N-FLAG-F	ATCGGATCCGGGAAGATGGACTACAAGGACGACGATGACAAG

SNUPN	Cloning Primers	SNUPN-ORF-N-MYC-F	ATCGGATCCGGGAAGATGGAGCAAAAG CTCATTTCTGAAGAGGACTTGG
SNUPN	Site-Directed Mutagenesis Primers	SNUPN-m1 (926 T>G) F	CACCAGCTCCAGCAGAGTATGGAGCAC AAGAAG
SNUPN	Site-Directed Mutagenesis Primers	SNUPN-m1 (926 T>G) R	CTTCTTGTGCTCCATACTCTGCTGGAGC TGGTG
SNUPN	Site-Directed Mutagenesis Primers	SNUPN-m6 (902-903DEL) F	GACCACCAAGCCAGTATGCTGGGCACC A
SNUPN	Site-Directed Mutagenesis Primers	SNUPN-m6 (902-903DEL) R	TGGTGCCCAGCATACTGGCTTGGTGGTC
SNUPN	Site-Directed Mutagenesis Primers	SNUPN-m7 (899-900DEL) F	GACCACCAAGCCAGTATGCTGGGCACC A
SNUPN	Site-Directed Mutagenesis Primers	SNUPN-m7 (899-900DEL) R	TGGTGCCCAGCATACTGGCTTGGTGGTC
SNUPN	Site-Directed Mutagenesis Primers	SNUPN-m9 (164G>A) F	GGCCTGCTCCATTTCTGCTGGATTATGT GAACC
SNUPN	Site-Directed Mutagenesis Primers	SNUPN-m9 (164G>A) R	GGTTCACATAATCCAGCAGAAATGGAG CAGGCC
SNUPN	Site-Directed Mutagenesis Primers	SNUPN m11 (c.476G>A) F	CACTTCTGCCAGGAGACAACAGGCGAA ACTC
SNUPN	Site-Directed Mutagenesis Primers	SNUPN m11 (c.476G>A) R	GAGTTTCGCCTGTTGTCTCCTGGCAGAA GTG
SNUPN	Site-Directed Mutagenesis Primers	SNUPN m12 (c.435_436delins AA) F	CAGTGCCTACACCAAGAGAAGCTACTG TGTCAACAGGT
SNUPN	Site-Directed Mutagenesis Primers	SNUPN m12 (c.435_436delins AA) R	ACCTGTTGACACAGTAGCTTCTCTTGGT GTAGGCACTG
SNUPN	RT-qPCR Primers	SNUPN-qPCR-F1	TTCCTTGGAGCAGAGTGAGC

SNUPN	RT-qPCR Primers	SNUPN-qPCR-R1	AGTCTAGGTCAATTAACCACTCAG
SMN	RT-qPCR Primers	SMN-qPCR-F	CCTGTGTTGTGGTTTACACTGG
SMN	RT-qPCR Primers	SMN-qPCR-R	GGGGGAATTATCTTTCCTGGTCC
TMEM41B	RT-qPCR Primers	TMEM41B-qPCR-F	AATCCTGGGTAGAAGCTGGA
TMEM41B	RT-qPCR Primers	TMEM41B-qPCR-F	AGAAAGAGGCACCAAGTCCA
LAMA5	RT-qPCR Primers	LAMA5-qPCR-F	CCCACCGAGGACCTTTACTG
LAMA5	RT-qPCR Primers	LAMA5-qPCR-R	GGTGTGCCTTGTTGCTGTT
SGCA	RT-qPCR Primers	SGCA-qPCR-F	AGACCACGCTACACCCACTT
SGCA	RT-qPCR Primers	SGCA-qPCR-R	GGTCCATGATGTCGTCAGCC
ITGB2	RT-qPCR Primers	ITGB2-qPCR-F	TGCGTCCTCTCTCAGGAGTG
ITGB2	RT-qPCR Primers	ITGB2-qPCR-R	GGTCCATGATGTCGTCAGCC
SFRP2	RT-qPCR Primers	SFRP2-qPCR-F	ACGGCATCGAATACCAGAACA
SFRP2	RT-qPCR Primers	SFRP2-qPCR-R	CTCGTCTAGGTCATCGAGGCA
SNUPN	CRISPR-Cas9	sgEx2	ACTTGGACTTGTACTGGGAT
SNUPN	CRISPR-Cas9	sgEx9	CCACCAAGGGAGTGCTTCCG

2.14 RNA sequencing and bioinformatics analysis

To evaluate differential gene expression and splicing events, RNA sequencing (RNA-seq) was performed using fibroblast RNA samples. The sequencing was carried out at Phi-Bioinformatics (Istanbul, Turkey).

2.15 RNA sequencing data processing

1. Alignment:
    - Raw FASTQ files were aligned to the human genome (GRCh37/hg19) using the STAR aligner under paired-end mode with default parameters.
2. Differential Gene Expression Analysis:
    - BAM files were processed with DESeq2, which was used to calculate gene expression levels and identify differentially expressed genes.
3. Alternative Splicing Analysis:
    - Splicing alterations were analyzed using rMATS 4.1.2 turbo software, which detected differentially spliced transcripts in the patient-derived fibroblasts.
4. Data Visualization:
    - Gene expression and splicing data were visualized using IDEP.951, an interactive web-based analysis tool.
    - Sashimi plots were generated using the rMATS2Sashimi plot package to depict exon skipping events.

2.16 Protein structure modeling and computational analysis

The impact of *SNUPN* mutations on protein structure was investigated using in silico modeling approaches.

2.16.1 Homology modeling and structure prediction

1. I-TASSER (Iterative Threading ASSEmbly Refinement) was used to generate 3D models of the wild-type and mutant SPN1 proteins.
2. Protein structures were analyzed for changes in secondary structure, active sites, and binding domains, with a focus on the m_3G cap-binding site, N-terminal, and C-terminal regions.
3. Structural Validation: Models were aligned with two crystallographic structures (PDB: 1XK5, PDB: 3GJX) to ensure structural accuracy.
4. Visualization: 3D protein structures were examined using PyMOL software (v2.4.1, Schrödinger LLC).

2.16.2 Multimerization analysis

To evaluate potential structural disruptions due to C-terminal SPN1 mutations, the AlphaFold 2 Colab notebook was utilized for dimer and multimer formation prediction.

- The highest-confidence structural models were selected based on lowest predicted aligned error (PAE) scores.
- Coiled-coil interactions within the SPN1 protein were assessed using Socket2 software, with a packing cutoff of 7 Å to determine potential multimerization effects.

2.17 Subcellular fractionation of fibroblasts and HeLa cells

To examine the localization of SPN1 in patient-derived fibroblasts and HeLa cells, nuclear and cytoplasmic fractionation was performed using the Cell Fractionation Kit-Standard (Abcam, #ab109719).

1. Cell pellets were lysed under gentle conditions to preserve nuclear integrity.
2. Cytoplasmic and nuclear fractions were separated by centrifugation and processed for Western blot analysis.
3. Purity assessment: The nuclear fraction was validated using H2A as a marker, while GAPDH was used to confirm cytoplasmic enrichment.

2.18 Immunoprecipitation assay

To investigate protein-protein interactions, co-immunoprecipitation (Co-IP) was performed using Anti-FLAG M2 agarose beads (Sigma-Aldrich, #A2220).

1. Cell lysates were pre-cleared and incubated overnight with FLAG-tagged SPN1 constructs.
2. Beads were washed six times with RIPA buffer and eluted in Laemmli buffer with 60 mM DTT at 95°C for 10 min.
3. Western blot analysis was performed to detect co-precipitated proteins using appropriate antibodies.

For visualization, HRP-conjugated light-chain-specific secondary antibodies (Abbkine, #A25012, #A25022) were used to avoid interference from heavy and light chains of IgG.

2.19 Web-based resources used for data analysis

A range of publicly available bioinformatics databases and software tools were used for variant annotation, gene function analysis, and structural modeling:

- Genome Aggregation Database (gnomAD) – https://gnomad.broadinstitute.org/
- Exome Sequencing Project (ESP) – http://evs.gs.washington.edu/EVS/
- ClinVar Database – ftp://ftp.ncbi.nlm.nih.gov/pub/clinvar/vcf_GRCh37/
- PolyPhen-2 for Variant Pathogenicity Prediction – http://genetics.bwh.harvard.edu/pph2/
- MutationTaster for Functional Impact Prediction – http://www.mutationtaster.org/
- I-TASSER for Protein Structure Prediction – https://zhanggroup.org/I-TASSER/
- AlphaFold 2 for Protein Structure Modeling – https://deepmind.com/research/highlighted-research/alphafold
- PyMOL for Structural Visualization – https://pymol.org/

2.20 Data analysis and statistical methods

Statistical analyses were conducted using GraphPad Prism 9 (GraphPad Software, Inc.) and Microsoft Excel. The following statistical tests were used:

- Comparisons between two groups: Unpaired Student's t-test
- Comparisons between multiple groups: One-way or two-way ANOVA with post hoc Tukey's test
- Correlation analyses: Pearson's correlation coefficient
- Significance threshold: p-value < 0.05

All experiments were performed in at least three independent biological replicates, and data are presented as mean ± SEM.

Chapter 3:**RESULTS**

3.1 Clinical and molecular characterization of a novel muscular dystrophy

3.1.1 Clinical, and histopathological investigation of patients' phenotype

The index patient (II.1), born into a non-consanguineous Kosovar family (F1), exhibited normal development until early childhood. At the age of 5 years, she began experiencing frequent falls and developed an abnormal gait. Over time, her symptoms progressively worsened, showing decreased muscle power in both upper and lower limbs, more pronounced on the left side. The patient presented with a waddling gait, mild anterior pelvic tilt, long face, and mild hypertelorism. Other systemic examinations were normal except for reduced pain sensitivity. Radiological investigations showed stable thoracic scoliosis. Biochemical investigations revealed elevated creatine kinase (CK) levels on two occasions (3133 U/L and 2577 U/L). Electromyography (EMG) indicated a myopathic pattern. Collectively, these clinical observations were consistent with a muscular dystrophy diagnosis.

Despite exhaustive molecular screening, including clinical exome sequencing of 4811 OMIM genes, Multiplex Ligation-dependent Probe Amplification (MLPA) of the 79 exons of the dystrophin (DMD) gene, array comparative genomic hybridization (CGH), and *SMN1/2* genes sequencing, no pathogenic variant was identified. Consequently, whole exome sequencing (WES) was performed, uncovering a novel germline homozygous pathogenic mutation in *SNUPN* (Chr15: c.926T>G, p.Ile309Ser), not reported in the ExAC, UK10K, or gnomAD databases. Sanger sequencing of the unaffected parents (I.1 and I.2) and a brother (II.2) confirmed that this private mutation segregated in the family, suggesting an autosomal recessive mode of inheritance. The p.Ile309Ser mutation was predicted to be deleterious by all pathogenicity classifiers tested (MCAP=0.121, PROVEAN, SIFT, and MutationTaster), and Ile309 is highly conserved across vertebrate SPN1 orthologues.

Subsequently, 20 additional patients from 17 unrelated families were identified with *SNUPN* mutations, sharing a similar clinical phenotype. This cohort comprised 21 patients from 18 unrelated families, including eleven females and nine males, from Kosovo, Italy, USA, Switzerland, Iraq, Iran, Macedonia, Romania, Guatemala, Colombia, Germany, and Türkiye. Consanguinity was noted in five families (second or third degree) (Figure 3.1). The age of onset varied, ranging from birth to ten years, with about 79% of patients developing symptoms before the age of ambulation (two years). Muscle weakness was progressive in all patients, with varying degrees of severity (Figure 3.2(a)). The disease was severe in almost half of the patients, particularly in two patients (F3-II:4 and F7-II:1), who died from respiratory failure at ages 10 and 15 years, respectively.

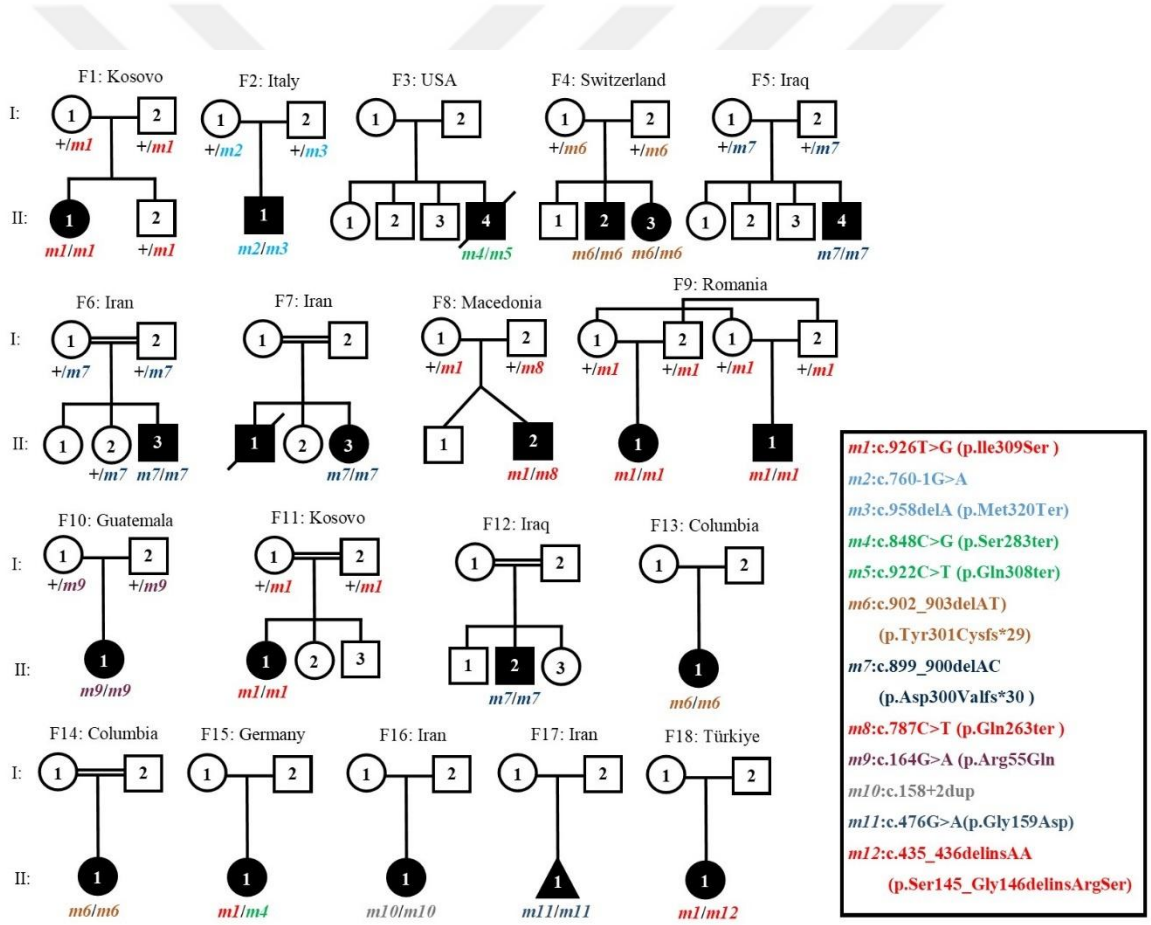

Figure 3.1: Family pedigrees and *SNUPN* mutations of the current cohort

The disease affected both proximal and distal limbs, with less involvement of axial muscles. Elevated creatine kinase (CK) levels were observed in the majority of patients, ranging from 1000 to 7000 U/L. Electromyography (EMG) conducted in 11 patients

showed a myopathic pattern. Some patients exhibited extra-muscular manifestations, including neurological, skeletal, and ocular symptoms. Brain magnetic resonance imaging (MRI) showed cerebellar atrophy in five of nine patients (F2, F3, F5, F12, and F14). Additionally, three patients had a thin corpus callosum (Figure 3.2(b)). Muscle biopsies from eleven patients revealed a dystrophic appearance with abnormal fiber size and endomysial fibrosis (Figure 3.2(c)). Skeletal symptoms included spinal abnormalities such as scoliosis and rigid spine in 76% of patients, and severe contractures were observed in 78%. Ocular symptoms, specifically congenital cataracts, were noted in six patients (F2, F3, F4-II:2, F5, F7-II:1, and F11). Notably, no cardiac problems were reported, but 63% of patients experienced respiratory insufficiency of varying severity.

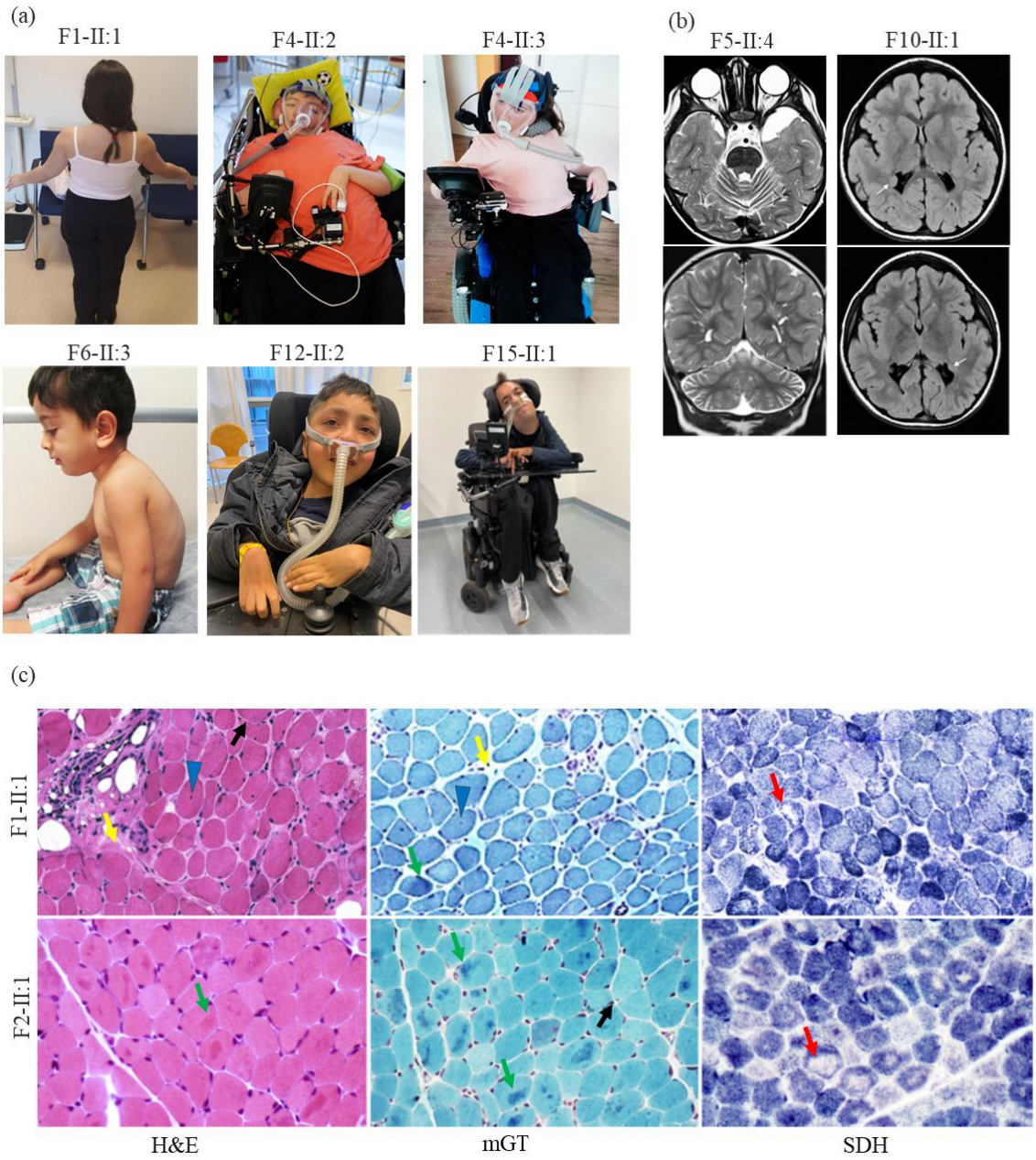

Figure 3.2: Clinical, radiological, and histopathological features of the patients: (a) Photos of six patients with variable degrees of severity, with some of the patients are still ambulant (F1), while others are wheel chair bound and on continuous respiratory support (F4, F12 and F15). (b) Brain MRI for patient F5-II:4 and patient F10-II:1 showing cerebellar atrophy and thinning of the corpus callosum (white arrow), respectively. (c) Cross-sectional muscle staining for patients F1-II:1 and F2-II:1, including H&E staining, mGT stain, and SDH stain. H&E and mGT stains show variability in the sizes of muscle fibers, with atrophic and hypertrophic fibers, with splitting fibers (black arrow), central nuclei (blue arrowhead), endomysial fibrosis (Yellow arrow), and heterogenous uptake of the

stain (green arrow). The SDH stain, a functional stain, shows variable uptake within the muscle fibers, indicating functional defects (red arrow). MRI, magnetic resonance imaging; H&E, Hematoxylin Eosin stain; mGT, modified Gomori Trichrome stain; SDH, succinate dehydrogenase stain.

3.1.2 Molecular diagnosis

The molecular diagnostic approach (Figure 3.3) in our study commenced with thorough clinical evaluation, including detailed medical history, clinical examinations, biochemical assessments (e.g., creatine kinase levels), and histopathological analysis of muscle biopsies when indicated. Initial genetic investigations for genes known to be associated with muscular dystrophy and myopathy phenotypes yielded unremarkable results. Consequently, whole exome sequencing (WES) was performed, leading to the discovery of novel variants in the *SNUPN* gene, which at the time had not been associated with any known clinical phenotype. To validate the findings obtained from WES, Sanger sequencing was subsequently performed on affected individuals as a confirmatory diagnostic measure.

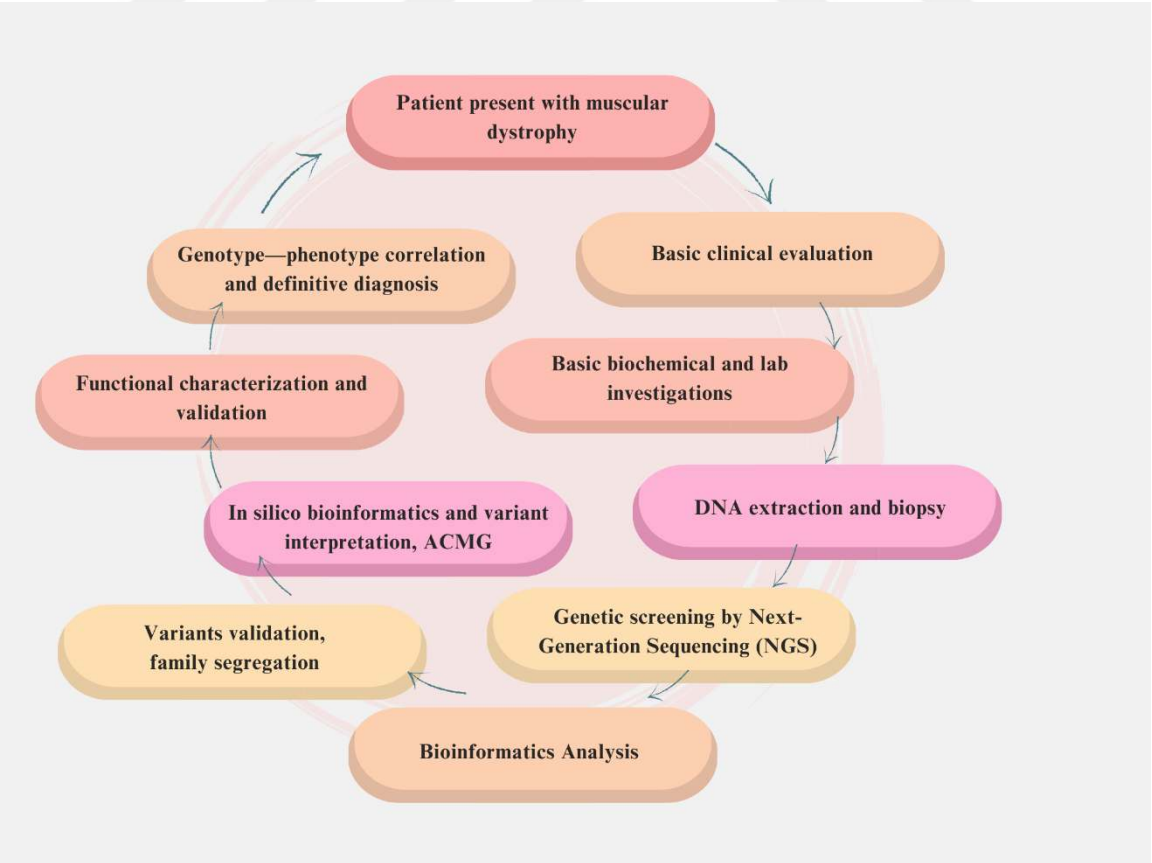

Figure 3.3 Molecular diagnosis workflow for the patients in the current cohort.

The identified variants were further assessed for pathogenicity using the guidelines established by the American College of Medical Genetics and Genomics (ACMG). According to the ACMG, variant classification involves analysis of population frequency data, computational predictions of pathogenic impact, functional evidence, and segregation analysis within the families (Richards et al., 2015). All identified *SNUPN* variants demonstrated disease-causing or likely damaging characteristics according to computational predictions (Table 3). Furthermore, segregation analyses confirmed that these variants co-segregated appropriately within families where parents were heterozygous carriers, while unaffected siblings were either wild-type or heterozygous carriers. Additionally, further functional characterization, were conducted to elucidate the pathogenic mechanisms underlying the identified *SNUPN* variants. Integrating these genetic, clinical, and functional analyses enabled us to establish robust genotype-phenotype correlations and provided comprehensive molecular diagnostic outcomes.

Notably, certain variants demonstrated a possible founder effect. Variant *m1*, for instance, was detected in multiple unrelated families (F1, F8, F9, F11, F15, and F18) originating from geographically adjacent regions, including Kosovo, Romania, Macedonia, and Türkiye. A similar observation was made for variant *m7*, identified in families F5, F6, F7, and F7, originating from geographically close regions. These findings indicate the potential presence of regional founder haplotypes. Table 3 summarizes the identified *SNUPN* variants, their pathogenic classifications, segregation data, and the predictions from various *in-silico* tools.

Table 3: Analysis of the discovered mutations according to ACMG criteria

Mutation No.	**Mutation at gene and protein**	**Population data gnomAD**	**Computational and predictive data**	**Segregation data**	**Conservation**
m1	c.926T>G (p.lle309Ser)	Allele Frequency: 0.000004957 Homozygous : 0	CADD: 29.1 (Pathogenic) PolyPhen (max): 0.964 (Pathogenic)	Segregates within family	phyloP: 6.33 (Conserved)

			FATHMM-MKL: 0.9908 (Pathogenic) MutationTaster : disease causing		
m2	c.760-1G>A (p.Splice)	Allele Frequency: 0.000009437 Homozygous : 0	CADD: 34.0 SpliceAI: 0.990 Pangolin: -0.850 FATHMM-MKL: 0.9835 (Pathogenic)	Segregates within family	PhyloP100: 7.376 (Conserved)
m3	c.958delA (p.Met320Ter)	Not found	MutationTaster : disease causing	Segregates within family	PhyloP 1.675 conserved
m4	c.848C>G (p.Ser283ter)	Allele Frequency: 0.0001617 Homozygous : 0	(Pathogenic) CADD: 42.0 DANN: 0.9959 FATHMM-MKL: 0.9931 MutationTaster : disease causing	Segregates within family	phyloP: 8.79 phyloP100: 9.361
m5	c.922C>T p.Gln308ter	Allele Frequency: 0.000009912 Homozygous : 0	(Pathogenic) CADD: 42.0 DANN: 0.9971 FATHMM-MKL: 0.9856 MutationTaster : Disease causing	Segregates within family	phyloP100: 7.408 (Conserved)
m6	c.902_903delAT (p.Tyr301Cysfs*29)	Allele Frequency: 0.00003283 Homozygous : 0	(Pathogenic) CADD: 33.0 MutationTaster : Disease causing	Segregates within family	phyloP: 7.11 phyloP100: 8.722
m7	c.899_900delAC (p.Asp300Valfs*30)	Allele Frequency: 6.195e-7 Homozygous : 0	(Pathogenic) CADD: 32.0 MutationTaster : Disease causing	Segregates within family	phyloP: 4.71 phyloP100: 3.736

m8	c.787C>T (p.Gln263ter)	Not found	(Pathogenic) CADD: 37 DANN: 0.9975 FATHMM-MKL: 0.9757 MutationTaster: Disease causing	Segregates within family	phyloP100: 6.014 phyloP: 4.68
m9	c.164G>A (p.Arg55Gln)	Allele Frequency: 0.000009342 Homozygous: 0	(Pathogenic) CADD: 29.8 PolyPhen (max): 1.00 DANN: 0.9995 FATHMM-MKL: 0.9912 MutationTaster: Disease causing	Segregates within family	phyloP: 8.81 phyloP100: 7.099
m10	c.158+2dup	Not found	(Pathogenic) SpliceAI: Donor loss 0.8	Not done	phyloP100: 7.839
m11	c.476G>A (p.Gly159Asp)	Not found	(Pathogenic) SIFT: deleterious, Polyphen: Possibly damaging Provean: Pathogenic, MutationTaster: Disease causing	Not done	PyhloP: 0.758
m12	c.435_436delinsAA (p.Ser145_Gly146delinsArgSer)	Not found	(Pathogenic) MutationTaster: Disease causing	Segregates within family	phyloP100: 4.318

The mutations discovered in *SNUPN* were as follows: F1: Homozygous *m1*: c.926T>G (p.Ile309Ser), F2: Compound heterozygous *m2*: c.760-1G>A (p.Splice) and *m3*: c.958delA

(p.Met320Ter), F3: Compound heterozygous *m4*: c.848C>G (p.Ser283Ter) and *m5*: c.922C>T (p.Gln308Ter), F4: Homozygous *m6*: c.902_903delAT (p.Tyr301Cysfs29), F5, F6, and F7: Homozygous *m7*: c.899_900delAC (p.Asp300Valfs30), F8: Compound heterozygous *m8*: c.787C>T (p.Gln263Ter) and *m1*: c.926T>G (p.Ile309Ser), F9: Homozygous *m1*: c.926T>G (p.Ile309Ser), F10: Homozygous *m9*: c.164G>A (p.Arg55Gln), F11: Homozygous *m1*: c.926T>G (p.Ile309Ser), F12: Homozygous *m7*: c.899_900delAC (p.Asp300Valfs30), F13: Homozygous *m6*: c.902_903delAT (p.Tyr301Cysfs29), F14: Homozygous *m6*: c.902_903delAT (p.Tyr301Cysfs*29), F15: Compound heterozygous *m1*: c.926T>G (p.Ile309Ser) and *m4*: c.848C>G (p.Ser283Ter), F16: Homozygous *m10*:c.158+2dup, F17: Homozygous *m11*:c.476G>A (p.Gly159Asp), and F18: Compound heterozygous *m12*:c.435_436delinsAA (p.Ser145_Gly146delinsArgSer) and *m1*: c.926T>G (p.Ile309Ser). Notably, all variants were located in the last exons, affecting the C-terminus of the SPN1 protein, except for the *m9* and *m10* mutations, which affected the IBB domain. This suggests that the C-terminus of the SPN1 protein is a hotspot for mutations. Additionally, a clear genotype-phenotype correlation was observed in patients with mutations near the C-terminus, where severe truncating mutations were associated with a more severe disease form. All clinical details, additional symptoms, and molecular details are summarized in Table 4.

Table 4**:** Clinical description of the patients

	HPO terms	**Family 1**	**Family 2**	**Family 3**	**Family 4**		**Family 5**	**Family 6**	**Family 7**		**Family 8**	**Family 9**		**Family 10**	**Family 11**	**Family 12**	**Family 13**	**Family 14**	**Family 15**	**Family 16**	**Family 17**	**Family 18**	**Ratio (%)**
Individual		**II:1**	**II:1**	**II:4**	**II:2**	**II:3**	**II:4**	**II:3**	**II:1**	**II:3**	**II:2**	**II:1**	**II:2**	**II:1**	**II:1**	**II:2**	**II:1**	**II:1**	**II:1**	**II:1**	**II:1**	**II:1**	
Origin		Kosovo	San Marino	USA	Switzerland		Iraq	Iran	Iran		Macedonia	Romania		Guatemala	Kosovo	Iraq	Columbia	Columbia	Germany	Iran	Iran	Türkiye	
Gender		F	M	M	M	F	M	M	M	F	M	F	M	F	F	M	F	F	M	F	ND	F	
Consanguinity (degree)		-	-	-	-	-	-	+ (3rd)	+ (2nd)		-	-	-	-	+	+ (2nd)	-	+	-	ND	ND	-	
Recessive inheritance	HP:0000007	+	+	+	+		+	+	+		+	+	+	+	+	+	+	+	+	+	+	+	
Gene (MIM607602)		*SNUPN*	*SNUPN*	*SNUPN*	*SNUPN*		*SNUPN*	*SNUPN*	*SNUPN*		*SNUPN*	*SNUPN*	*SNUPN*	*SNUPN*	*SNUPN*	*SNUPN*	*SNUPN*	*SNUPN*	*SNUPN*	*SNUPN*	*SNUPN*	*SNUPN*	
Variant (NM_005701.3)		Hom. *m1*:c.926T>G	Cmpd. Het. *m2*:c.760-1G>A *m3*:c.958delA	Cmpd. Het. *m4*:c.848C>G *m5*:c.922C>T	Hom. *m6*:c.902_903delAT		Hom. *m7*:c.899_900delAC				Cmpd. Het *m8*:c.787C>T *m1*:c.926T>G	Hom. *m1*:c.926T>G		Hom. *m9*:c.164G>A	Hom. *m1*:c.926T>G	Hom. *m7*:c.899_900delAC	Hom. *m6*:c.902_903delAT	Hom. *m6*:c.902_903delAT	Cmpd. Het *m1*:c.926T>G *m4*:c.848C>G	Hom. *m10*:c.158+2dup	Hom. *m11*:c.476G>A	Cmpd. Het. *m12*:c.435_436delinsAA *m1*:c.926T>G	
Protein prediction		p.Ile309Ser	p.Splice p.Met320Ter	p.Ser283ter p.Gln308ter	p.Tyr301Cysfs*29		p.Asp300Valfs*30				p.Gln263ter p.Ile309Ser	p.Ile309Ser		p.Arg55Gln	p.Ile309Ser	p.Asp300Valfs*30	p.Tyr301Cysfs*29	p.Tyr301Cysfs*29	p.Ile309Ser p.Ser283ter	p.splice	p.Gly159Asp	p.Ser145_Gly146delinsArgSer p.Ile309Ser	
CLINICAL SYNOPSIS																							
Age at onset		5 y	2 y	Birth	Birth	Birth	Birth	Birth	Birth	Birth	17 m	10 y	4 y	18 m	3 y	2 y	8 m	1 y	Birth	ND	ND	2 y	**15/19 (79)**

Age at last examination		9 y	10 y	10 m	18y	15 y	3y	3 y	ND	4 y	3.5 y	18 y	16 y	11 y	13 y	7 y	5 y	5 y	36 y	ND	ND	16 y	
Deceased (age of death)		-	-	15 y	-	-	-	-	10 y	-	-	-	-	-	-	-	-	-	-	ND	ND	-	**2/19 (10)**
MUSCULAR PHENOTYPES																							
Muscle weakness	HP:0001324	Progressive, mild to moderate	Non-progressive, mild	Progressive, severe	Progressive, severe		Progressive, mild	Progressive, moderate	Progressive, severe		Progressive, mild to moderate	Progressive, mild to moderate	Progressive, moderate	Progressive, severe	Progressive, moderate	Progressive, severe	Progressive mild to moderate	Progressive Moderate	Progressive severe	ND	ND	Progressive Moderate to severe	
Proximal upper limb	HP:0008997	+	+	++	+++	+++	+	+	+++	+++	+	++	++	++	++	++	+	+	++	ND	ND	++	**19/19 (100)**
Distal upper limb	HP:0008959	+	-	ND	+++	+++	+	+	+++	+++	-	-	+	+	ND	++	+	-	+	ND	ND	++	**13/17 (76)**
Proximal lower limbs	HP:0008994	+	+	++	+++	+++	+	+	+++	+++	+	+	++	+++	++	++	+	+	++	ND	ND	++	**19/19 (100)**
Distal lower limb	HP:0009053	+	-	++	+++	+++	+	+	+++	+++	-	+	++	+++	+	++	+	+	+	ND	ND	++	**17/19 (89)**
Axial	HP:0003327	++	+	+	+++	+++	+	++	+++	+++	++	-	++	-	++	++	+	+	++	ND	ND	++	**17/19 (89)**
Unsteady or no gait	HP:0002317	+	+	NA	NA	NA	+	NA	NA	NA	+	+	NA	NA	NA	NA	+	+	NA	ND	ND	++	**8/8 (100)**
Gowers sign	HP:0003391	+	-	NA	NA	NA	ND	NA	NA	NA	+	+	NA	NA	NA	NA	+	ND	NA	ND	ND	+	**5/6 (83)**
Difficulty walking	HP:0002355	-	-	NA	NA	NA	+	NA	NA	NA	+	+	NA	NA	NA	NA	+	+	NA	ND	ND	+	**6/8 (75)**
Difficulty climbing stairs	HP:0003551	+	+	NA	NA	NA	+	NA	NA	NA	+	+	NA	NA	NA	NA	+	+	NA	ND	ND	+	**8/8 (100)**

Non-ambulatory (age)	HP:0002540	-	-	+	6 y	5 y	-	6 y	7 y	7 y	-	-	16 y	11 y	13 y	3.5 y	-	-	6.5 y	ND	ND	-	**11/19 (57)**
Calf muscle pseudohypertrophy	HP:0003707	+	-	-	+	+	ND	+	-	-	+	-	-	-	-	-	+	-	-	ND	ND	-	**6/18 (33)**
CK high (> 500)	HP:0030234	2577-3133	normal	1500	2000 - 7000	1000	5459	3806	ND	2961	3170	2529	5750	480–6601	>6000	3500	2348	High	465-1300	ND	ND	260-1295	**17/18 (94)**
EMG / myopathy	HP:0003198	myopathy	myopathy	myopathy	ND	ND	ND	myopathy	ND	myopathy	ND	ND	myopathy	ND	myopathy	myopathy	myopathy	myopathy	myopathy	ND	ND	ND	**11/11 (100)**
MUSCLE BIOPSY																							**11/21 (52)**
age		7 y	10 y	5 m	2 y and 6 y	NA	NA	NA	6 y	NA	NA	17 y	15 y	3 y	NA	3 y	NA	NA	1.5 y, 2.5 y & 8 y	ND	ND	16 y	
site		deltoid	quadriceps femoris	left thigh	quadriceps femoris	NA	NA	NA	quadriceps femoris	NA	NA	thigh	thigh	left thigh	NA	NA	NA	NA	quadriceps femoris & paravertebral	ND	ND	ND	
Abnormal muscle fiber	HP:0004303	+	+	+	+	NA	NA	NA	+	NA	NA	+	+	+	NA	+	NA	NA	+	ND	ND	+	**11/11 (100)**
Endomysial fibrosis	HP:0100297	+	+	+	+	NA	NA	NA	ND	NA	NA	+	+	+	NA	+	NA	NA	+	ND	ND	+	**11/11 (100)**
NEUROLOGIC																							**7/9 (78)**
Cerebellar atrophy	HP:0001272	ND	+	+	-	ND	+	-	ND	ND	ND	ND	ND	-	ND	+	ND	+	-	ND	ND	ND	**5/9 (56)**
Thin corpus callosum	HP:0200012	ND	-	ND	-	ND	+	ND	ND	ND	ND	ND	ND	+	ND	+	ND	-	-	ND	ND	ND	**3/7 (43)**
Exploration		ND	MRI	MRI at 18 m	MRI at 2 y	ND	MRI at 22 m	Brain CT	ND	ND	ND	ND	ND	MRI at 3 y	ND	MRI	ND	MRI	MRI	ND	ND	ND	**9/21 (43)**

OTHERS																							
Pain insensitivity	HP:0007021	+	-	ND	-	-	ND	-	-	-	ND	-	-	-	-	+	-	-	-	ND	ND	ND	**2/14 (14)**
Abnormal facial shape	HP:0001999	+	-	-	-	-	-	-	-	-	+	-	-	-	-	-	-	-	+	ND	ND	-	**3/19 (16)**
Motor delay	HP:0001270	+	+	+++	+++	+++	+	+	+++	+++	+	-	-	+++	-	+	+	+	++	ND	ND	++	**16/19 (84)**
Cataract	HP:0000518	-	+	+	+	-	+	-	+	-	-	-	-	-	-	-	-	+	-	ND	ND	-	**6/19 (31)**
Respiratory insufficiency	HP:0002093	-	-	+++	+++	+++	-	-	+++	+++	-	+	++	+	-	+	+	-	++	ND	ND	++	**12/19 (63)**
Cardiomyopathy	HP:0001638	ND	-	ND	-	-	-	-	ND	-	NA	-	-	-	-	-	-	-	-	ND	ND	-	**0/15 (0)**
Abnormal vertebral column	HP:0000925	Mild scoliosis	-	ND	Scoliosis, rigid spine	Scoliosis, rigid spine	ND	Mild scoliosis	Scoliosis	Scoliosis	-	-	Hyper-lordosis, scoliosis	Scoliosis	Scoliosis, rigid spine	Scoliosis, rigid spine	Hyper-lordosis	-	Scoliosis	ND	ND	Kyphosis	**13/17 (76)**
Limb joint contracture	HP:0003121	+	-	+++	+++	+++	+	-	+++	+++	+	+	++	+++	+	+++	-	-	+++	ND	ND	++	**15/19 (78)**
Others		NA	Mild upper limb left dysmetria Scanned speech	Never reached ambulation Difficulty in swallowing	Reduced fetal movement, difficulty in swallowing	Reduced fetal movement, difficulty in swallowing	Strabismus pectus excavatum	Flat feet.	Death due to cardiac arrest.	Flat feet.	Big eyes, hypertelorism, anteverted nasal tip.	Absent deep tendon reflexes.	Absent deep tendon reflexes.	Microcephaly, intellectual disability, difficulty in swallowing.	ND	Cachexia, sensorineural hearing loss, difficulty in swallowing.	Tricuspid regurgitation, pectus carinatum.	Tricuspid regurgitation, neurodevelopmental delay.	Low global brain volume reduction.	ND	ND	Hyperextension in the neck, dropped-head	

Hom, Homozygote; Cmpd. Het., Compound Heterozygote; *m1* to *m12*: mutations; ND, Not Determined; NA, Not Applicable; M, Male; F, Female; y, year(s); m, month(s); h, hour(s); %, percentage; +, mild; ++, moderate; +++, severe.

3.1.3 Comparative analysis with established muscular dystrophy phenotypes

To better understand and clinically classify the current disease, Table 5 summarizes the clinical classification from the review by Mercuri and Muntoni (2013) (Mercuri & Muntoni, 2013). Since almost all patients in our cohort are characterized by an early childhood onset, only congenital muscular dystrophies and childhood-onset muscular dystrophies are included in the table. The phenotype observed in our patients shares characteristics with many types of muscular dystrophies (MD). However, the presence of central nervous system (CNS) defects helps narrow the diagnosis. This phenotype closely resembles congenital muscular dystrophy with merosin deficiency or muscle-eye-brain disease (MD type A5), similar to that seen in *FKRP* mutations. In such cases, patients may experience cataracts, CNS symptoms, and respiratory issues.

On the other hand, the presentation of some patients after the age of ambulation provides grounds for comparison with other limb-girdle muscular dystrophies (LGMD). This observation aligns the disease phenotype within a category that includes various conditions sharing similar clinical behavior. Examples of diseases classified both as congenital muscular dystrophies and limb-girdle muscular dystrophies include collagen VI-related dystrophies (Ullrich and Bethlem myopathies), dystroglycanopathies, and LAMA2-related muscular dystrophy (Barton et al., 2020; Zambon & Muntoni, 2021), each presenting as either congenital or limb-girdle muscular dystrophy depending on the severity and timing of their clinical manifestation.

Table 5**:** Summery of clinical features of congenital and childhood onset muscular dystrophies

Muscular dystrophy	**Motor function**	**Distribution of weakness**	**Rigid spine**	**Respiratory impairment**	**Disease course**	**Increased CK**	**Other signs**
Congenital muscular dystrophy with merosin deficiency	Independent ambulation	Upper limbs>lower limbs	-	++	Slowly progressive	++	White matter changes on brain MRI

	generally, not achieved in patients with absent merosin						
Congenital muscular dystrophy and abnormal glycosylation of Dystroglycan (Walker-Warburg syndrome, muscle-eye-brain disease, congenital muscular dystrophy type 1C, etc.)	Independent ambulation generally not achieved	Upper limbs>lower limbs	-	+	Slowly progressive	++	Frequent structural brain changes
Congenital muscular dystrophy with rigid spine syndrome type 1 (SEPN1)	Ambulation achieved	Axial muscles>limbs	++	Early respiratory failure	Progression of respiratory signs>motor signs	Normal or +	Scoliosis
Ullrich syndrome	Ambulation achieved in ~50% but lost by middle teens	Proximal and axial	++	Early respiratory failure	Progression of respiratory and motor signs	Normal or +	Distal laxity
Duchenne muscular dystrophy	Independent ambulation achieved, but lost before age of	Proximal>distal	-	++	Progression of motor, cardiac, and respiratory signs	++	Mental retardation in 30%

	13 years						
Emery-Dreifuss muscular dystrophy with Lamin AC deficiency (type 2)	Ambulation achieved in all cases except for rare cases with congenital onset	Scapulo peroneal	++	In adulthood in the typical form, but also in childhood (congenital variants)	Slowly progressive	+	Frequent association with Dunningham type lipodystrophy Cardiomyopathy
Limb girdle muscular dystrophy with Lamin AC deficiency (type 1B)	Independent ambulation achieved, variable progression	Proximal>distal	+	In adulthood	Progression of cardiac signs>motor signs	+	none
Limb girdle muscular dystrophy with calpain deficiency (type 2A)	Ambulation achieved	Proximal>distal	+	Not frequent	Slow progression	++	None
Limb girdle muscular dystrophy with sarcoglycan deficiency (type 2C, 2D, 2E, 2F)	Independent ambulation achieved, generally lost in the second decade	Proximal>distal	-	++	Progression of motor, cardiac and respiratory signs	++	None
Limb girdle muscular dystrophy with abnormal glycosylation of dystroglycan (type 2I, 2K, 2L, 2M, 2N, 2O)	Independent ambulation achieved, variable progression	Proximal>distal	-	+	Progressive	++	Mental retardation reported in some cases

Limb girdle muscular dystrophy with dysferlin deficiency (type 2B)	Independent ambulation always achieved	Proximal and distal involvement	-	-	Progressive in adulthood	++	None
Limb girdle muscular dystrophy with telethonin deficiency (type 2G)	Independent ambulation achieved, generally lost in the fourth decade	Proximal>distal	-	+	Progressive in adulthood	+	None
Limb girdle muscular dystrophy with titin deficiency (type 2J)	Independent ambulation achieved	Proximal>distal	-	-	Roughly half lose ambulation in adulthood	++	None
Facioscapulohumeral dystrophy	Independent ambulation achieved, variable progression	Fascial muscles, Scapulae, proximal upper limbs and distal lower limbs	-	Uncommon and mild	Slowly progressive	Normal or +	Neurosensory hearing loss and retinal degeneration
Emery-Dreifuss muscular dystrophy with merin deficiency (type 1)	Independent ambulation achieved, variable progression	Scapuloperoneal	+	Not frequent	Progression of cardiac signs>motor signs	+	None
SPN1 deficiency muscular dystrophy	Independent ambulation achieved in some	Proximal > distal, Axial involvement	+, scoliosis	++	Variable progression two thirds lost ambulatio	++	Cerebellar atrophy, thin corpus callosum, Cataract.

	patients but lost in early childhood. Variable progression				n in early childhood		

+, mild; ++, moderate; -, negative; >, more than.

3.2 Characterization of *SNUPN* variants pathogenicity

3.2.1 Cellular models

Primary dermal fibroblasts

Primary dermal fibroblasts were collected from patients F1, F2, F4-II:2, F4-II:3, and F10. We assessed the expression levels of *SNUPN* mRNA in these patients and compared them with those in three healthy controls. For this purpose, RNA was extracted from the patients' fibroblasts, and cDNA was synthesized for qPCR analysis. The results indicated no significant difference in *SNUPN* expression between patients and controls (Figure 3.4(a)).

To investigate the protein level, whole protein extracts were obtained from both patients and controls primary fibroblasts. Western blot analysis was performed using an SPN1 antibody to compare levels across the samples (Figure 3.4(b)). The results revealed a significant decrease in SPN1 protein levels in samples from F1, F2, F4-II:2, and F4-II:3, but not from F10 (Figure 3.4(c)). The observed decrease in SPN1 protein levels, without a corresponding compensatory increase at the RNA level, suggests protein instability and consequent loss of function, potentially contributing to the pathogenic mechanism observed in this cell type.

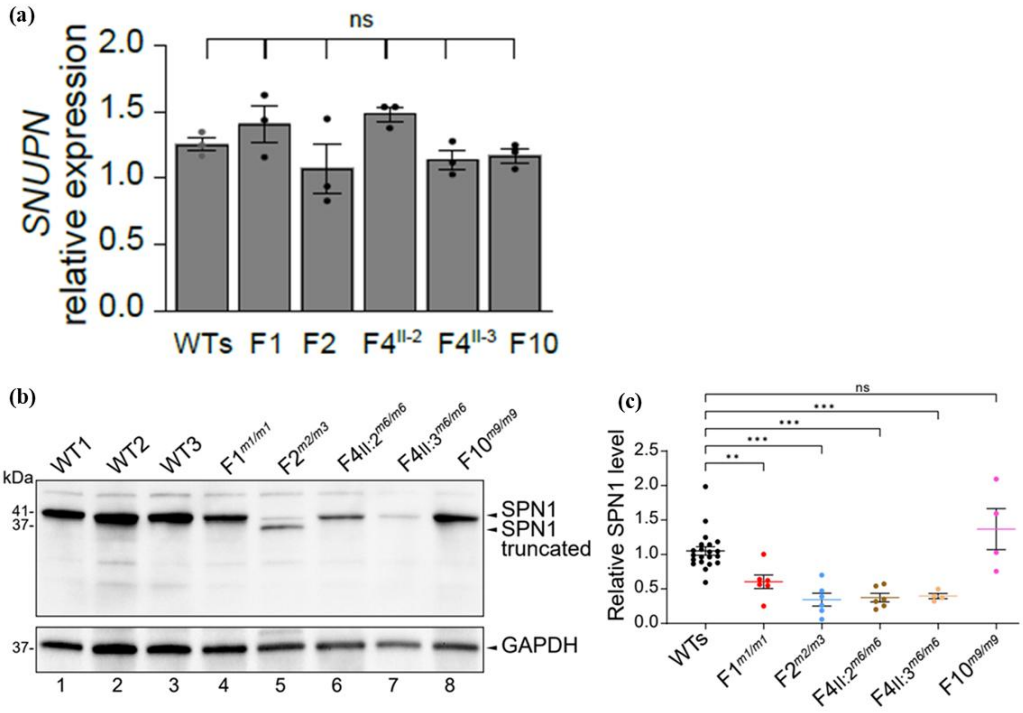

Figure 3.4: *SNUPN* expression and SPN1 protein levels in primary dermal fibroblasts: (a) Relative expression of *SNUPN* in samples from three healthy controls and five patients; the differences were not statistically significant. (b) Western blot analysis showing SPN1 levels in three healthy controls and five patient samples, with decreased SPN1 levels in all patients except F10. Additionally, a truncated SPN1 protein is evident in patient F2 with a splice site mutation. (c) Quantification of the western blot using ImageJ, indicating a statistically significant decrease in SPN1 levels in patients F1, F2, F4-II:2, and F4-II:3.

Modeling SNUPN mutations in mutant HeLa

To model the disease, mutant HeLa cell lines were generated using CRISPR-Cas9 technology. Two distinct cell lines were created, each targeting different regions of the *SNUPN* gene. The first cell line targeted exon 2, aiming to produce a complete knockout model by disrupting the N-terminal region of the protein. The second cell line targeted exon 9 to generate mutants mimicking patient-specific mutations near the C-terminus of the protein. Figure 3.5(a) provides an overview of the single guide RNAs (sgRNAs) designed for this purpose, illustrating the location of sgEx2 and sgEx9. The resulting *SNUPN* mutant cell lines exhibited a variety of mutations, either in the N-terminal region (Figure 3.5(b)) or the C-terminal region

(Figure 3.5(c)), reflecting the intended disruption of the protein. In this way, we successfully generated two distinct cellular models with potentially different levels of SPN1 functionality, facilitating a deeper understanding of the disease pathophysiology.

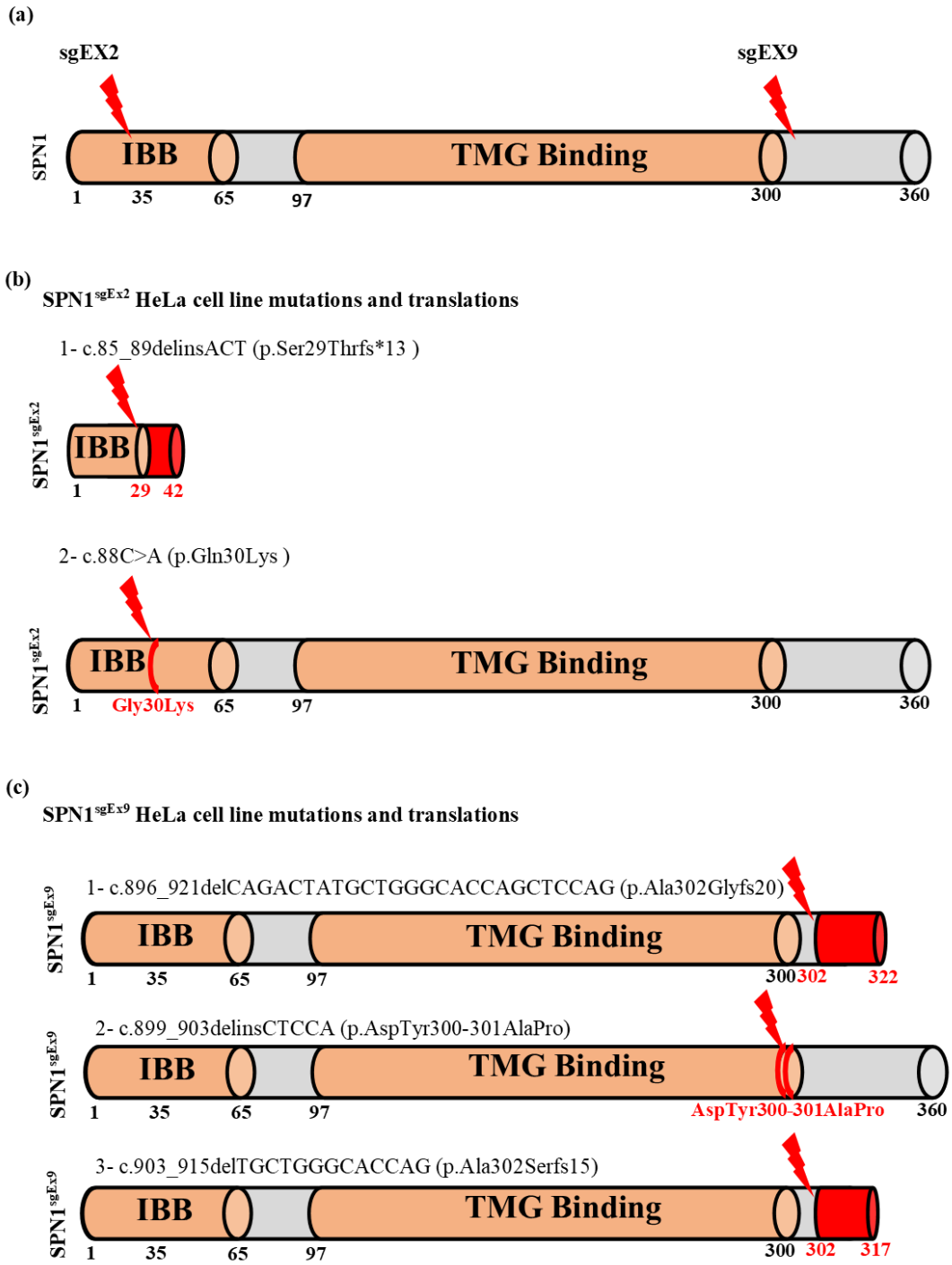

Figure 3.5: CRISPR-Cas9-generated HeLa cell mutants: (a) A schematic representation of the wild-type SPN1 protein, illustrating the regions targeted by the single guide RNAs (sgRNAs)

at the protein level. sgEx2 refers to the sgRNA targeting exon 2 of the *SNUPN* gene, resulting in mutations near the N-terminus of the protein. sgEx9 refers to the sgRNA targeting exon 9, resulting in mutations near the C-terminus of the protein. (b) A schematic representation of the SPN1^{sgEx2} proteins and mutations resulting from sgEx2 targeting. Sequencing of the generated cell lines identified two mutations: c.85_89delinsACT (p.Ser29Thrfs*13) and c.88C>A (p.Gln30Lys). (c) A schematic representation of the SPN1^{sgEx9} proteins and mutations resulting from sgEx9 targeting. Sequencing revealed three mutations: a 26 bp deletion (c.896_921delCAGACTATGCTGGGCACCAGCTCCAG, p.Ala302Glyfs20), a 5 bp deletion with a 5 bp insertion (c.899_903delinsCTCCA, p.AspTyr300-301AlaPro), and a 13 bp deletion (c.903_915delTGCTGGGCACCAG, p.Ala302Serfs15). (CRISPR-Cas-9 was done with Nasrinsadat Nabavizadeh and Elanur Yılmaz).

The expression of *SNUPN* was significantly increased in SPN1 mutant HeLa cell lines (SPN1^{sgEx2} and SPN1^{sgEx9}) compared to wild-type (WT) controls, a finding not observed in primary dermal fibroblasts. This discrepancy may arise from intrinsic cellular differences between HeLa cells and primary dermal fibroblasts, potentially influencing gene regulation and protein stability in distinct manners. Furthermore, protein level assessments revealed significantly reduced SPN1 protein in both SPN1 mutant HeLa cell lines compared to WT controls, with a more pronounced reduction in SPN1^{sgEx2} compared to SPN1^{sgEx9}. This variation might reflect distinct functional consequences associated with different mutation positions within the *SNUPN* gene. Collectively, these findings suggest that the observed reduction in SPN1 protein levels is likely due to increased protein instability or enhanced degradation pathways triggered by the mutations, rather than alterations in transcriptional regulation alone (Figure 3.6).

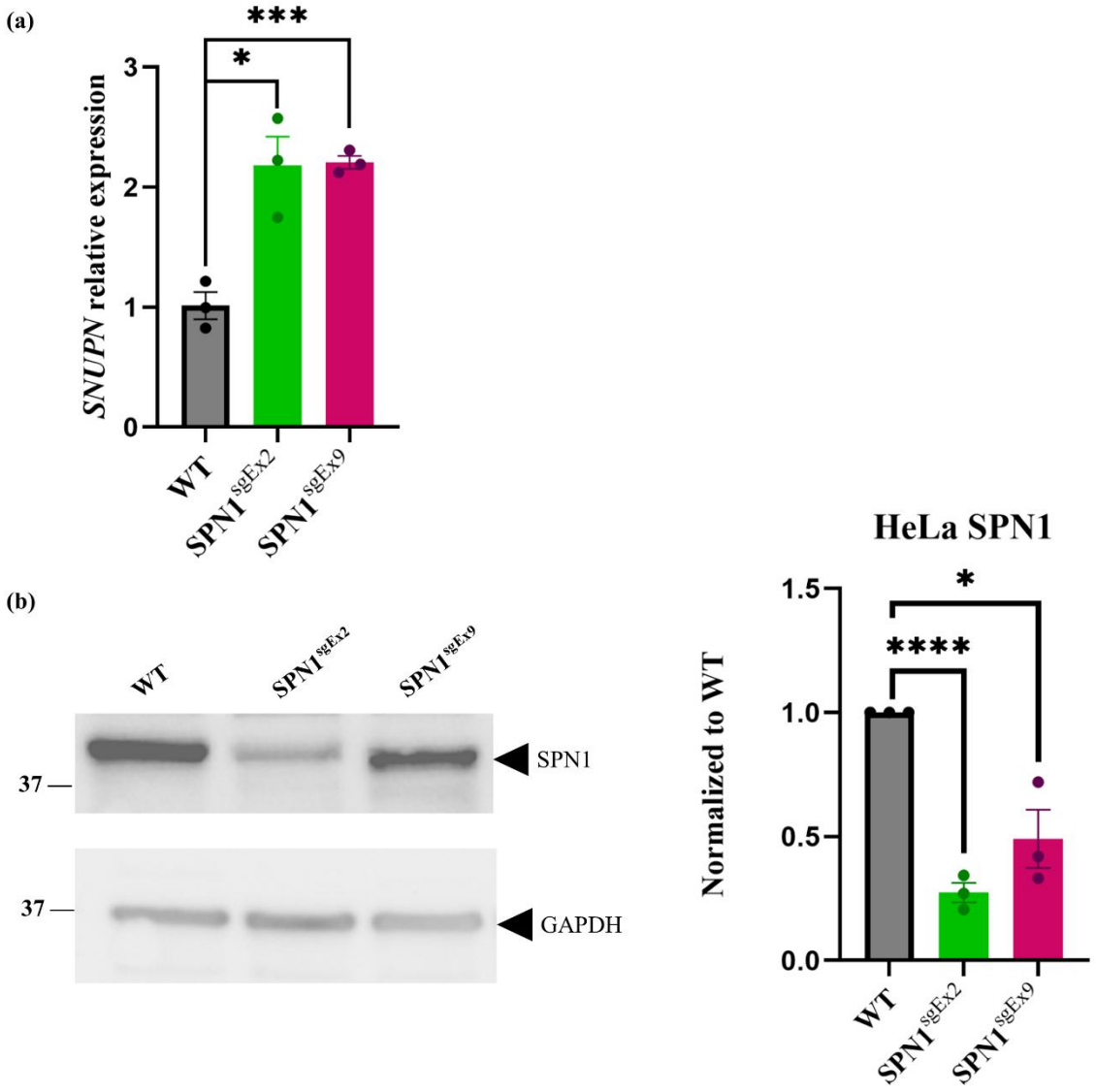

Figure 3.6: *SNUPN* expression and SPN1 protein levels in SPN1 mutant HeLa cells: (a) Relative expression of *SNUPN* in WT HeLa cells compared to SPN1 mutant HeLa cell lines ($SPN1^{sgEx2}$ and $SPN1^{sgEx9}$), showing a significant increase in *SNUPN* expression in mutant cell lines relative to controls. (b) SPN1 protein levels in WT HeLa cells compared to SPN1 mutant HeLa cell lines. There is a significant reduction in SPN1 protein levels in mutant HeLa cells compared to WT cells.

3.2.2 Mislocalization of SPN1 mutant cells

Mislocalization of SPN1 in primary dermal fibroblasts

To assess the localization of the SPN1 protein in patients compared to controls, immunofluorescence assays targeting SPN1 were performed using primary fibroblasts from both groups, as well as muscle cross-sections. In primary fibroblasts from patients, SPN1 demonstrated pronounced aggregation around the nuclei compared to controls, which displayed more uniform network like distribution throughout the cytoplasm (Figure 3.7(a)). Quantitative analysis of the perinuclear region confirmed a significant increase in SPN1 accumulation in patient fibroblasts (Figure 3.7(b)). Similarly, muscle cross-sections from patients revealed SPN1 aggregation predominantly in the subsarcolemmal and perinuclear areas, contrasting with the control fibers, where SPN1 was uniformly dispersed within the sarcoplasm. These observations suggest altered intracellular localization of SPN1 associated with disease pathology (Figure 3.7(c)).

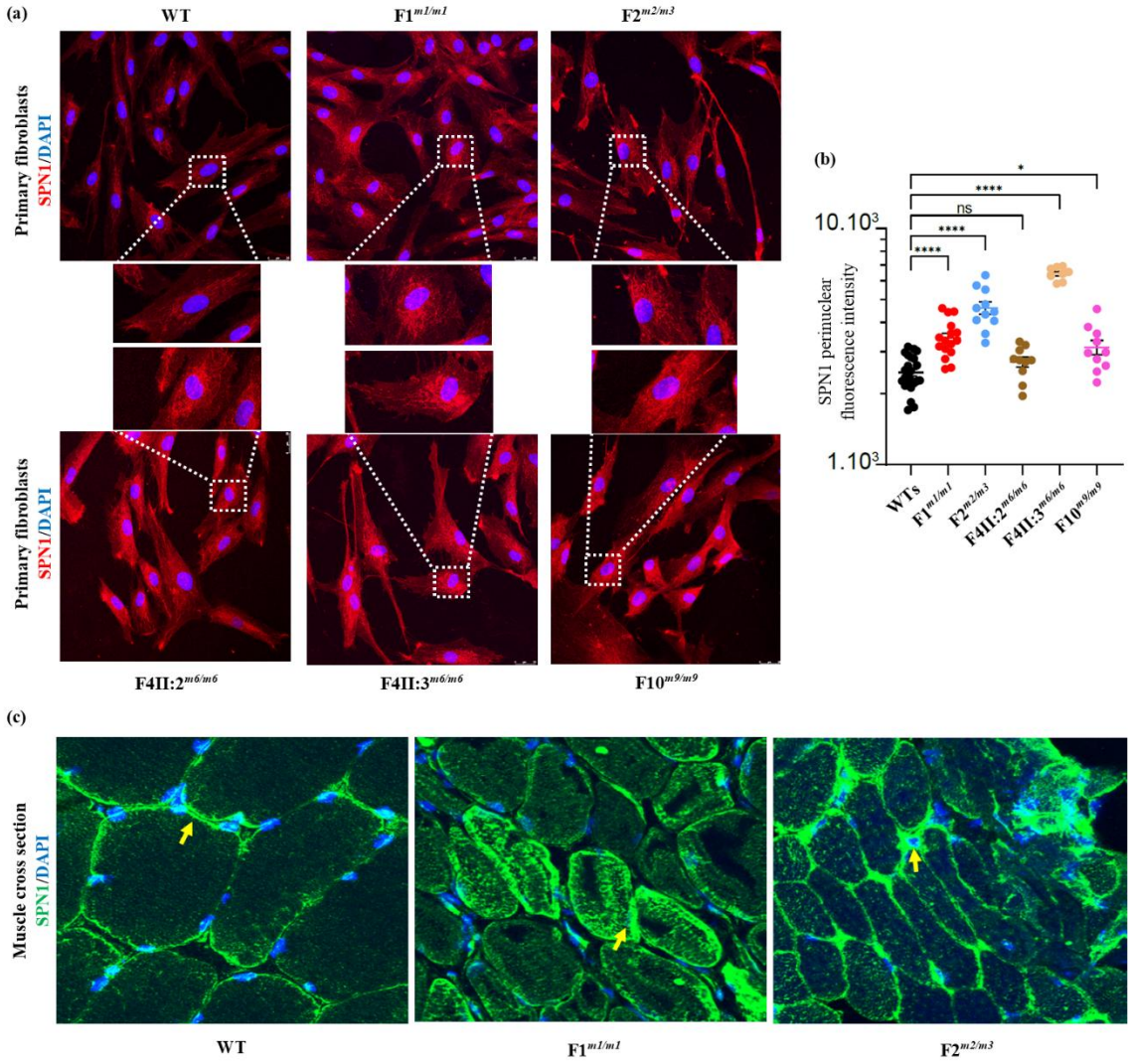

Figure 3.7: SPN1 mutant protein aggregation in patient fibroblasts and muscle tissues (a) Immunofluorescence staining of primary fibroblasts demonstrating SPN1 localization (red) and nuclei labeled by DAPI (blue). Areas of SPN1 aggregation around the nuclei in patient samples ($F1^{m1/m1}$, $F2^{m2/m3}$, F4-II:2 $^{m6/m6}$, F4-II:$3^{m6/m6}$, *and* $F10^{m9/m9}$ are highlighted by dotted squares and compared to control. (b) Quantification of SPN1 signal intensity, revealing significantly increased perinuclear aggregation in most patient fibroblasts compared to controls. (c) Immunofluorescence staining of muscle cross-sections from control and patients ($F1^{m1/m1}$ and $F2^{m2/m3}$), showing SPN1 (green) and DAPI (blue). Yellow arrows indicate SPN1

aggregates located subsarcolemmally and around nuclei in patient muscle tissues. (IF imaging done by Hilal Pırıl Saraçoğlu).

Mislocalization of SPN1 in mutant HeLa cells

In addition to the reduced SPN1 levels described previously, the network-like distribution of SPN1 observed in the wild-type cells was disrupted in the mutant cell lines (Figure 3.8). These results confirm the successful generation of a disease model for SPN1 deficiency, demonstrating both reduced levels, particularly in SPN1^{sgEx2}, and altered localization of the SPN1 protein. Additionally, these results confirm what was observed in patients' samples.

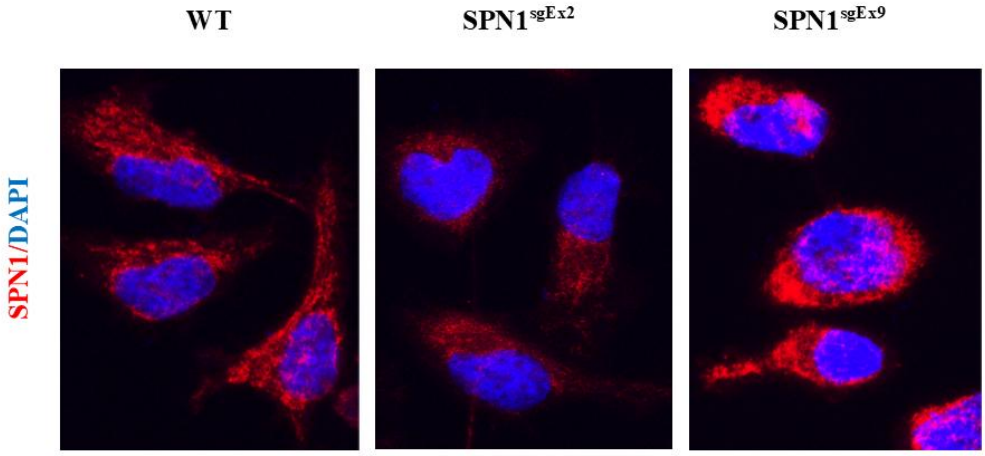

Figure 3.8: SPN1 mislocalization in HeLa mutant cell lines: Immunofluorescence images of WT and mutant HeLa cells (SPN1^{sgEx2} and SPN1^{sgEx9}). SPN1 is shown in red, while nuclei are stained with DAPI (blue). The network-like distribution of SPN1 observed in WT cells is disrupted in mutant cell lines. (IF imaging done by Hilal Pırıl Saraçoğlu).

3.3 Characterizing the role of SPN1 as a nuclear import adaptor of UsnRNP complex

3.3.1 SPN1 mutations lead to impaired nuclear import of UsnRNPs in patients' samples

The primary function of SPN1 is to act as an import adaptor, facilitating the transport of the UsnRNP complex from the cytoplasm to the nucleus after its maturation to form spliceosomes.

If the structure of SPN1 is compromised, it may fail to interact either with the m_3G cap on UsnRNP or with the primary import protein Imp-β1 (KPNB1). In either scenario, UsnRNPs would be mislocalized, likely resulting in their aggregation in the cytoplasm.

To test this hypothesis, we extracted proteins from patient and control samples, followed by fractionation to separate nuclear, cytoplasmic, and mitochondrial fractions. As previously mentioned, UsnRNPs consist of UsnRNA and seven Sm proteins. To determine the localization of the UsnRNPs, we used an anti Sm antibody for western blot analysis. Examination of the cytoplasmic fraction from primary fibroblasts of patients and controls revealed an increase in Sm protein bands in the patients' samples compared to controls (Figure 3.9(a)).

To further validate these findings, we performed immunofluorescence to visualize the Sm proteins within the cells. In fibroblasts from patients, the Sm signal was more aggregated in the cytoplasm, whereas in control cells, the signal was predominantly nuclear (Figure 3.9(b)). Notably, the quantification analysis of the nuclear Sm signal was significantly less in truncating mutations in comparison to controls (Figure 3.9(c)). These results clearly indicate a loss of SPN1 function and its subsequent inability to facilitate the transport of the UsnRNP complex to the nucleus.

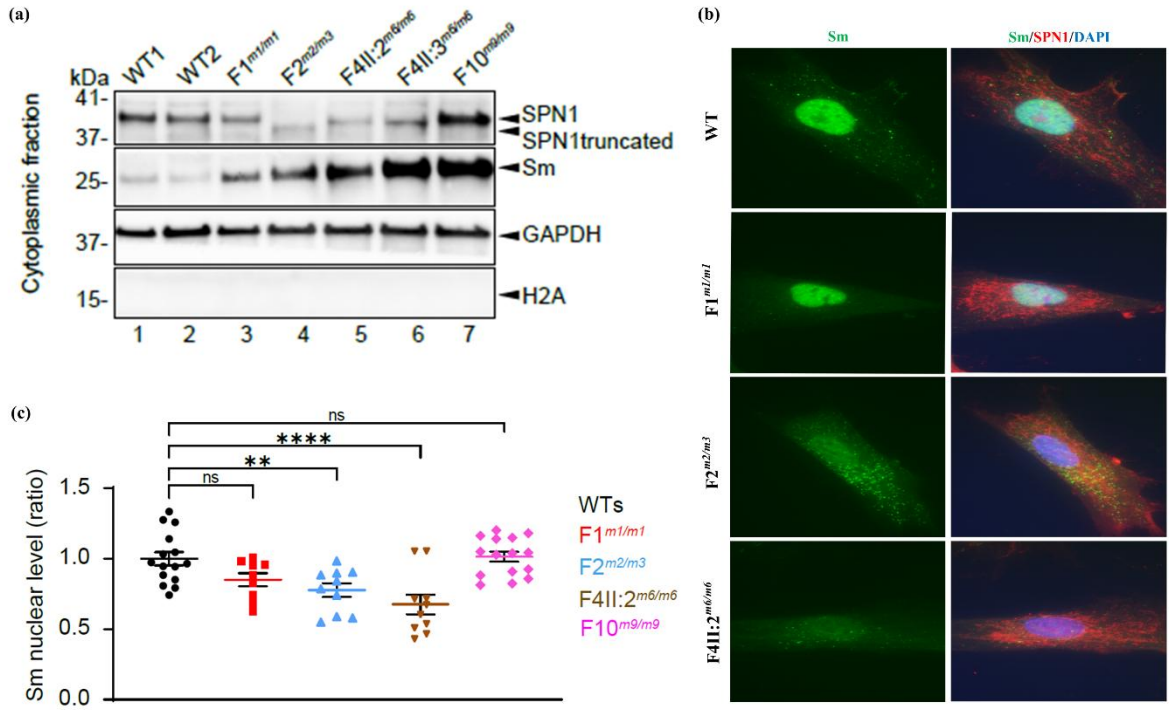

Figure 3.9: Disrupted Sm protein nuclear import and mislocalization: (a) Western blot analysis of the cytoplasmic fraction from primary fibroblasts protein extracts of patients and controls. The upper panel of the Western blot shows the SPN1 antibody, which is less abundant in patients compared to controls, except for $F10^{m9/m9}$. The second panel shows the Sm protein, which is clearly aggregated in patients' samples compared to the two controls. (b) Immunofluorescence analysis of fibroblasts from patients and controls. Sm is stained in green, SPN1 in red, and nuclei are counterstained with DAPI (blue). In patients' samples, Sm proteins are predominantly localized in the cytoplasm and less in the nucleus. (c) Quantification of nuclear Sm fluorescent intensity between patients and controls. The intensity was less in all the patients' cells in comparison to controls, however the difference was significantly less in $F2^{m2/m3}$ and $F4II:2^{m6/m6}$ (Fractionation was done by Nasrinsadat Nabavizadeh and IF imaging done by Hilal Pırıl Saraçoğlu).

3.3.2 Impaired nuclear import of UsnRNPs in SPN1 mutant HeLa cells

To evaluate the functional impact of SPN1 mutations in HeLa cell mutants and determine whether the phenotype observed in patients' primary fibroblasts is recapitulated, the localization of Sm proteins was examined and compared between mutant and wild-type (WT)

HeLa cells. The results revealed a marked decrease in the levels of Sm proteins within the nuclei of mutant cells compared to the WT. This finding indicates a defect in the ability of SPN1 to mediate the nuclear import of the Sm protein-containing import complex in the SPN1 mutant HeLa cells (Figure 3.10).

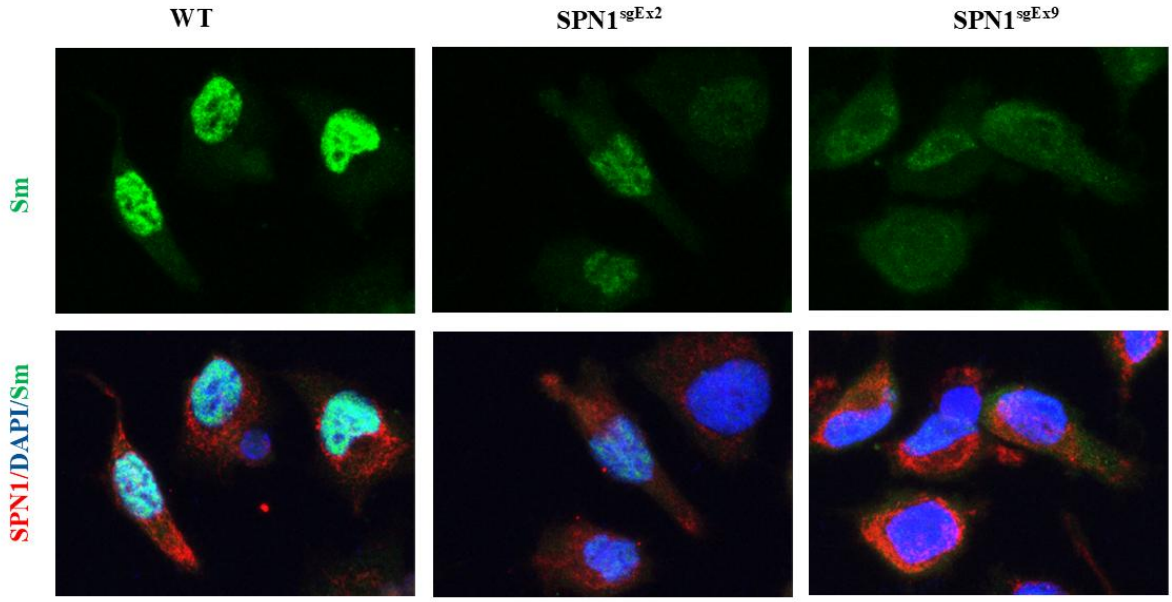

Figure 3.10: Sm protein disrupted nuclear import and mislocalization in HeLa cell lines: Immunofluorescence staining of Sm proteins (green) revealed their characteristic nuclear aggregation in wild-type (WT) HeLa cells. However, this nuclear aggregation was absent in SPN1 mutant HeLa cell lines, indicating impaired nuclear localization of Sm proteins. In the lower panel, SPN1 protein staining (red) shows a reduced level of SPN1 protein in SPN1^{sgEx2} mutant cells, additionally the loss of the SPN1 cytoplasmic network like distribution is lost in both mutant HeLa cell lines compared to the WT. (IF imaging done by Hilal Pırıl Saraçoğlu).

3.3.3 Cajal bodies disruption in SPN1 mutant cells

Cajal bodies disruption in patients' cells

Cajal bodies (CBs) are distinct, non-membrane-bound intranuclear structures found in both vertebrate and invertebrate cells. Their numbers and sizes vary depending on the cell type. Cajal bodies are molecularly defined by the presence of a protein called COILIN, which dynamically exchanges between the CB and the nucleoplasm. CBs primarily consist of components involved in RNA processing, including UsnRNPs and SMN (Lemm et al., 2006). The presence of these components is essential for the maintenance of CBs. A failure of SMN and subsequently UsnRNPs to reach the CBs results in their disruption, evidenced by the dispersion of COILIN in the nucleoplasm and its partial relocalization in the nucleoli, which is usually marked by FIBRILLARIN (Lemm et al., 2006). To investigate this phenomenon, we utilized an anti-COILIN antibody to visualize CBs in patient-derived cells compared to controls. The patient cells exhibited notable disruption of CBs, demonstrated by the significantly increased prevalence of dispersed COILIN compared to control cells (Figure 3.11(a)). Quantitative analysis further confirmed this observation, showing a significantly higher frequency of nuclei with disrupted CBs in patient samples relative to controls (Figure 3.11(b)). These findings strongly suggest impaired nuclear import of essential CB constituents, such as UsnRNPs and the SMN complex, resulting from SPN1 dysfunction.

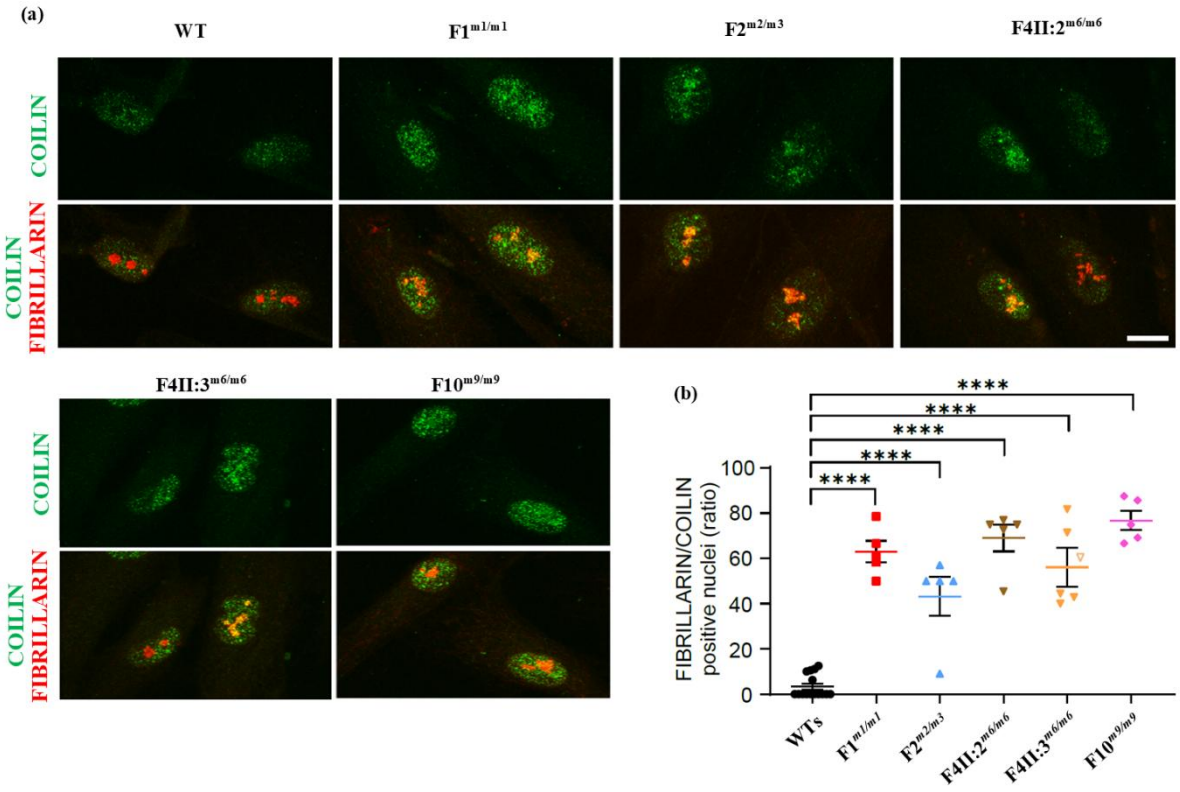

Figure 3.11: Cajal bodies disruption in SPN1 mutant patients' primary fibroblasts: (a) The upper panel of the figure shows immunostaining of COILIN (green) in control and patient primary fibroblasts. In patient samples, COILIN appears more dispersed throughout the nucleoplasm, while in controls it is more concentrated in CBs. The lower panel shows co-immunostaining with FIBRILLARIN (red), a known biomarker for the nucleolus. In patient samples, the colocalization of COILIN and FIBRILLARIN is more apparent compared to control samples, suggesting a relocalization of COILIN due to the disruption of CBs. (b) Quantification of the FIBRILLARIN/COILIN positive nuclei ratio. In patients' cells the number of FIBRILLARIN/COILIN positive nuclei is significantly more than the controls. (IF imaging done by Hilal Pırıl Saraçoğlu).

Cajal bodies disruption in SPN1 mutant HeLa cells

As previously described, the nuclear import of SMN and UsnRNPs is critical for maintaining Cajal bodies. In normal conditions, WT HeLa cells display distinct, punctate Cajal bodies characterized by precise co-localization of COILIN with SMN. In contrast, mutant HeLa cells

showed a disruption of this pattern, evidenced by the loss of COILIN-SMN co-localization, indicating compromised structural integrity of Cajal bodies (Figure 3.12(a)). Additionally, COILIN exhibited a dispersed distribution throughout the nucleoplasm rather than being confined to discrete punctate structures. This dispersion further confirms the disruption of CBs in mutant cells. Quantitative assessment of COILIN foci showed significantly reduced and altered patterns of localization in mutant HeLa nuclei (Figure 3.12(b,c)). These findings are consistent with the phenotypic observations in patient-derived primary fibroblasts, supporting the validity of our cellular disease model. Based on previous results indicating a perturbation in the nuclear transport of spliceosome components and the disruption of CBs, the next would be to investigate whether patients exhibited any abnormal splicing events compared to controls.

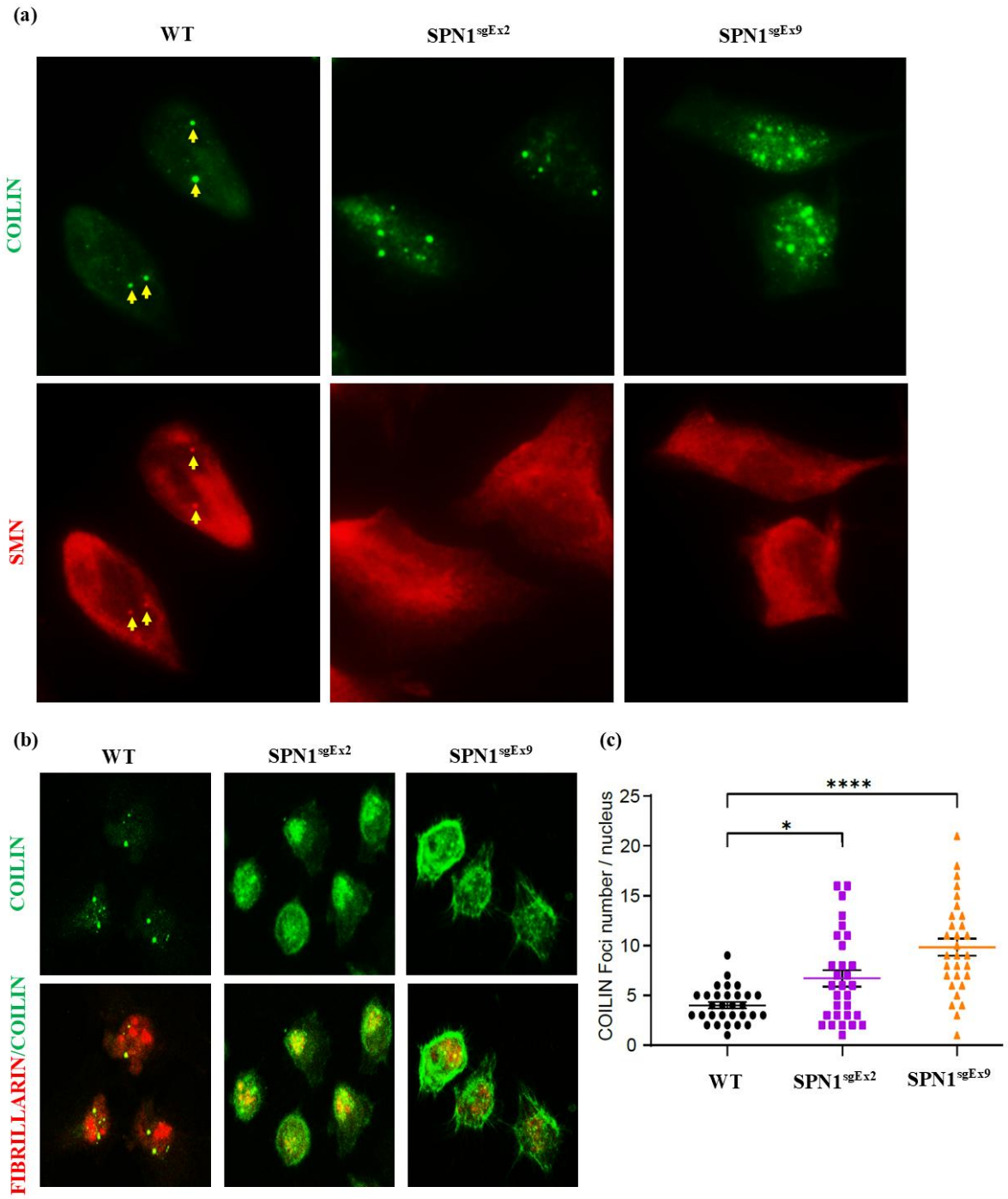

Figure 3.12: Cajal bodies disruption in SPN1 mutant HeLa cell lines: (a) Wild-type (WT) and SPN1 mutant HeLa cell lines (SPN1^{sgEx2} and SPN1^{sgEx9}) were stained with COILIN (green) and SMN (red) antibodies. In WT HeLa cells, COILIN forms normal Cajal bodies, visible as distinct, sparkling spots in the nucleus, with clear co-localization with SMN (yellow arrows). In contrast, SPN1 mutant cell lines showed dispersed COILIN staining throughout the

nucleoplasm, indicating disrupted Cajal bodies. Additionally, COILIN-SMN co-localization was absent in the mutants. (b) In WT cells, COILIN staining (green) represents intact Cajal bodies and does not co-localize with FIBRILLARIN (red), as shown in the lower panel. However, in SPN1 mutant cell lines (SPN1^{sgEx2} and SPN1^{sgEx9}), COILIN is dispersed in the nucleoplasm, reflecting disrupted Cajal bodies, and re-localizes to the nucleolus, where it co-localizes with FIBRILLARIN. (c) Quantification of nuclear COILIN foci in WT and SPN1 mutant HeLa cells showing a significantly higher number of foci in mutants indicating Cajal bodies disruption. (IF imaging done by Hilal Pırıl Saraçoğlu).

3.4 Structural characterization of SPN1

3.4.1 3D modeling and identification of C-terminus alpha helix

The complete crystallographic 3D model of the SPN1 protein, without being in a complex, is not available in the literature. All studies have only visualized parts of the protein or the protein in a complex. For example, the model with Protein Data Bank (PDB) identifier 1XK5 visualized the 3D structure from amino acid 97 to 300, along with the m_3G cap (Strasser et al., 2005). In contrast, 3GJX visualizes SPN1 in a complex with CRIM1, exportin 1, and RAN-GTP (Monecke et al., 2009). All attempts to visualize the complete SPN1 resulted in degradation at the N- and C-termini of the protein in solution, suggesting that these regions are unstructured and likely interact continuously with other substrates, either through homo- or hetero-oligomerization (Ospina et al., 2005; Strasser et al., 2005).

An alternative way to visualize the SPN1 protein and its interactions with its ligands (TMG or m_3G) is to use prediction programs that generate predicted 3D structures with varying degrees of accuracy. We used I-TASSER, an online protein 3D structure prediction tool (Y. Zhang, 2008) and Alphafold2 (Jumper et al., 2021) to obtain models of the SPN1 wild-type and mutated versions of the protein, focusing on homozygous mutations.

Figure 3.13 shows the differences mainly in the C-terminus of the WT and other mutants, where the alpha helix in the C-terminus is distorted in the mutants. The prediction of mutated SPN1 varies based on the on the location and severity of the mutations. Notably in almost all the predicted models the N- and the C-terminus mutations affected the C-terminus alpha helix,

either by mild point mutation like *m1* or complete loss like *m6*, *m7*, *m9*, and *m12* or by changing its orientation like in *m11*. The alpha helices close to the N-terminus, which are important for the interaction with Imp-β1, have been affected significantly in mutations closer to the N-terminus like *m11* and *m12*.

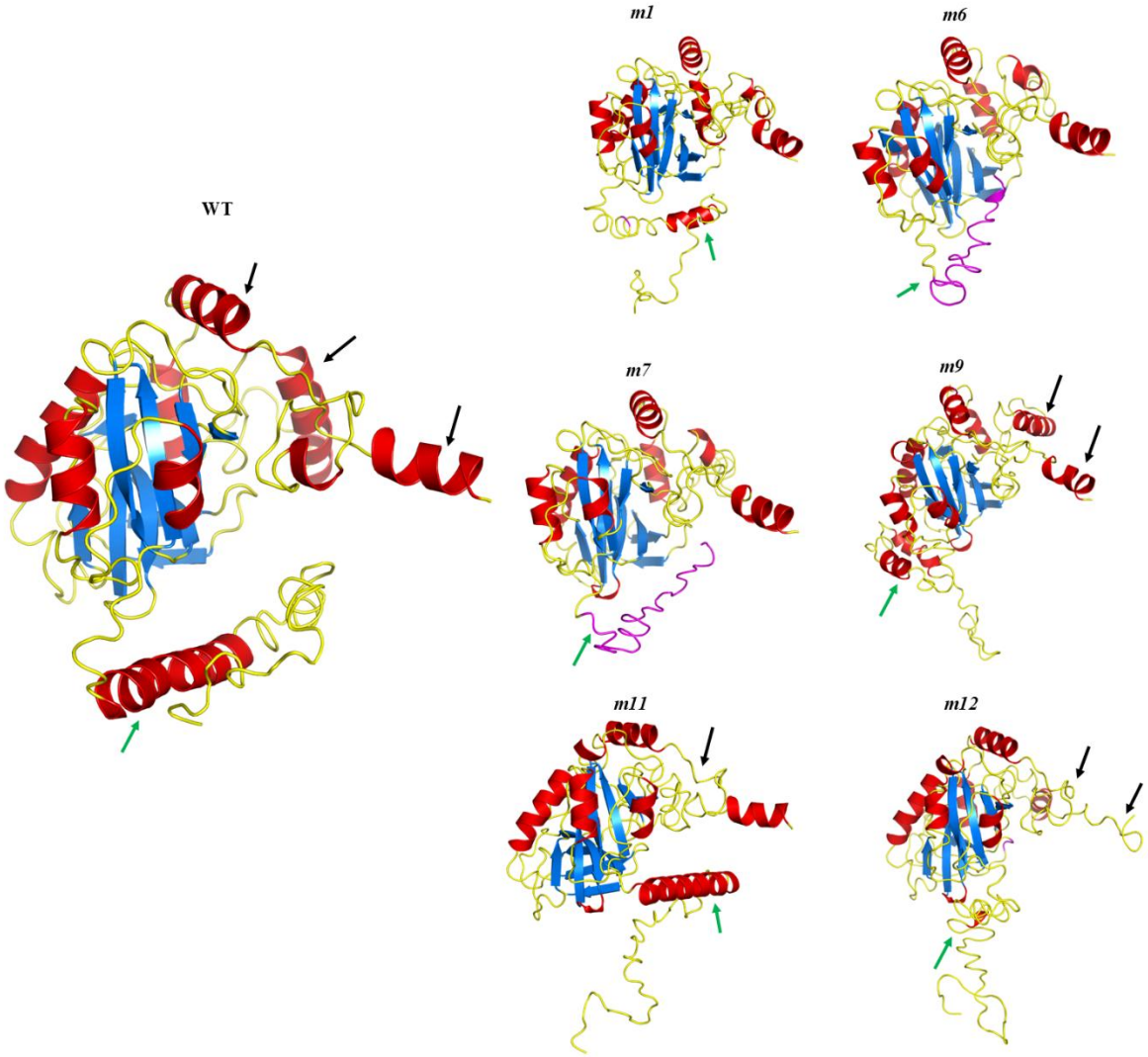

Figure 3.13: SPN1 WT and mutants 3D modeling predictions: Alpha helices are depicted in red, beta-sheets in blue, and coils in yellow (black arrows point to the alpha helices close to the N-terminus, and green arrows point to the C-terminus alpha helix). The mutated C-terminus in *m1, m6*, and *m7* is colored in magenta. The alpha helix in the WT C-terminus is distorted in the *m1* model and completely lost in *m6* and *m7*. Although the *m9* mutation is close to the N-terminus, it affects the C-terminus alpha helix. *m11* is closer to N-terminus and

it changed the orientation of the C-terminus and affected the alpha helices close to the N-terminus. *m12* affected significantly the N- and C-terminus alpha helices.

It is well known that the TMG (m_3G) cap binds SPN1 specifically through a tight pocket in the protein. By aligning the crystallographic model 1XK5 to the predicted models in the PyMOL program, we were able to dock the ligand in the mutants in its natural spatial dimensions. Visualizing the binding pocket of the ligand in Figure 3.14 clearly shows how the ligand fits tightly in the WT protein. However, in the predicted mutants, there are numerous clashes between the ligand and protein residues, which might decrease the binding efficiency between the protein and ligand. Additionally, the hydrogen bonds numbers, orientations, and lengths are predicted to be different in mutant proteins.

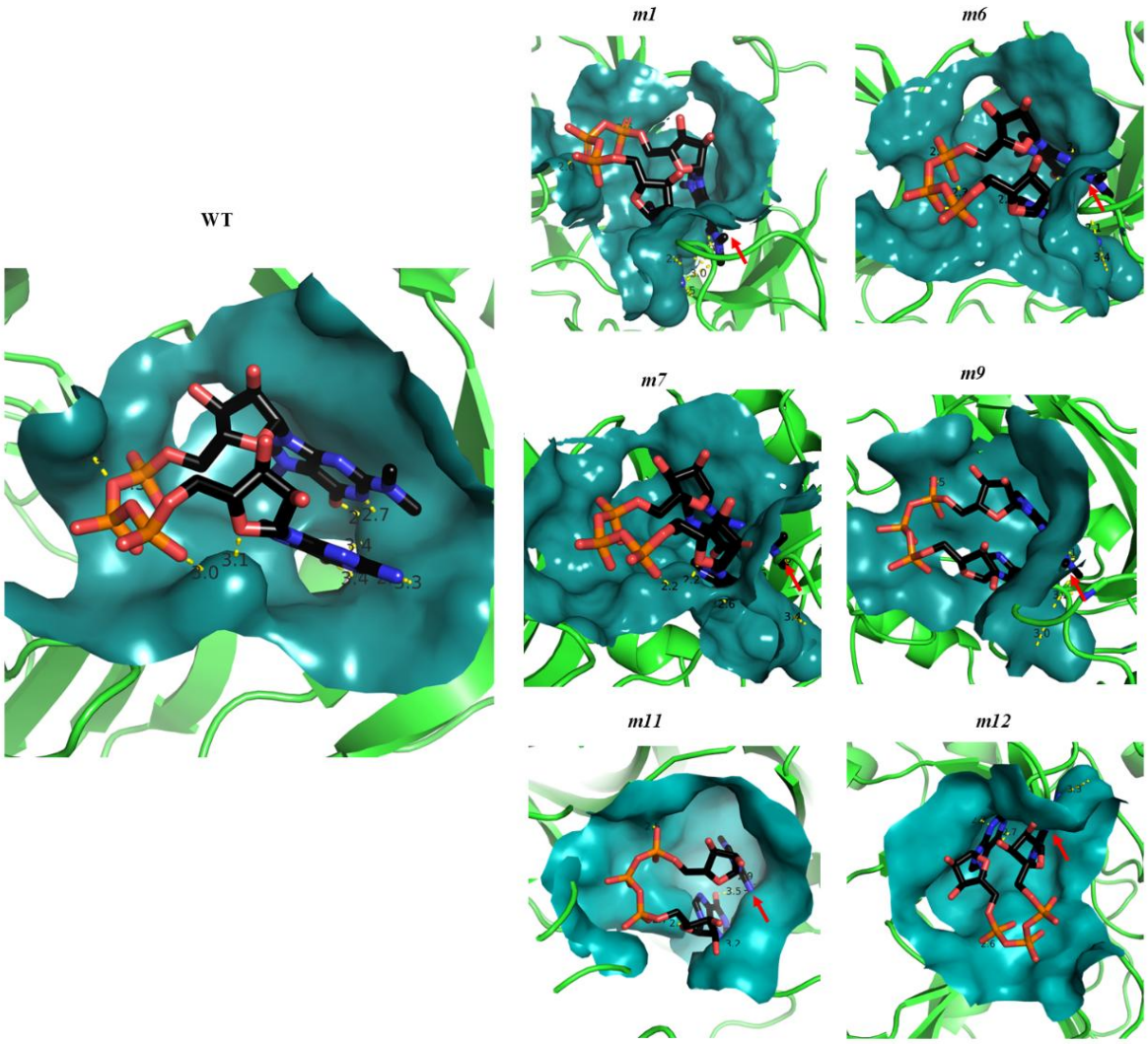

Figure 3.14: A zoomed-in view of the TMG (m_3G cap) and its binding pocket: The TMG is presented in stick representation, and the surface of the binding pocket is in deep-teal color. Hydrogen bonds are shown as yellow dotted lines. In the WT, the ligand fits tightly into the pocket; however, in all the mutants, there are clashes between the ligand and the surface of the protein (indicated by the red arrows). This might affect the binding efficiency and the stability of the hydrogen bonds and hydrophobic interactions. In *m12* the orientation of the pocket is completely changed, which might further affect the binding capacity of the ligand to the protein.

3.4.2 SPN1 oligomerization required intact C-terminus

It is known from the literature that there is crosstalk between the C-terminus and the N-terminus of SPN1(Ospina et al., 2005). However, the oligomerization of SPN1 was not previously documented. When we analyzed the Western blot (WB) of SPN1 from control and patient samples, we observed a higher band at around 150 kDa in the wild-type (WT), which became fainter in F1$^{m1/m1}$ and was completely absent in F2$^{m2/m3}$ and F4II:3$^{m6/m6}$. Conversely, this band was maintained in the F10$^{m9/m9}$ sample (Figure 3.15(a)). To confirm these results, HEK 293T cells were transfected with WT and SPN1 C-terminus-mutant constructs (Myc-SPN1^{WT}, Myc-SPN1^{Ile309Ser}, Myc-SPN1^{Tyr301Cysfs*29}, Myc-SPN1^{Asp300Valfs*30}). When protein extracts from the transfected cells were analyzed via WB, the same pattern was observed: the 150 kDa band appeared in the Myc-SPN1^{WT} and Myc-SPN1^{Ile309Ser} constructs but not in SPN1^{Tyr301Cysfs*29} and Myc-SPN1^{Asp300Valfs*30}. To verify that this band represented an oligomer of SPN1, we repeated the WB with the addition of DTT, a reducing agent. After adding DTT, the band disappeared from the Myc-SPN1^{WT} and Myc-SPN1^{Ile309Ser} samples, indicating that the band was specific to the SPN1 oligomer (Figure 3.15(b)).

To further confirm these results, we employed co-immunoprecipitation (IP), co-transfecting HEK 293T cells with similar Flag- and Myc-tagged SPN1 WT and mutant constructs. In the IP, we mixed protein extracts with Flag-antibody conjugated agarose beads and then checked for Myc-SPN1 in the pull-down. As shown in Figure 3.15(c), Myc bands appeared in the Myc-SPN1^{WT} and Myc-SPN1^{Ile309Ser} constructs but were absent in the SPN1^{Tyr301Cysfs*29} and Myc-SPN1^{Asp300Valfs*30} constructs.

Additionally, we performed the same experiment by co-transfecting HEK 293T cells with the Flag-WT SPN1 constructs along with Myc-SPN1 WT and mutant constructs. Co-IP was then conducted to determine if the WT-SPN1 could interact with the mutant constructs. The results were comparable to the previous experiment, where the WT successfully pulled down the Myc-SPN1^{WT}, Myc-SPN1^{Ile309Ser}, and the construct with the N-terminus mutation (Myc-SPN1^{Arg55Gln}), but not the SPN1^{Tyr301Cysfs*29} and Myc-SPN1^{Asp300Valfs*30} constructs with truncating C-terminus mutations (Figure 3.15(d)). These results confirmed that the C-terminus mutations in SPN1 prevented the oligomerization of SPN1.

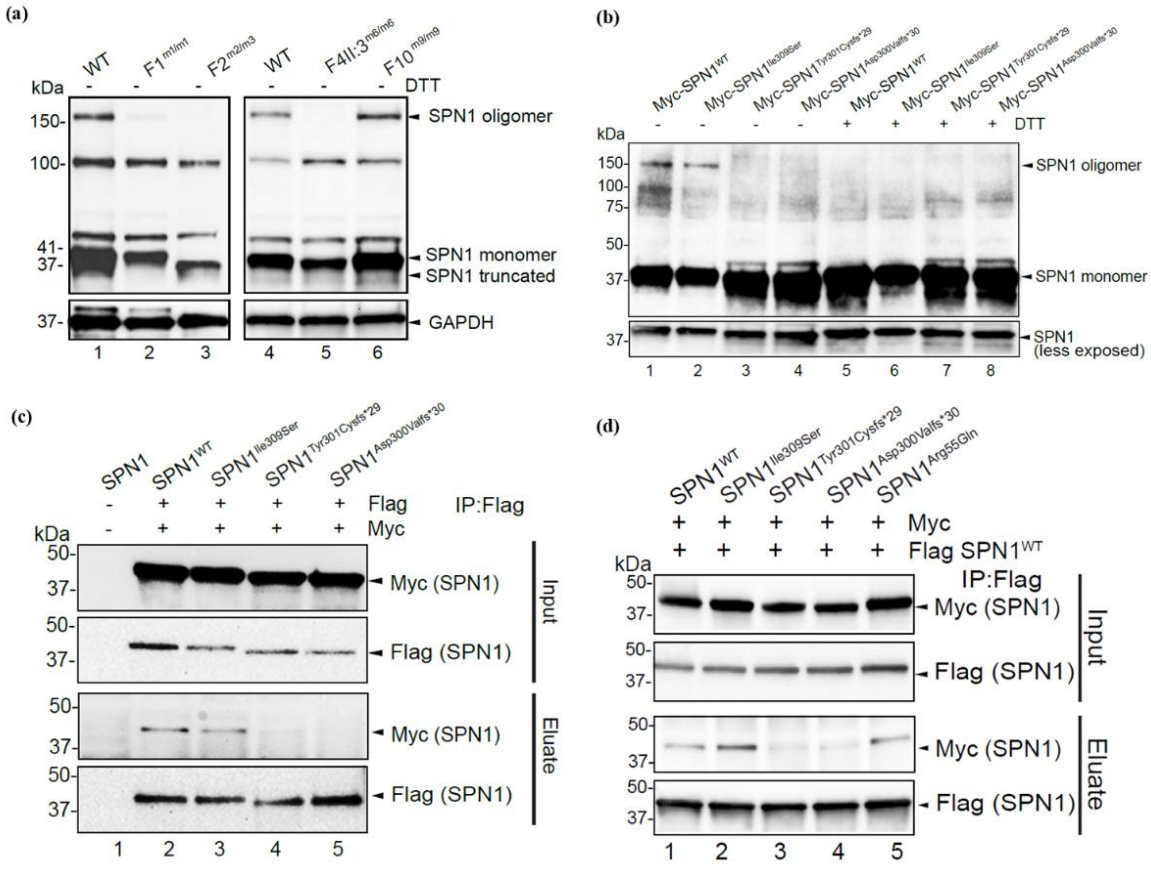

Figure 3.15: SPN1 oligomerization characterization: (a) Western blot (WB) analysis of samples from patients and controls without the use of the reducing agent DTT. The higher band at 150 kDa, which might represent SPN1 oligomerization, was evident in the control, very faint in F1$^{m1/m1}$, but completely absent in patients F2$^{m2/m3}$, and F4II:3$^{m6/m6}$. (b) Transfected HEK 293T cells with Myc-tagged SPN1 constructs representing the WT and patient mutations: Myc-SPN1^{WT}, Myc-SPN1^{Ile309Ser}, SPN1^{Tyr301Cysfs29}, and Myc-SPN1^{Asp300Valfs30}. The samples were loaded twice on the same gel, with and without the addition of the reducing agent DTT. The same 150 kDa upper band, which appeared in Myc-SPN1^{WT} and Myc-SPN^{1Ile309Ser} without DTT, did not appear in the other two constructs (SPN1^{Tyr301Cysfs29} and Myc-SPN1^{Asp300Valfs30}). However, with the addition of DTT, the bands did not appear in any of the constructs. (c) Co-immunoprecipitation (Co-IP) using samples from co-transfected HEK293T cells with Flag- and Myc-tagged constructs. The samples were pulled down using Flag-tagged agarose beads. In the pull-down (PD) incubated with Myc antibody, bands were observed only in Myc-SPN1^{WT} and Myc-SPN1^{Ile309Ser}. (d) Co-

transfection of HEK293T cells with Flag-tagged SPN1^{WT} constructs and Myc-tagged constructs including Myc-SPN1^{WT}, Myc-SPN1^{Ile309Ser}, SPN1^{Tyr301Cysfs29}, Myc-SPN1^{Asp300Valfs30}, and the N-terminus mutation construct Myc-SPN1^{Arg55Gln}. The PD showed bands only for Myc-SPN1^{WT}, Myc-SPN1^{Ile309Ser}, and Myc-SPN1^{Arg55Gln}. (Constructs were prepared with Burak Sarıbaş).

3.4.3 Coiled – coil hydrophobic interactions SPN1 tetramerization

To understand the possible mechanism of this oligomerization, we analyzed further the predicted structures of the C-terminus of SPN1, which we noted previously that the C-terminal alpha-helix present in the WT was disrupted in F1$^{m1/m1}$ and completely lost in the truncating mutations. To assess the ability of this alpha-helix to form an oligomer, we checked its potential for coiled-coil hydrophobic interactions. The online prediction tool LOGICOIL predicted a high likelihood of the C-terminus region of SPN1 forming a tetramer. Next, we used AlphaFold2-Colab to create a C-terminus tetramer model, which was tested again using the Socket2 online tool to assess the potential for hydrophobic interactions.

The results indicated a high likelihood of forming multiple coiled-coil interactions. Interestingly, the Ile309 residue, which is mutated in the F1$^{m1/m1}$ patient, was located in the middle of this coiled-coil interaction, suggesting its importance in the stability of the SPN1 oligomer. (Figure 3.16 (a), (b))

(a)

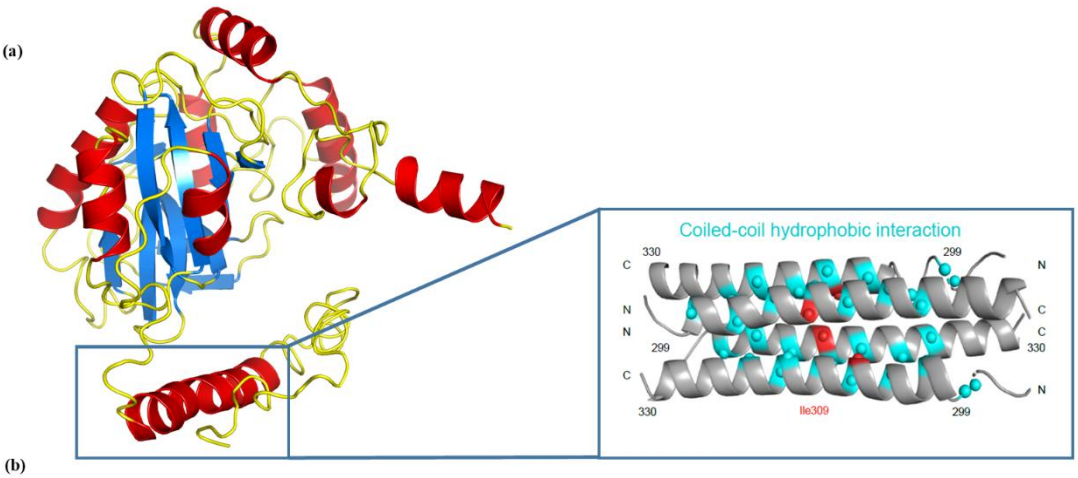

(b)

Residue number	Residue name	heptad Position	Packing Angle(Deg)	Residue number	Residue name	heptad Position	Packing Angle(Deg)	Residue number	Residue name	heptad Position	Packing Angle(Deg)	Residue number	Residue name	heptad Position	Packing Angle(Deg)
Chain A				Chain B				Chain C				Chain D			
305	GLN	d	64.249	323	LYS	g	64.194	320	MET	a	155.868	305	GLN	c	113.298
309	ILE	a	61.52	320	MET	d	50.049	317	LYS	e	141.6	306	LEU	d	100.142
312	HIS	d	97.048	317	LYS	a	96.638	316	GLN	d	123.495	309	ILE	g	108.563
313	LYS	a	12.788	313	LYS	d	58.854	315	SER	c	53.395	312	HIS	c	54.5
316	GLN	d	65.06	312	HIS	g	54.169	313	LYS	a	29.55	313	LYS	d	48.979
320	MET	e	19.868	309	ILE	d	80.438	312	HIS	c	54.909	315	SER	f	52.313
				306	LEU	a	122.32	309	ILE	g	114.072	316	GLN	a	147.643
								308	GLN	g	52.287	320	MET	e	145.348
								305	GLN	d	119.324				

Figure 3.16: SPN1 C-terminus coiled-coiling prediction: (a) Predicted 3D model for wild-type SPN1 with a zoom-in on the C-terminus of the protein, showing the predicted tetramer coiled-coil interaction of the C-terminus alpha-helix. The cyan-colored residues represent the hydrophobic residues involved in the coiled-coil interaction. The red-colored residue is Isoleucine 309, which is also involved in the coiled-coiling and is mutated in patient $F1^{m1/m1}$. (b) Table listing C-terminal residues involved in SPN1 tetramer formation predicted by Socket2 coiled-coil analysis.

3.5 *SNUPN* mutants cause splicing defects in primary fibroblasts

The spliceosomal machinery is primarily responsible for excising introns from transcribed immature mRNA (pre-mRNA) and joining the exons to produce mature mRNAs ready for translation. UsnRNPs as core components of spliceosomes, require precise maturation and structural integrity to ensure correct splicing, thereby facilitating the synthesis of functionally competent proteins (Scotti & Swanson, 2016). Given the central role of UsnRNPs in this

pathway, we aimed to investigate the impact of *SNUPN* mutations on RNA splicing. For this purpose, RNA sequencing (RNA-Seq) was performed on samples derived from patients' primary fibroblasts to assess splicing patterns and differential gene expression profiles in patients compared to wild-type controls, to identify molecular alterations underlying the observed phenotypes.

3.5.1 SPN1 deficiency results in mis-splicing events in key components of extracellular matrix sarcolemma and cytoskeleton

RNA sequencing was performed using RNA extracted from patient and control fibroblasts. The rMATS program was utilized to analyze variable splicing events in patients and controls, including exon skipping (ES), intron retention (IR), alternative 5' splice site (A5SS), alternative 3' splice site (A3SS), and mutually exclusive spliced exons (MXE) events. Over 1,000 genes exhibited alternative splicing events in patients compared to controls, with the majority being ES events, followed by IR (Figure 3.17(a)). To visualize the main genes involved in these alternative splicing events, a volcano plot was used (Figure 3.17(b)).

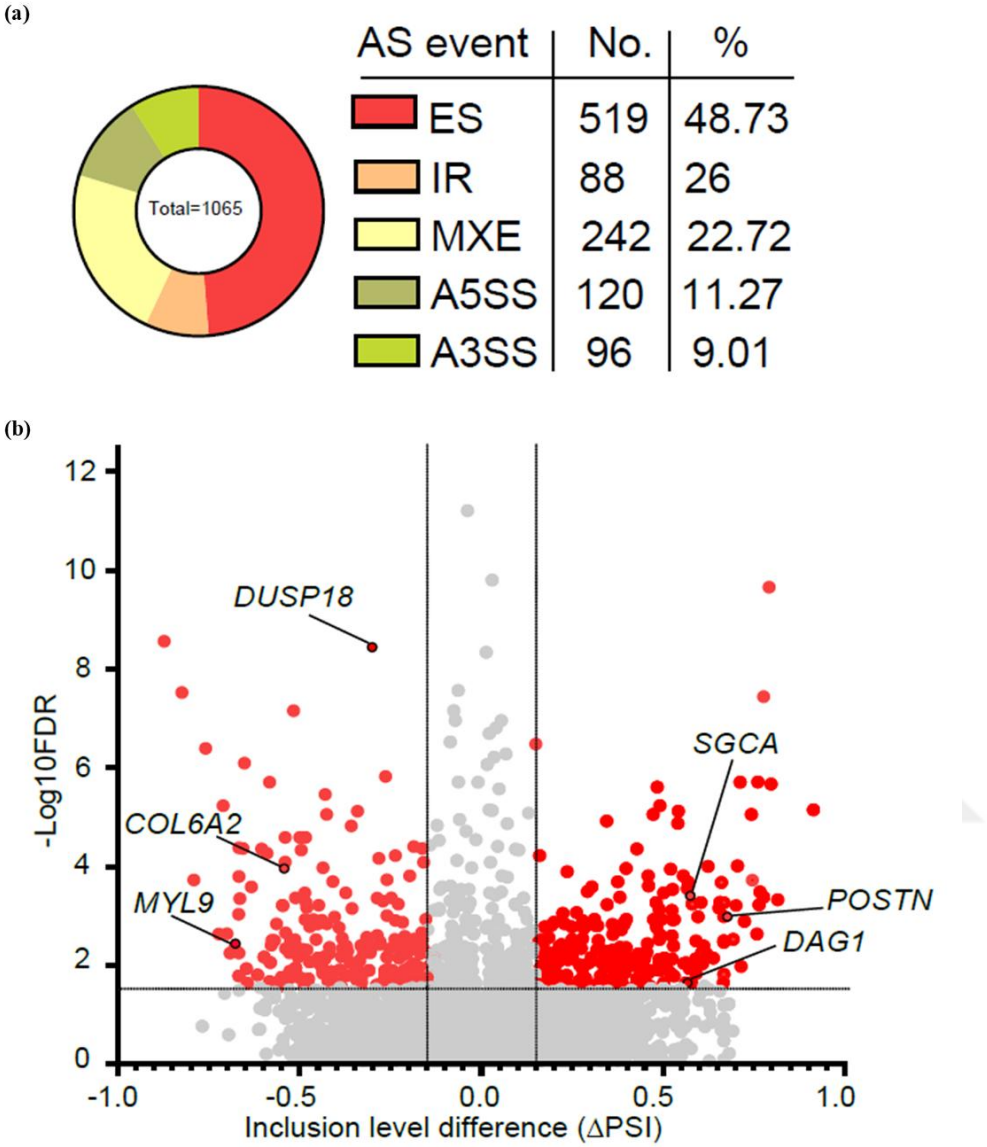

Figure 3.17: Alternative splicing events in primary fibroblasts: (a) Pie chart displaying the number and percentages of various types of alternative splicing events identified by rMATS from RNA sequencing data of patients and controls. The majority of events were exon skipping, followed by intron retention. (b) Volcano plot showing the alternative splicing analysis comparing two wild-type (WT1 and WT2) and three mutants ($F1^{m1/m1}$, $F2^{m2/m3}$ and $F4^{m6/m6}$) primary fibroblasts. The -Log10 (FDR) (False Discovery Rate) is plotted on the y-axis, whereas the x-axis represents the exon inclusion level (ΔPSI) where PSI = Percent Splicing Inclusion. ΔPSI is the difference between the average PSI of the patients compared

to the WTs. ES: exon skipping; IR: intron retention; A5SS: alternative 5' splice site; A3SS: alternative 3' splice site; MXE: mutually exclusive spliced exons.

Subsequently, we aimed to visualize the splicing events of genes with statistically significant differential alternative splicing events. Using the rMATS2Sashimi program, we highlighted the most important and significantly different genes (Figure 3.18). Among these genes were *SGCA, COL6A2, DAG1, POMGNT1, MYL9, POSTN, DUSP18, SYNE1,* and *PLEC*. Many of these genes encode proteins crucial for muscle homeostasis, with mutations in some known to cause muscular dystrophy. For example, *SGCA* mutations cause autosomal recessive limb-girdle muscular dystrophy (LGMDR3) (Vainzof, Souza, Gurgel-Giannetti, & Zatz, 2021). Mutations in *COL6A2* are associated with Ullrich congenital muscular dystrophy 1B (Di Martino et al., 2023). Dystroglycan, encoded by *DAG1*, is a central component of the dystrophin-glycoprotein complex (DGC) (Holt, Crosbie, Venzke, & Campbell, 2000). Mutations in *DAG1* potentially cause muscular dystrophies of varying severity, including severe congenital muscular dystrophy-dystroglycanopathy with brain and eye anomalies (type A) (MDDGA9) (Riemersma et al., 2015), and the milder form muscular dystrophy-dystroglycanopathy (limb-girdle), type C9 (LGMDR16) (LGMD2P) (Hara et al., 2011). Loss of function of *POMGNT1* affects dystroglycan glycosylation, leading to muscular dystrophy (Muntoni, Torelli, & Brockington, 2008). *SYNE1* encodes nesprin-1, a structural protein linking the plasma membrane with actin filaments, with mutations known to cause Emery-Dreifuss muscular dystrophy (Heller, Shih, Kalra, & Kang, 2020). Mutations in the *PLEC* gene, which encodes plectin, an intermediate filament-binding protein, may result in autosomal recessive limb-girdle muscular dystrophy type 17 (Georganopoulou et al., 2021; Gundesli et al., 2010).

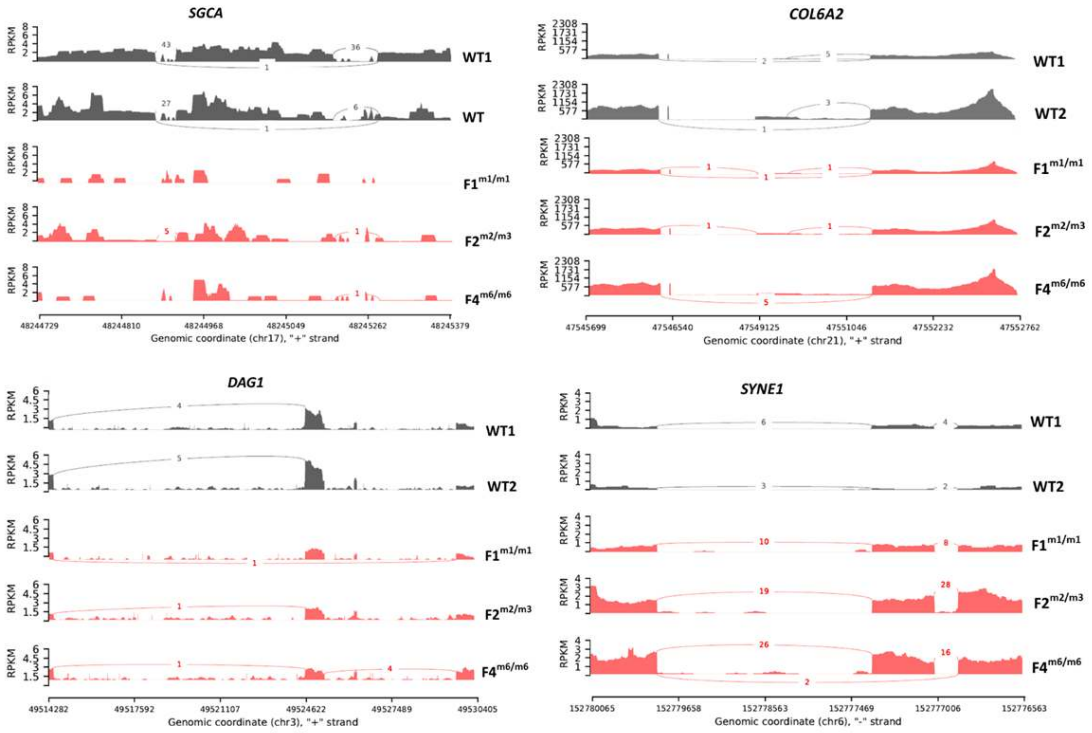

Figure 3.18: Sashimi plots of selected genes: Sashimi plots for *SGCA, COL6A2, DAG1*, and *SYNE1*, highlighting significant alternative splicing events observed in patient samples compared to controls. RPKM: Reads Per Kilobase per Million mapped reads.

3.5.2 Key components for muscle fiber function had variable differential expression in patients' samples.

To gain a comprehensive understanding of the interacting and affected genes, we analyzed transcriptomic data to assess differential gene expression. By comparing RNA sequencing results between patients and controls, numerous genes were identified with varying relative expression levels (Figure 3.19(a)-(b)). These genes were subsequently classified and grouped based on the pathways they are involved in. Interestingly, many of the differentially expressed genes are associated with the extracellular matrix, muscle cell differentiation, and adhesion (Figure 3.19(c)-(d)).

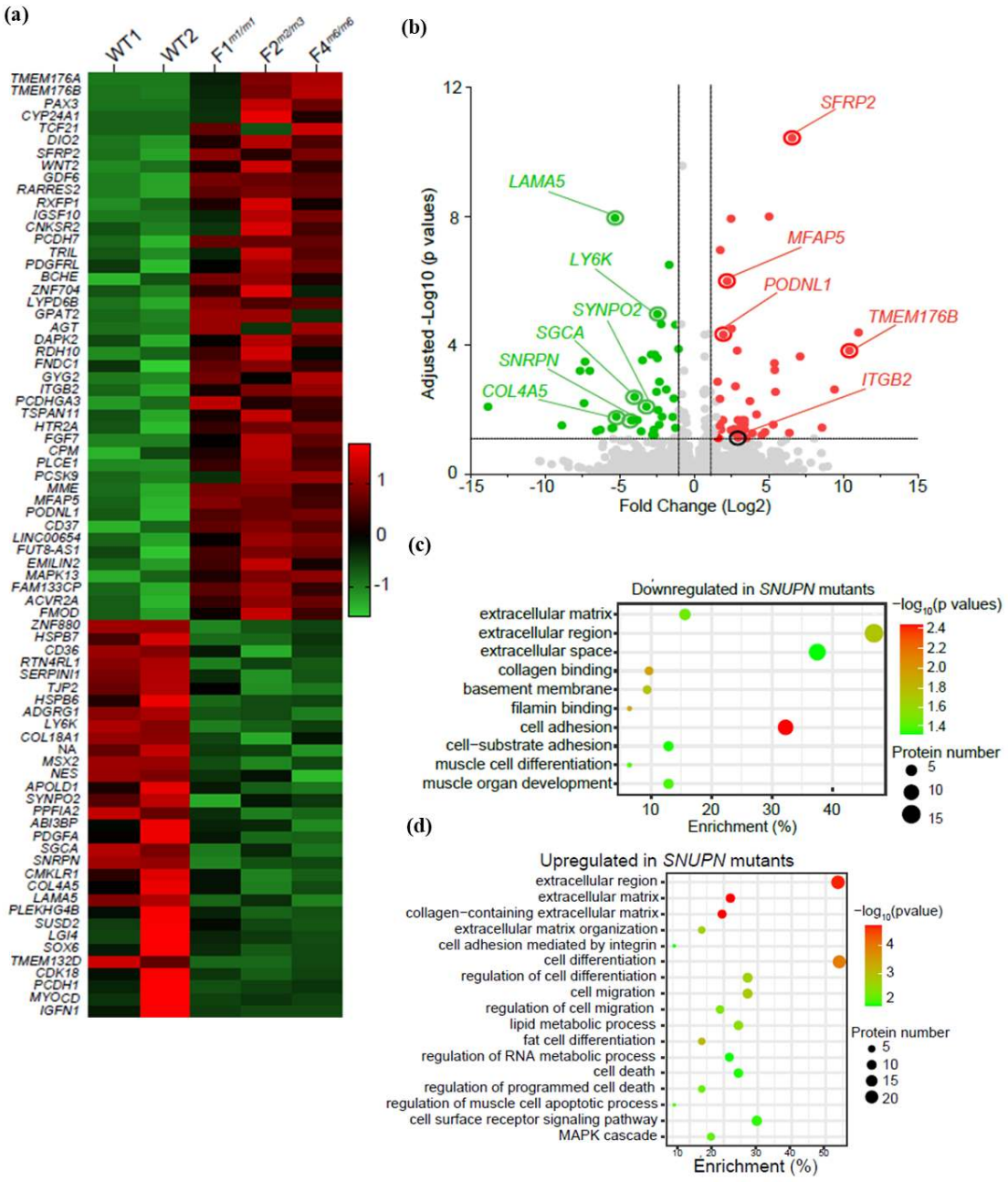

Figure 3.19: RNA sequencing differential expression: (a) Heatmap representing differentially expressed genes between WTs (WT1 and WT2) and patients ($F1^{m1/m1}$, $F2^{m2/m3}$, and $F4^{m6/m6}$). Green and red colors represent lower and higher relative expression levels, respectively. (b) Volcano plot illustrating the upregulated genes (red) and the downregulated genes (green). The gray-colored dots represent genes with statistically insignificant fold changes. (c) Bubble plot depicting gene ontology (GO) enrichment analyses of the downregulated genes. The top 10 affected biological pathways are primarily involved in collagen and extracellular matrix

biology. Circle size indicates the number of differentially expressed genes enriched in each pathway, and circle color represents the enrichment significance, with red indicating high statistical significance. (d) Bubble plot showing the GO enrichment analyses of the upregulated genes. The most affected biological pathways are primarily involved in collagen and extracellular matrix biology. Circle size indicates the number of differentially expressed genes enriched in each pathway, and circle color represents the enrichment significance, with red indicating high statistical significance.

To validate these findings, we selected two of the most downregulated genes (*LAMA5* and *SGCA*) and two of the most upregulated genes (*SFRP2* and *ITGB2*) and performed RT-qPCR. The RT-qPCR results confirmed the RNA sequencing findings (Figure 3.20).

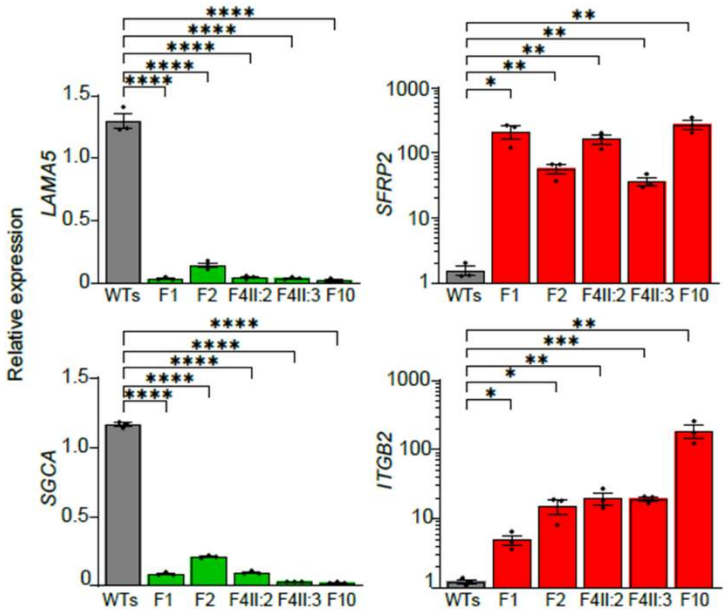

Figure 3.20: RT-qPCR for upregulated and downregulated genes: RT-qPCR validation assay conducted for two downregulated (*LAMA5* and *SGCA*) and two upregulated (*SFRP2* and *ITGB2*) genes identified by RNA-seq. Fold change relative to WTs (n=3) is plotted as mean ± SEM with n=3 biological replicates. *P < 0.05; **P < 0.01; ***P < 0.001; ****P < 0.0001 (two-tailed unpaired t-test).

Several genes exhibiting differential expression in our patient samples play critical roles in maintaining skeletal muscle homeostasis and regeneration. One such gene is *LAMA5*, which encodes Laminin type 5, a crucial component of the basal lamina. LAMA5 has previously been associated with the homeostasis and activation of satellite cells during muscle regeneration (Rayagiri et al., 2018). Additionally, the loss of LAMA5 function has been correlated with systemic disorders, including muscle weakness (Sampaolo et al., 2017). Additionally, loss of LAMA5 function has been linked to disruptions in the actin and vinculin cytoskeletal networks and alterations in the WNT signaling pathway. These molecular changes have been associated with bent bone dysplasia in affected individuals, who also exhibit muscle weakness (Barad et al., 2020). The observed significant downregulation of *LAMA5* in all the patients' samples could have a significant impact on the muscle regeneration and homeostasis.

In addition to the aberrant alternative splicing of *SGCA* previously described, our results demonstrate significant downregulation of *SGCA* in all patients' samples. *SGCA* encodes sarcoglycan alpha, a crucial component of the sarcoglycan complex located at the sarcolemma. It plays a significant role in regulating DAG1 expression, as described previously. The loss of SGCA function is well-documented to cause muscular dystrophy (Trabelsi et al., 2008). These observations further underscore the essential role of *SNUPN* in maintaining and regulating critical components of muscle homeostasis.

SFRP2 encodes soluble frizzled-related protein 2, a known modulator of the Wnt signaling pathway. Wnt proteins are secreted signaling molecules crucial for embryonic development, cell proliferation, and differentiation (Logan & Nusse, 2004). Interestingly, recombinant SFRP2 has been shown to inhibit myoblast differentiation in C2C12 cells, as well as in primary satellite cell cultures from mouse and rabbit, in a dose-dependent manner (Descamps et al., 2008). The observed significant upregulation of *SFRP2* in our patient samples could potentially have similar inhibitory effects on muscle regeneration and differentiation.

ITGB2 encodes Integrin Beta-2, a member of the integrin family of membrane glycoproteins. Loss of function mutations in ITGB2 are associated with leukocyte adhesion deficiency. ITGB2 has also been implicated in satellite cell proliferation and differentiation via

inflammatory responses triggered by mechanical stress (Marino et al., 2008). Recently, an upregulation of *ITGB2* was observed in a LAMA2-deficient mouse model (Tan et al., 2025), which aligns with the elevated *ITGB2* expression observed in our patients' samples.

3.6 SPN1 dysfunction affects the integrity of key components of extracellular matrix sarcolemma and cytoskeleton

Previous results clearly demonstrated aberrant expression levels and alternative splicing events of numerous genes that play critical roles in muscle fiber function and integrity. Consequently, we investigated these components at the protein level. One of the downregulated genes identified was *COL4A5*, an isoform of COLLAGEN IV, which was markedly reduced in patients' fibroblasts compared to controls (Figure 3.21(a)). Immunofluorescence assays on cross-sectional muscle fibers from patients $F1^{m1/m1}$ and $F2^{m2/m3}$ confirmed a decrease in COLLAGEN IV levels (Figure 3.21(b)). COLLAGEN type IV forms the essential network of the basal lamina within the extracellular matrix (ECM) (Sanes, 2003).

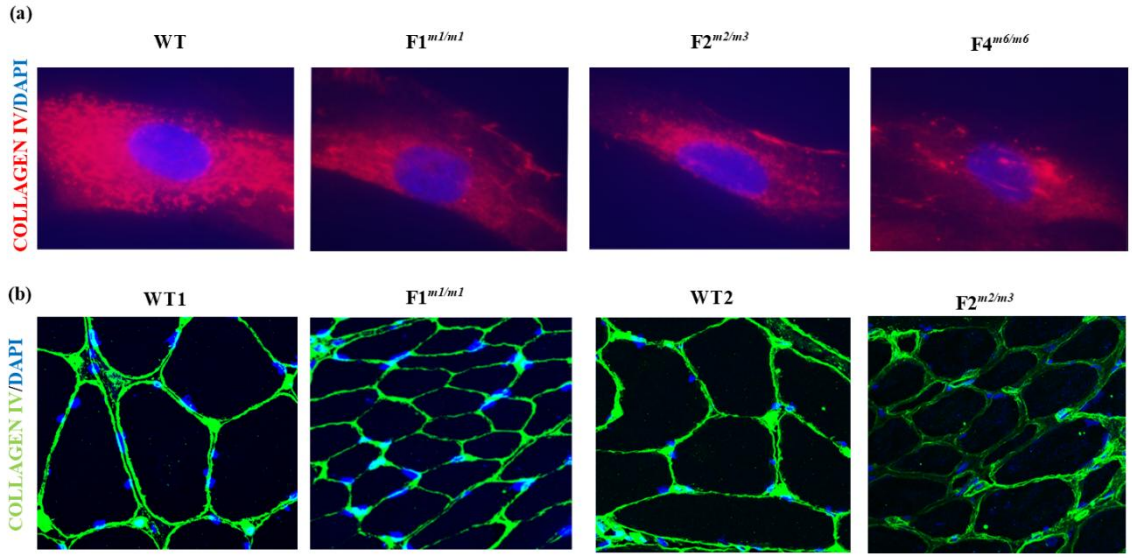

Figure 3.21: COLLAGEN IV decrease in SPN1 mutant fibroblasts and muscle: (a) Immunofluorescence staining of COLLAGEN IV (red) in fibroblasts. COLLAGEN IV levels are reduced in patient fibroblasts ($F1^{m1/m1}$, $F2^{m2/m3}$, and $F4^{m6/m6}$) compared to controls. Nuclei are stained with DAPI (blue). (b) Immunofluorescence staining of COLLAGEN IV (green) in muscle cross-sections. Patient muscle fibers ($F1^{m1/m1}$, and $F2^{m2/m3}$) exhibit reduced

COLLAGEN IV levels compared to wildtype (WT) controls. Nuclei are stained with DAPI (blue). (IF imaging done by Hilal Pırıl Saraçoğlu).

Sarcoglycan α (SGCA), a component of the sarcoglycan complex located on the sarcolemma, was also reduced in immunofluorescence assays of patients' muscle sections compared to controls (Figure 3.22(a)). The sarcoglycan complex is adjacent to the dystrophin-associated glycoprotein (DAG) complex, which consists of two subunits: the extracellular α-DAG and the transmembrane β-DAG. This complex functions to firmly connect the ECM to the cytoskeleton. SGCA plays a protective role by preventing the cleavage of β-DAG^{43} into the non-functional β-DAG^{30} by metalloproteinases, a process typically observed in muscle tissue of patients with sarcoglycanopathies (Fukai et al., 2017). To assess whether decreased SGCA levels impacted the integrity of β-DAG^{43}, we performed Western blot analysis of β-DAG from patients' primary fibroblasts and compared the results to controls. Strikingly, in the patients, the primary band observed was the cleaved, non-functional β-DAG^{30}, whereas in the controls, the upper β-DAG^{43} band predominated (Figure 3.22(b)).

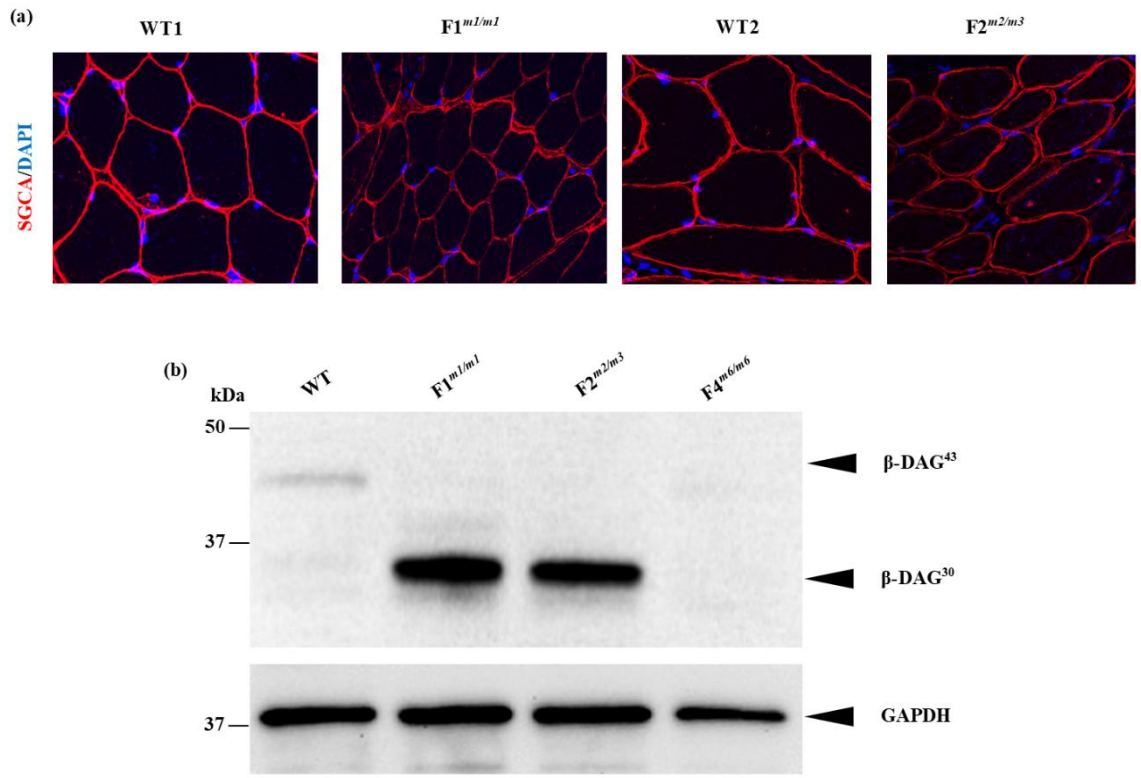

Figure 3.22: Dystroglycan components are dysregulated in SPN1 mutant primary fibroblasts and muscle: (a) Immunofluorescence staining of SARCOGLYCAN α (red) in muscle cross-sections. SARCOGLYCAN α levels are reduced in patients $F1^{m1/m1}$ and $F2^{m2/m3}$ compared to WT controls. Nuclei are stained with DAPI (blue). (b) Western blot analysis of β-DYSTROGLYCAN (β-DAG) in fibroblast protein samples from patients $F1^{m1/m1}$, $F2^{m2/m3}$, and $F4^{m6/m6}$, compared to WT controls. In patients $F1^{m1/m1}$ and $F2^{m2/m3}$, the predominant β-DAG band corresponds to the cleaved, non-functional form (30 kDa), indicating insufficient protection by the reduced SARCOGLYCAN α levels. In contrast, the WT samples predominantly show the full-length β-DAG (43 kDa). In sample $F4^{m6/m6}$, β-DAG bands were not detectable. (IF imaging done by Hilal Pırıl Saraçoğlu).

Finally, we examined whether the defects observed in the ECM and the dystrophin-glycoprotein complex (DGC), known to directly affect cytoskeletal integrity, resulted in dysregulation of the cytoskeleton. Immunofluorescence analysis of patients' fibroblasts revealed aggregates of F-ACTIN, β-TUBULIN (a microtubule subunit), VIMENTIN (a type III intermediate filament), and VINCULIN (a scaffolding protein critical for cell–matrix

adhesion). Both F-ACTIN and β-TUBULIN exhibited disorganization and aggregation, while VIMENTIN and VINCULIN levels were elevated in patients' cells compared to controls (Figure 3.23(a)-(d)). Additionally, in muscle cross-sections from patients $F1^{m1/m1}$ and $F2^{m2/m3}$, abnormal sarcoplasmic aggregates of DESMIN, an intermediate filament protein, were observed. DESMIN aggregates are usually seen in desminopathies, a sub-type of muscular dystrophies. This finding was corroborated by the presence of αβ-CRYSTALLIN, a small heat shock protein associated with DESMIN. Aggregates of F-ACTIN were also evident in the muscle section of patient $F2^{m2/m3}$, which conforms what was observed in the fibroblasts (Figure 3.23(e)-(g)).

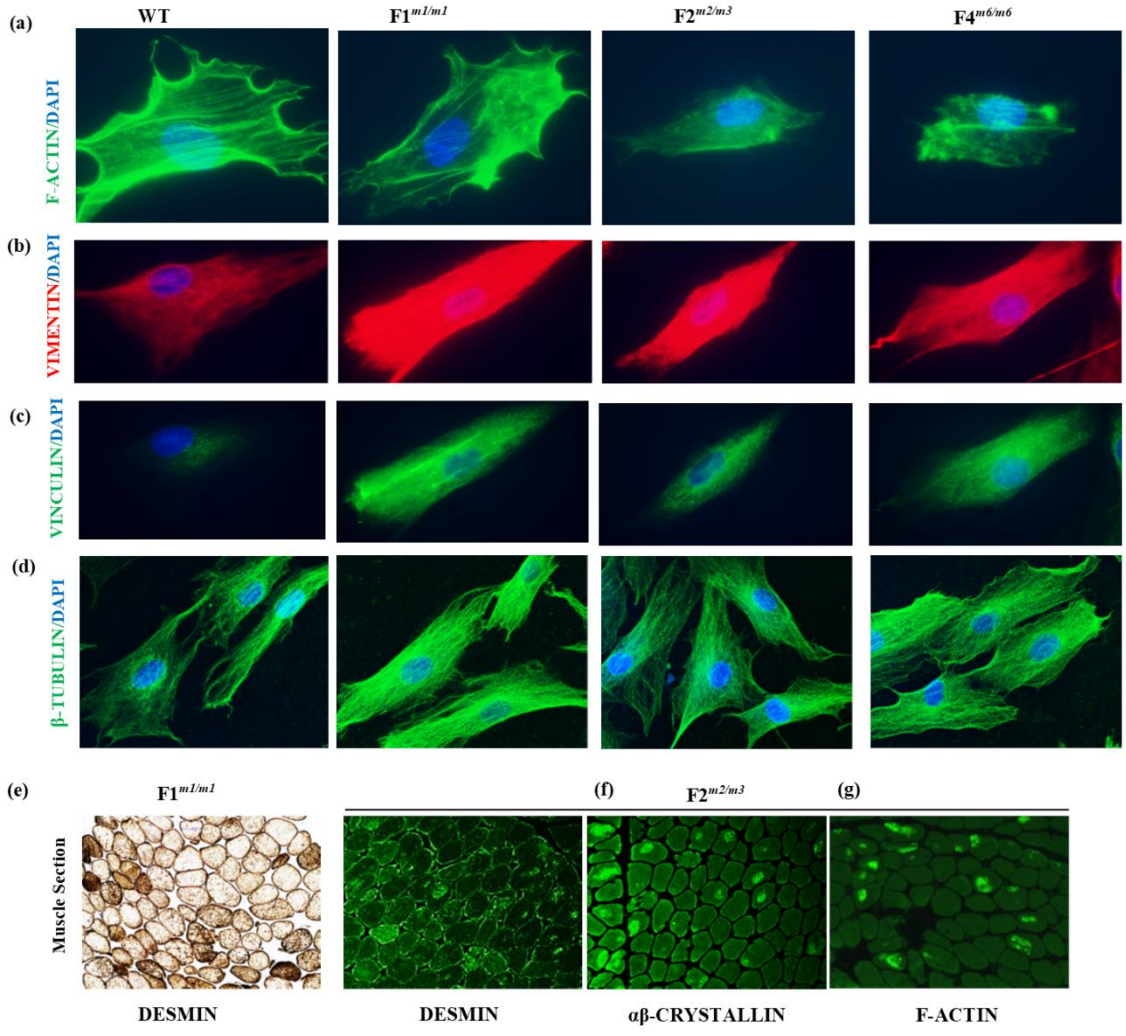

Figure 3.23: Cytoskeleton components aggregation in SPN1 mutant fibroblasts and muscle: (a) Immunofluorescence staining of F-ACTIN (green) in primary fibroblasts from patients

(F1$^{m1/m1}$, F2$^{m2/m3}$, and F4$^{m6/m6}$) shows decreased levels of F-ACTIN and its aggregated distribution within the cytoplasm. (b)-(d) Immunofluorescence staining of VIMENTIN (red) (b), VINCULIN (green) (c), and β-TUBULIN (green) (d) demonstrates increased levels of these proteins in patient fibroblasts compared to controls. (e) Immunostaining of DESMIN in muscle cross-sections from patients F1$^{m1/m1}$, F2$^{m2/m3}$ reveals abnormal intra-sarcoplasmic aggregates of DESMIN. (f) Abnormal aggregates of αβ-CRYSTALLIN are observed in muscle cross-sections from patient F2$^{m2/m3}$, a hallmark feature often associated with Desminopathies. (g) Immunostaining of F-ACTIN (green) in the muscle cross-section of patient F2$^{m2/m3}$ confirms abnormal sarcoplasmic aggregates, consistent with observations in fibroblasts. (IF imaging done by Hilal Pırıl Saraçoğlu).

3.7 SPN1 mutations and SMN dysregulation

As part of the import complex analysis, we investigated the levels of additional key components beyond UsnRNPs. As previously established, SMN is essential to UsnRNP assembly and their localization into Cajal bodies is critical for maintaining them. To assess its expression, we first examined *SMN* mRNA levels in primary fibroblasts derived from patients. Notably, *SMN* transcript levels were consistently and significantly upregulated in patient samples compared to controls (Figure 3.24(a)). This upregulation was also evident in SPN1 mutant HeLa cell lines, where *SMN* mRNA expression was markedly elevated relative to wild-type (WT) cells (Figure 3.24(b)).

Surprisingly, despite the increased *SMN* transcript levels, total SMN protein levels were reduced in patients' fibroblasts (Figure 3.24(c)). A comparable trend was observed in SPN1 mutant HeLa cells, where SMN protein expression was significantly lower in mutants relative to WT cells (Figure 3.24(d)).

These findings suggest a potential feedback mechanism between SPN1 and SMN. Furthermore, they indicate that SPN1 may be essential for the post-transcriptional stability of SMN, underscoring a previously unrecognized regulatory interplay between these two proteins.

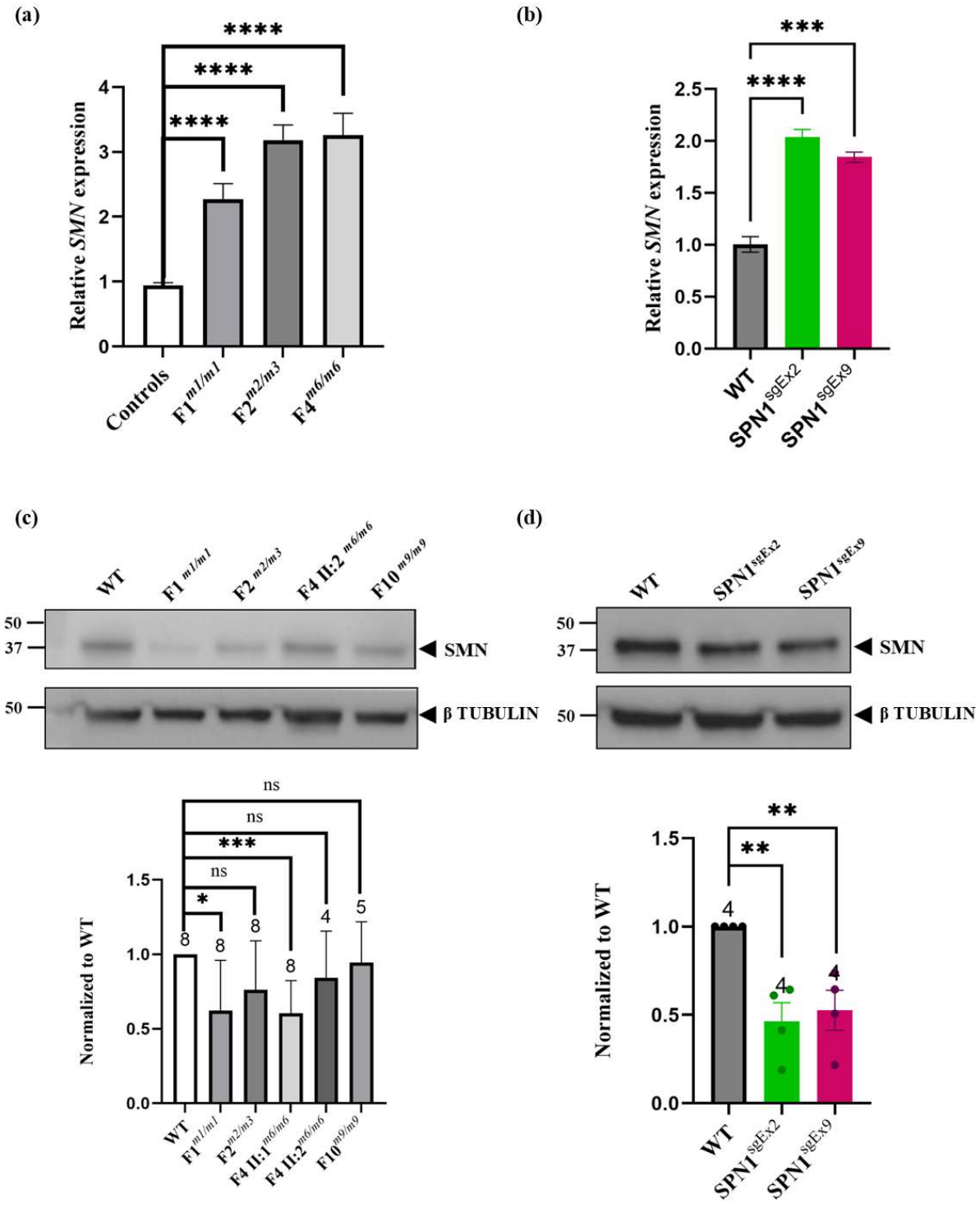

Figure 3.24: SMN dysregulation in SPN1 mutant cells: (a) qPCR analysis of *SMN* mRNA expression in primary fibroblasts from patients and controls. All patient samples exhibited a significant upregulation of *SMN* gene expression compared to controls ($P < 0.0001$ for all comparisons). (b) qPCR analysis of *SMN* mRNA expression in wild-type (WT) and SPN1

mutant HeLa cells. Both mutant cell lines displayed a significant upregulation of *SMN* expression relative to WT ($P < 0.0001$). (c) Western blot analysis of SMN protein levels in total protein extracts from patient and control fibroblasts. Although a general trend of reduced SMN protein levels was observed in all patient samples, statistical significance was reached only in $F1^{m1/m1}$ and F4 $II{:}1^{m6/m6}$ samples ($P = 0.006$ and $P = 0.0002$, respectively). (d) Western blot analysis of SMN protein levels in WT and SPN1 mutant HeLa cells. SMN protein levels were significantly reduced in mutant cell lines compared to WT ($P < 0.0001$).

3.7.1 C-terminus is essential for SPN1-SMN interaction

Previous studies have demonstrated a direct interaction between SPN1 and SMN in the cytoplasm. Notably, the same study reported that SMN was capable of interacting with an N-terminally deleted SPN1 variant (Narayanan, Ospina, Frey, Hebert, & Matera, 2002). In line with these findings, we investigated the heterodimerization of SPN1 and SMN through immunoprecipitation assays using wild-type (WT) and mutant SPN1 constructs transfected into HeLa cells alongside an SMN WT construct. Our results revealed that SPN1-WT, as well as the *m1* ($SPN1^{Ile309Ser}$) and *m9* ($SPN1^{Arg55Gln}$) mutants, were effectively pulled down by the SMN construct. In contrast, the *m6* ($SPN1^{Tyr301Cysfs*29}$) and *m7* ($SPN1^{Asp300Valfs*30}$) mutants failed to interact with SMN, while *m11* ($SPN1^{Gly159Asp}$) and *m12* ($SPN1^{Ser145\_Gly146delinsArgSer}$) exhibited only a weak interaction (Figure 3.25).

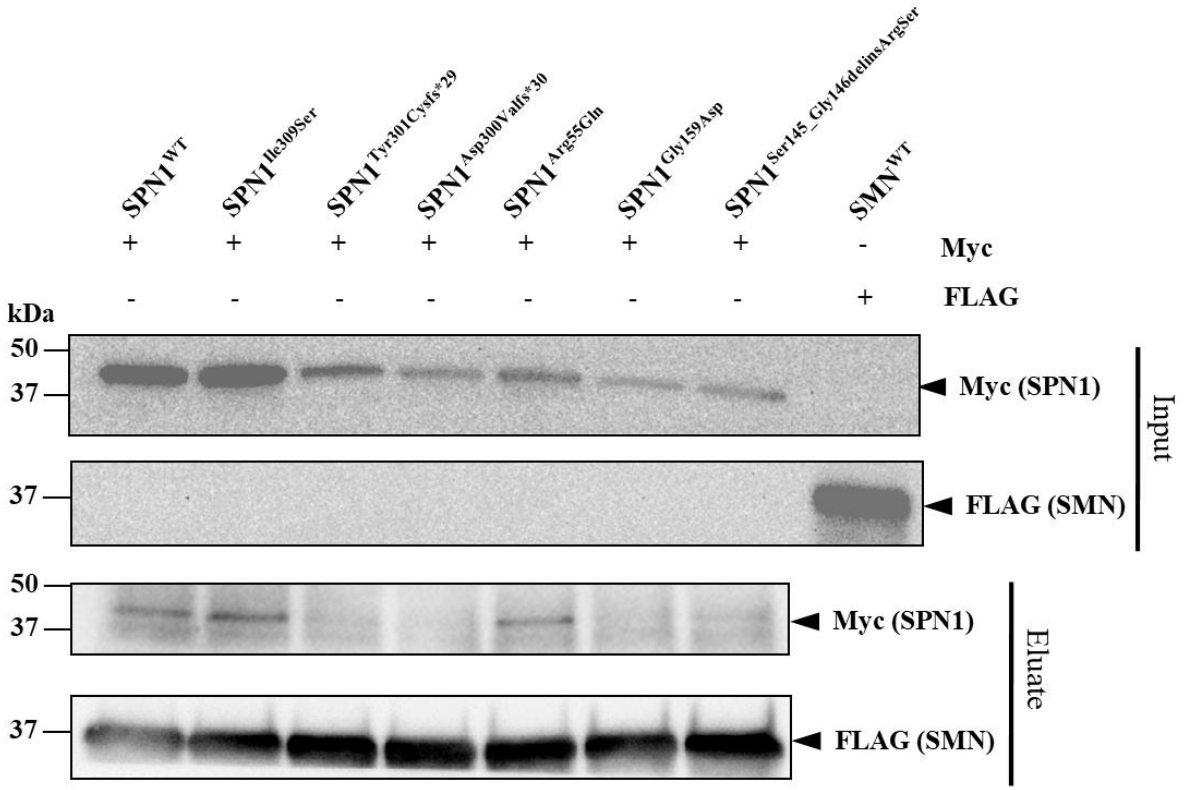

Figure 3.25: SPN1 C-terminus mutations leads to SPN1-SMN interaction defect: Immunoblot analysis depicting the co-immunoprecipitation of transfected HeLa cell extracts. Cells were transfected with either Myc-tagged SPN1 constructs ($SPN1^{Ile309Ser}$, $SPN1^{Arg55Gln}$, $SPN1^{Tyr301Cysfs*29}$, $SPN1^{Asp300Valfs*30}$, $SPN1^{Gly159Asp}$, $SPN1^{Ser145\_Gly146delinsArgSer}$, or a FLAG-tagged SMN construct. Immunoprecipitation was performed using FLAG agarose beads to assess the interaction between SPN1 variants and SMN in vitro.

3.8 SPN1 mutations impact autophagy homeostasis

3.8.1 Dysregulated expression and mis-splicing for key autophagy genes in patients' cells

RNA sequencing analysis of primary fibroblasts derived from patients, compared to healthy controls, revealed dysregulation in the expression of multiple autophagy-related genes. Figure 3.26(a) illustrates the changes in expression levels of selected key autophagy markers. Among the most upregulated genes in patients' fibroblasts was Phospholipase C, Epsilon-1 (*PLCE1*), a member of the phospholipase family known to activate the MAPK cascade pathway (Lopez,

Mak, Ding, Hamm, & Lomasney, 2001). *PLCE1* activation has been associated with autophagy inhibition and disruption of autophagosome formation. Furthermore, PLCE1 overexpression in cancer cells has been linked to p53 downregulation (Chen et al., 2020; Shimozawa, Anzai, Satow, & Fukami, 2017). Another significantly upregulated gene was Mitogen-Activated Protein Kinase 13 (*MAPK13*), also known as p38δ, which is a key regulator of extracellular stress signaling (Zhong et al., 2014). p38 MAPKs are known to modulate autophagy, where their activation enhances autophagy, while their inhibition leads to its suppression. MAPK13 phosphorylates and activates p62, a critical regulatory factor in autophagy (Linares et al., 2015; C. Zhang, Gao, Li, Deng, & Jiang, 2018). Additionally, Death-Associated Protein Kinase 2 (*DAPK2*) was significantly upregulated in patients' fibroblasts. DAPK2 interacts with and phosphorylates mTORC1, leading to its inhibition and subsequent activation of autophagy (Ber et al., 2015). Conversely, *CD36*, a scavenger receptor that co-localizes with LC3B on autophagosomes, was significantly downregulated in patient samples. Loss of CD36 has been associated with impaired autophagosome formation in immune cells (He et al., 2021).

Further analysis focused on alternative splicing events in autophagy-related genes using transcriptomic data (Figure 3.26(b), (c)). Among the most notable findings was significant exon skipping (SE) in the Damage-Regulated Autophagy Modulator (*DRAM2*) gene, which is localized to the lysosomal membrane and facilitates autophagy induction by catalyzing the conversion of LC3BI to LC3BII. Inhibition of DRAM2 has been shown to interfere with starvation-induced autophagy (Yoon, Her, Kim, Jang, & Park, 2012). Another key autophagy regulator, Beclin1 (*BECN1*), also exhibited exon skipping. BECN1 is a critical regulatory subunit of the PI3KC3 complex, which is essential for autophagosome formation and membrane elongation (Tran, Fairlie, & Lee, 2021). Additionally, significant SE alternative splicing was observed in *ATG13*, a gene crucial for autophagy initiation (Yamamoto et al., 2016). Among the genes exhibiting intron retention (RI), Unc-51-like kinase 3 (*ULK3*) was identified. Increased ULK3 expression has been linked to autophagy activation. (Goruppi et al., 2017)

One of the key components of the autophagy machinery, *TMEM41B*, was also investigated. TMEM41B plays a fundamental role in lipid scrambling from the ER to the autophagosome during the elongation phase of autophagy. Additionally, *TMEM41B* mis-splicing has been implicated in spinal muscular atrophy (SMA) and the neurodegeneration associated with the disease (Lotti et al., 2012). *TMEM41B* was significantly upregulated in patient fibroblasts, and this result was further validated in HeLa SPN1 mutant cells (Figure 3.26(d), (e)).

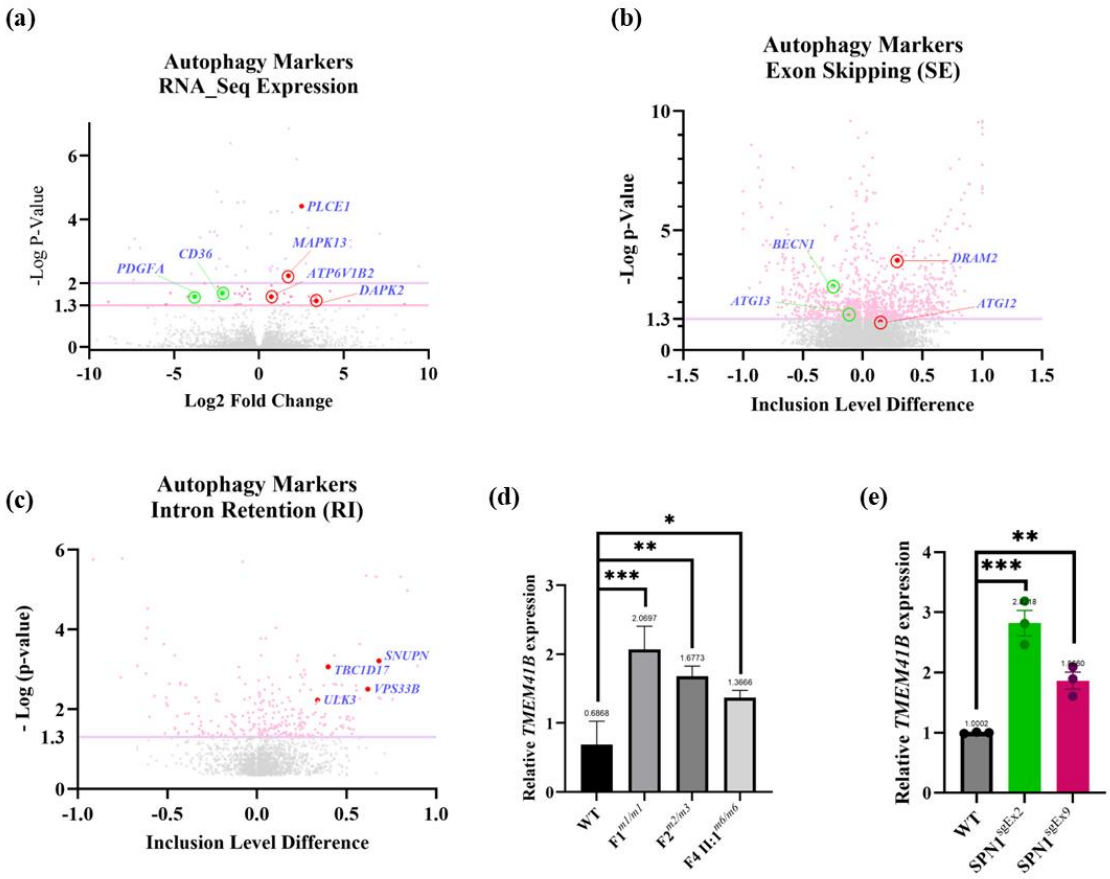

Figure 3.26: Dysregulated autophagy-related genes in SPN1 mutant cells: (a) Volcano plot representing differential gene expression from RNA-Seq data analyzed from patients compared to controls. The annotated genes in the plot are involved in the autophagy pathway. A -log p-value of 1.3 corresponds to $p < 0.05$, while a -log p-value of 2 corresponds to $p < 0.01$. Genes highlighted in green are downregulated, whereas genes represented by red dots are upregulated. (b) & (c) Volcano plots depicting alternative splicing events identified from RNA-Seq data in patients compared to controls. (b) represents mRNA exon skipping events,

while (c) illustrates intron retention events. (d) qPCR analysis of *TMEM41B* gene expression in patients' fibroblasts compared to controls. (e) qPCR analysis of *TMEM41B* gene expression in SPN1 mutant HeLa cells compared to wild-type cells. Statistical significance is indicated as follows: (*: $p < 0.01$, **: $p < 0.001$, ***: $p < 0.0001$)

3.8.2 Autophagy proteins' dysregulation in SPN1 mutant HeLa cells

To further validate autophagy dysregulation, we assessed the expression levels of key autophagy markers in SPN1 mutant HeLa cells compared to wild-type (WT) controls. The primary markers analyzed were p62 and LC3B (Figure 3.27(a), (b)).

As previously described, p62 functions as an autophagy adaptor, recognizing polyubiquitinated target proteins during the early phase of autophagy. Subsequently, p62 is incorporated into autophagosomes and degraded within autolysosomes along with the targeted proteins or organelles. LC3B-I, a cytosolic form of LC3, is converted to LC3B-II upon autophagy activation, facilitating autophagosome membrane expansion.

When analyzing SPN1 mutant HeLa cells, we observed fluctuating p62 levels across independent experiments, with no consistent trend compared to WT cells. In contrast, LC3B-II levels and, more importantly, the LC3B-II/LC3B-I ratio, were significantly increased in mutant cells compared to WT. These findings suggest autophagy activation, with a potential disruption in autophagic flux, as indicated by the inconsistent p62 levels.

Interestingly, p53 protein levels were dramatically reduced in SPN1 mutant HeLa cells compared to WT (Figure 3.27(c)). This reduction could be attributed to dysregulation of p53 regulatory mechanisms, potentially leading to its suppression, as previously discussed.

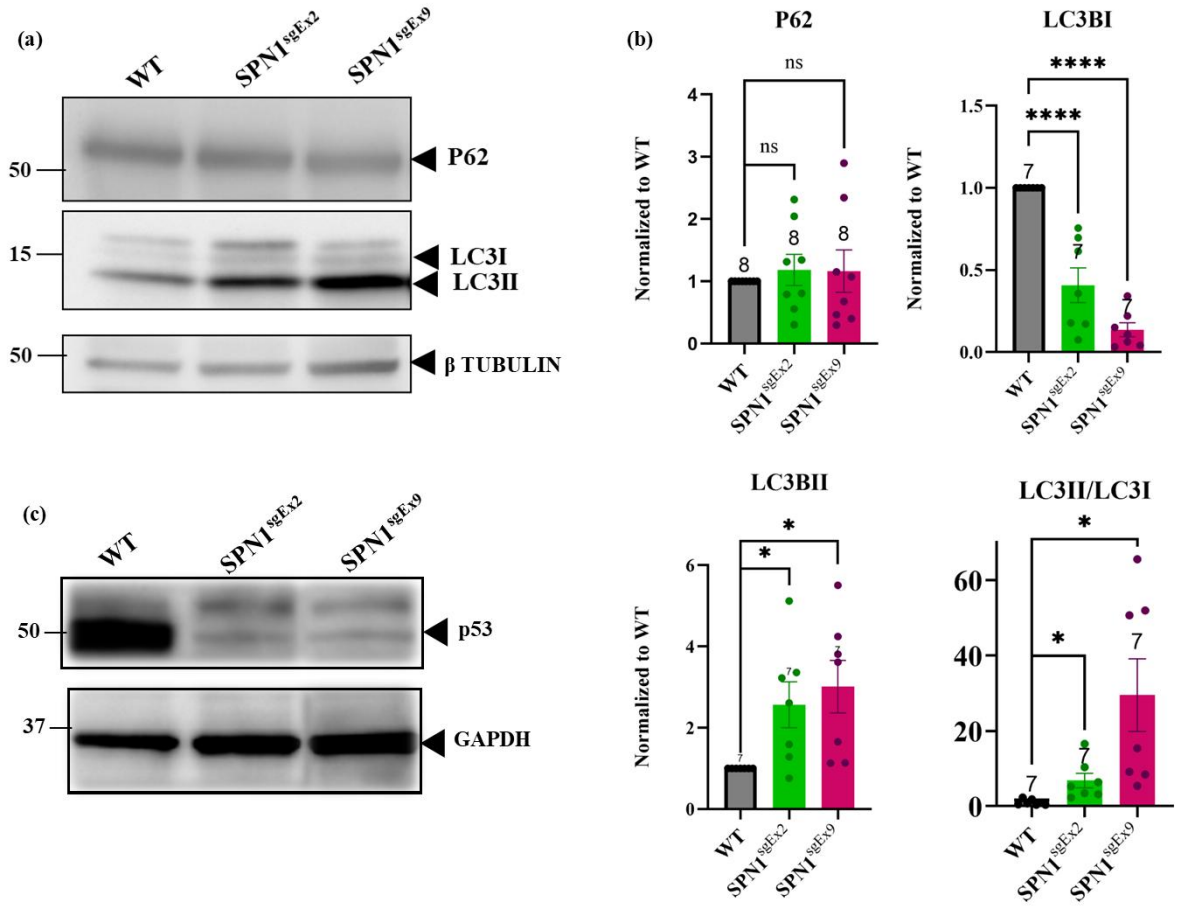

Figure 3.27: Autophagy markers dysregulation in SPN1 mutant HeLa cells: (a) Western blot analysis of p62, LC3B-I, and LC3B-II in WT and SPN1 mutant HeLa cells. β-Tubulin was used as a loading control. (b) Quantification of western blot data for p62, LC3B-I, LC3B-II, and the LC3B-II/LC3B-I ratio. p62 quantification was performed from 8 biological replicates, showing high variability between replicates with no significant difference between WT and mutant cells. LC3B-I quantification was performed from 7 biological replicates, demonstrating significantly lower levels in SPN1 mutant cells compared to WT. Conversely, LC3B-II levels were significantly higher in SPN1 mutants compared to WT. The LC3B-II/LC3B-I ratio was also significantly elevated in SPN1 mutant cells compared to WT. (c) Western blot analysis of p53 protein levels in WT and SPN1 mutant HeLa cells. GAPDH was used as a loading control. p53 levels were consistently and dramatically reduced in SPN1 mutant cells compared to WT across three biological replicates.

Chapter 4:**DISCUSSION**

In this study, we present 21 patients from 18 unrelated families who share a common clinical phenotype characterized by progressive muscle weakness with varying degrees of severity, associated to *SNUPN* gene mutations. In addition to muscular dystrophy, several patients exhibited extra-muscular manifestations, including central nervous system abnormalities, such as cerebral and cerebellar atrophy, and congenital cataracts.

SNURPORTIN protein (SPN1) plays a crucial role in facilitating the nuclear transport of key spliceosomal components (UsnRNPs) in conjunction with SMN. Notably, most identified mutations were clustered within the C-terminal domain of SPN1, emphasizing the functional significance of this region. Furthermore, this pattern suggests that the C-terminus may represent a mutational hotspot within the *SNUPN* gene.

Dysfunctional SPN1 impairs UsnRNP nuclear import, leading to abnormal alternative splicing events in multiple genes encoding proteins essential for muscle homeostasis and autophagy processes. Among the affected proteins are extracellular matrix components (COLLAGEN IV and COLLAGEN VI), sarcolemmal proteins (DYSTROGLYCAN and SARCOGLYCAN), and cytoskeletal proteins (ACTIN, VINCULIN, and DESMIN). This dysregulation likely compromises the structural integrity and function of skeletal muscle fibers, resulting in muscle damage and fibrosis. The loss of the SPN1-SMN complex may influence both the stability and functionality of SMN. Furthermore, the observed alterations in autophagic markers suggest a disruption in the autophagy process, particularly affecting autophagic flux. Figure 4.1 illustrates the proposed pathophysiology underlying SPN1-deficient muscular dystrophy.

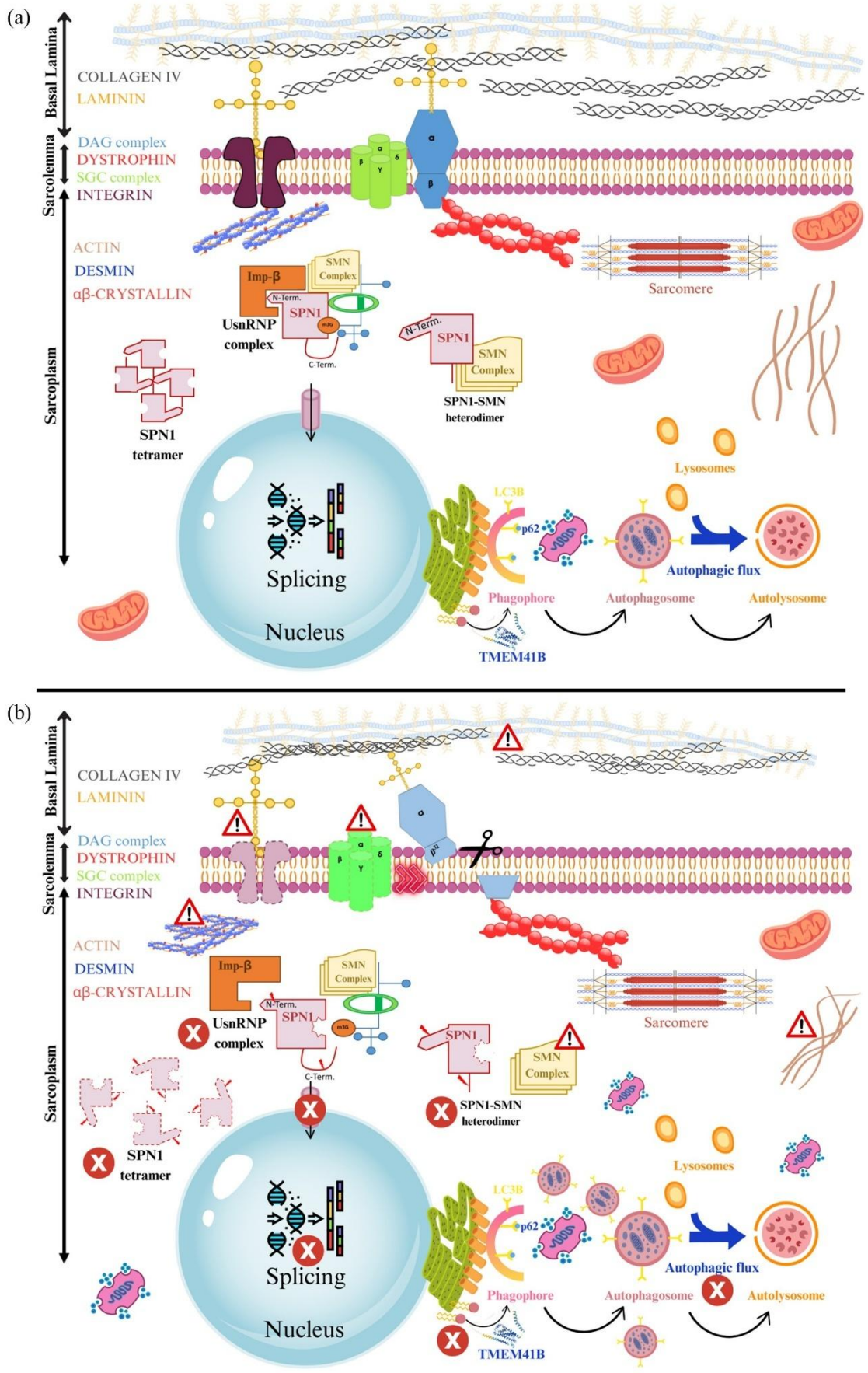
(a)
Basal Lamina
COLLAGEN IV
LAMININ
Sarcolemma
DAG complex
DYSTROPHIN
SGC complex
INTEGRIN
Sarcoplasm
ACTIN
DESMIN
αβ-CRYSTALLIN
Imp-β
SMN Complex
N-Term.
SPN1
UsnRNP complex
C-Term.
SPN1 tetramer
SPN1-SMN heterodimer
Sarcomere
Lysosomes
LC3B
p62
Ub
Autophagic flux
Phagophore
Autophagosome
Autolysosome
TMEM41B
Splicing
Nucleus
(b)
Basal Lamina
COLLAGEN IV
LAMININ
Sarcolemma
DAG complex
DYSTROPHIN
SGC complex
INTEGRIN
Sarcoplasm
ACTIN
DESMIN
αβ-CRYSTALLIN
Imp-β
SMN Complex
N-Term.
SPN1
UsnRNP complex
C-Term.
SPN1 tetramer
SPN1-SMN heterodimer
Sarcomere
Lysosomes
LC3B
p62
Ub
Autophagic flux
Phagophore
Autophagosome
Autolysosome
TMEM41B
Splicing
Nucleus

Figure 4.1: Proposed pathophysiology of SPN1-deficient muscular dystrophy: (a) In healthy muscle fibers, SPN1 undergoes oligomerization, facilitating the normal nuclear transport of UsnRNPs and ensuring accurate pre-mRNA splicing. This process maintains the proper production of mature transcripts and proteins essential for skeletal muscle integrity, thereby preserving the structure and function of the extracellular matrix, basal lamina, sarcoplasm, and cytoskeleton. Furthermore, SPN1 interacts with SMN, forming a heteromeric complex that contributes to the stability and functionality of the SMN protein. Additionally, the autophagy pathway remains intact, with core components such as LC3B, P62, and TMEM41B, along with regulatory elements, functioning normally. This ensures efficient clearance of damaged organelles, including mitochondria. (b) In contrast, *SNUPN* mutations result in SPN1 loss-of-function, impairing its ability to oligomerize and maintain protein interactions necessary for nuclear transport. Consequently, disruption in nuclear import of UsnRNPs leads to aberrant alternative splicing events and the generation of mis-spliced mRNA. Abnormal protein products accumulate in critical structural regions, including the extracellular matrix, basal lamina, sarcoplasm, and cytoskeleton, ultimately resulting in cytoskeletal disorganization, muscle fiber dysfunction, and fibrosis. Additionally, SMN functionality is compromised due to impaired interaction with SPN1. This disruption extends to the autophagic process, including the autophagic flux, causing perturbations in autophagic markers such as LC3B and P62, and impairing autophagic clearance. As a result, damaged mitochondria and other organelles accumulate, contributing further to muscular pathology and dysfunction.

4.1 Genotype-phenotype correlation and clinical variability

The clinical presentation of affected individuals was consistent with muscular dystrophy, exhibiting a spectrum of disease severity. The age of onset varied from early infancy (prior to ambulation) to later childhood, with variable disease progression and prognosis. While some patients retained ambulatory ability, others died early in life due to respiratory insufficiency.

The phenotypic variability correlated with the nature of the underlying mutations, wherein patients harboring missense mutations exhibited a milder disease course, whereas those with truncating mutations presented with a more severe phenotype. This genotype-phenotype correlation aligns with observations in other muscular dystrophies. For instance, in Duchenne muscular dystrophy (DMD), out-of-frame deletions in the *DMD* gene result in severe Duchenne muscular dystrophy (DMD), whereas in-frame deletions lead to the milder Becker muscular dystrophy (BMD) phenotype (Lim, Nguyen, & Yokota, 2020). Similarly, in merosin-deficient congenital muscular dystrophy type 1A (MDC1A) caused by *LAMA2* mutations, the clinical severity correlates with mutation severity and merosin expression levels (Geranmayeh et al., 2010).

Interestingly, in most patients in this study, SPN1 protein levels were relatively preserved, suggesting that the mutant protein remains stable but exhibits dysfunctional activity with varying degrees of residual function. SPN1 mutations alter the topographic structure of the tight TMG binding pocket within the protein, reducing its affinity for UsnRNPs. It is likely that SPN1 mutants retain partial binding capability, which disproportionately affects tissues with high splicing activity, such as skeletal muscles. The extent of this impact appears to correlate with the nature and location of the mutations.

4.2 Structural and functional implications of SPN1 mutations

This study underscores the critical role of the C-terminal region of SPN1, which remained poorly characterized in the literature. Previous crystallographic modeling of isolated SPN1 demonstrated instability in both the N-terminal and C-terminal regions when analyzed in solution (Strasser et al., 2005). Notably, successful structural modeling of these domains was only achieved when SPN1 was complexed with other proteins (Monecke et al., 2009).

Our findings indicate that mutations in the C-terminus impair SPN1 oligomerization, reinforcing the hypothesis that SPN1 must exist in a homomeric or heteromeric complex for stability and function. This observation is consistent with reports by Ospina et al. (2005), which describe a functional cross-talk between the N-terminal and C-terminal domains of SPN1, with implications for regulating interactions with Imp-β1 (Ospina et al., 2005).

Similarly, a comparable structural requirement is evident in SMN protein, where C-terminal dimerization is essential for stability and function (Gupta et al., 2021).

Our experiments validated the previously reported interaction between SPN1 and SMN, demonstrating that SPN1 can interact with SMN even in the absence of its N-terminus (Narayanan et al., 2002). This finding and our results highlight the crucial role of the C-terminus in maintaining this interaction. Further studies are required to elucidate the feedback mechanisms between these two proteins, particularly the C-termini, and to investigate whether this complex has additional, yet undiscovered, functional roles.

4.3 Comparison with other reports of *SNUPN*-associated disorders

Our study represents the first and most comprehensive investigation in the literature describing SPN1-deficient muscular dystrophy (Nashabat et al., 2024). Concurrently, Iruzubieta et al. reported confirmatory findings from a cohort of five patients from two unrelated families, all of whom harbored the same missense mutation (*m1*:c.926T>G (p.Ile309Ser)). All affected individuals exhibited progressive muscular dystrophy, predominantly affecting the proximal muscles of the upper and lower limbs. Their functional experiments confirmed the accumulation of UsnRNP components in the cytoplasmic fraction of fibroblasts and muscle fibers derived from these patients in comparison to controls. Furthermore, aberrant alternative splicing events were observed in mRNA transcripts encoding proteins essential for muscle function. RNA sequencing (RNA-Seq) analysis additionally revealed differential gene expression, particularly affecting genes involved in neuronal biology and motor neuron function. To further investigate the pathogenic role of *SNUPN* mutations, the group developed a Drosophila melanogaster knockdown model, which exhibited reduced mobility and survival rates compared to wild-type (WT) controls (Iruzubieta et al., 2024). Following the publication of these two studies, SPN1-related muscular dystrophy was officially classified as Limb-Girdle Muscular Dystrophy autosomal recessive type 29 (LGMDR29) in the Online Mendelian Inheritance in Man (OMIM) database (MIM 620793). This classification was based on the recommendations of Iruzubieta et al., who reached their conclusion based on the phenotype associated with a single mutation. In contrast, our assessment was more comprehensive, as we analyzed a broader spectrum of mutations and phenotypic variations.

This wider perspective led us to propose classifying the disorder as a congenital muscular dystrophy.

Interestingly, an independent study from Japan (Okubo et al., 2024) published on medRxiv described *SNUPN* mutations associated with spinocerebellar ataxia (SCA). This cohort included three patients from two unrelated families, all of whom presented with intellectual disability, and in two cases, congenital cataracts, findings that closely resemble manifestations observed in our cohort. The affected individuals harbored compound heterozygous mutations in *SNUPN*, including c.611G>A (p.Arg204Gln), c.927dupT (p.Met310Tyrfs21), and c.163C>T (p.Arg55Trp), c.927dupT (p.Met310Tyrfs21). Notably, the N-terminal mutation identified in their cohort (p.Arg55Trp) is highly similar to the mutation reported in our study (*m9*:c.164G>A p.Arg55Gln). Although a dystrophic phenotype was not explicitly reported in their patients' muscle biopsies, the clinical findings of muscle weakness, atrophy, and elevated creatine kinase (CK) levels strongly suggest muscle involvement and damage. Further functional analysis demonstrated impaired nuclear transport of mutant SPN1. Specifically, GFP-tagged Arg55Trp-SPN1 exhibited abnormal nuclear import, whereas GFP-tagged Arg204Gln-SPN1 displayed defective nuclear export in HeLa cells. To further elucidate the biological significance of *SNUPN* deficiency, the group attempted to generate a complete *Snupn* knockout mouse model; however, they found that complete loss of *SNUPN* was embryonically lethal, underscoring the essential role of SPN1 in normal development. Consequently, they developed a knock-in mouse model harboring the same mutations identified in their patient cohort (Ile312Tyr/Arg55Trp). The mutant mice exhibited abnormal Purkinje cell dendrite development, cerebellar atrophy, and an SCA phenotype, in addition to muscle weakness, further reinforcing the critical role of SPN1 in both neuromuscular function and central nervous system development (Okubo et al., 2024).

The variability in phenotypic presentation among the three reported cohorts may be attributed to differences in the type and combination of mutations present in affected individuals. Mutations in the N-terminal and C-terminal regions of *SNUPN* could lead to distinct functional consequences, potentially impacting different tissues. While C-terminal mutations were predominantly associated with varying degrees of muscular dystrophy, mutations located toward the N-terminus appeared to result in extra-muscular manifestations, primarily

neurological symptoms. For instance, patient F10-II:1 and the patients described by Okubo et al. (2024) exhibited SCA as a primary phenotype, accompanied by muscle weakness and evidence of muscle fiber damage.

A parallel phenomenon is observed in *LMNA* gene mutations, which encode the LAMIN A and LAMIN C intermediate filaments, both generated via alternative splicing of the same gene. These proteins are ubiquitously expressed and serve as essential components of the nuclear lamina. Interestingly, different *LMNA* mutations, or in some cases even the same mutation, can give rise to completely distinct clinical phenotypes, including Emery-Dreifuss muscular dystrophy (EDMD), congenital muscular dystrophy, dilated cardiomyopathy, and lipodystrophy (Shin & Worman, 2022).

These observations suggest previously unrecognized functional roles of SPN1, indicating that it extends beyond its established function as a nuclear import adaptor for UsnRNPs. The differential impact of various mutations on distinct cellular pathways, resulting in diverse clinical manifestations, further supports this hypothesis. Therefore, additional in-depth studies are essential to precisely define the mechanisms by which *SNUPN* mutations lead to tissue-specific effects and influence disease pathology in neuromuscular and neurodegenerative disorders. Moreover, further research with larger patient cohorts will be necessary to better establish genotype-phenotype correlations and to advance our understanding of the molecular basis underlying the phenotypic variability associated with *SNUPN* mutations.

4.4 Splicing machinery defects and muscular dystrophy pathogenesis

All three reports on *SNUPN*-related muscular dystrophy have highlighted mRNA mis-splicing as the primary pathogenic mechanism underlying the patients' clinical phenotypes. Disruptions in the spliceosome machinery are well-documented contributors to other forms of muscular dystrophy, including facioscapulohumeral muscular dystrophy (FSHD) and myotonic dystrophy type 1 (DM1). Patients with DM1 often exhibit a combination of muscular dystrophy, neurological manifestations, and cataracts, which further emphasize the widespread impact of splicing defects on muscle and neural tissues (Johnson, 2019).

Notably, skeletal muscle is among the tissues with the highest number of differentially expressed alternative exons, making it particularly vulnerable to disruptions in splicing regulation (Pistoni et al., 2010). Consequently, any defect in this highly regulated machinery is expected to affect the skeletal muscle fibers more than other tissues in the body, which could also be affected but to a lesser extent.

Another well-characterized example of splicing machinery dysfunction is spinal muscular atrophy (SMA), caused by mutations in the *SMN* gene. In SMA, the primary affected tissue is the motor neuron, leading to progressive neuromuscular degeneration, which defines the disease phenotype (Mercuri et al., 2022). The splicing defect in SMA is primarily associated with dysfunction in the minor spliceosome machinery, which is essential for the proper processing of certain intron-containing transcripts.

Recent studies and animal model experiments have demonstrated direct effects of SMN deficiency on skeletal muscles. In mouse models where SMN was selectively depleted in skeletal muscle, a clear dystrophic phenotype was observed, characterized by muscle fiber degeneration and impaired regeneration (Jha, Kim, Her, & Monani, 2023). These findings indicate that skeletal muscle pathology is an intrinsic feature of SMA, although its clinical detection is often masked by the predominant neurogenic phenotype. In many patients, muscle degeneration may not be fully evident, as individuals often die due to respiratory failure before the manifestation of overt muscular dystrophy. Moreover, muscle biopsy is no longer a standard diagnostic tool for SMA, as it does not significantly currently contribute to diagnosis, clinical management, or therapeutic strategies, which further limit the ability to detect dystrophic features in SMA patients (Jha et al., 2023).

The functional interaction between SPN1 and SMN, along with their overlapping pathophysiological consequences, underscores the need for further investigation into their potential interaction. The downregulation of SMN in SPN1 mutant cell lines further reinforces this connection, suggesting a previously uncharacterized role of SPN1 in the stability or regulation of SMN protein and its associated complex. Future studies are essential to elucidate the precise molecular relationship between SPN1 and SMN, as this could provide critical

insights into the shared mechanisms underlying *SNUPN*-related muscular dystrophy and SMA, potentially uncovering new therapeutic targets.

4.5 Autophagy dysfunction in SPN1 mutant cells

Autophagy dysfunction has recently been identified as a key consequence of SMN loss of function. Several studies have reported autophagic flux impairment in primary cells and various cell lines with SMN deficiency, characterized by the accumulation of autophagy markers, including p62 and LC3-II, compared to controls (Rashid & Dimitriadi, 2023). These findings are consistent with our observations, where LC3-II accumulation was significantly higher in SPN1 mutant cell lines compared to wild-type (WT) cells in addition to the fluctuating p62 levels, indicating a possible autophagic flux impairment. Additionally, the muscle cross-section analysis reported by Iruzubieta et al. (2024) further supports this, as they observed increased p62 and LC3-II accumulation within the sarcoplasm of muscle fibers, reinforcing the hypothesis that autophagy dysregulation plays a significant role in SPN1-associated muscular dystrophy.

As previously highlighted in the Introduction section, autophagy defects have been implicated in several forms of muscular dystrophy, including Duchenne muscular dystrophy (DMD), limb-girdle muscular dystrophy R9 (LGMDR9), and merosin-deficient congenital muscular dystrophy type 1A (MDC1A) (De Palma, Morisi, et al., 2014; Franekova et al., 2021; Mastrapasqua et al., 2023). These studies, along with others, have demonstrated the detrimental effects of autophagy dysregulation on disease progression and clinical phenotype of the affected patients.

The growing understanding of autophagy regulation and its role in neuromuscular disorders has paved the way for therapeutic exploration, including potential targeted treatments or adjuvant therapies for various muscular dystrophies, including DMD (De Palma, Morisi, et al., 2014). Strategies aimed at enhancing autophagic activity have shown promising results in preclinical models. Notably, autophagy activation, either through nutritional interventions such as starvation or pharmacological modulation, has been demonstrated to rescue cellular

homeostasis and ameliorate the dystrophic phenotype in COLLAGEN VI-deficient mouse models (Grumati et al., 2010; Grumati et al., 2011).

Given these findings, the potential of autophagy modulation as a therapeutic target for SMA has also been investigated by multiple research groups. However, despite encouraging preliminary data, further studies are required to validate the efficacy of this approach in SMA and other neuromuscular diseases (Rashid & Dimitriadi, 2023). Understanding the precise molecular mechanisms underlying autophagy dysfunction in *SNUPN*-associated muscular dystrophy and related disorders could provide critical insights into novel therapeutic interventions aimed at modulating autophagy to mitigate disease progression.

Chapter 5: **CONCLUSION AND FUTURE DIRECTIONS**

This study establishes *SNUPN* mutations as the underlying cause of a newly identified form of muscular dystrophy with extramuscular manifestations. Through comprehensive molecular and cellular analyses, we have demonstrated that SPN1 dysfunction leads to widespread mis-splicing of genes essential for maintaining muscle homeostasis. The novel characterization of SPN1 self-oligomerization has provided deeper insights into its structural and functional properties. Furthermore, the identification of SPN1-SMN interactions and the subsequent SMN perturbation suggest a potential mechanistic link between these two proteins, emphasizing their shared roles in RNA processing and cellular homeostasis. The observed cellular phenotypes, including Cajal body disruption, protein aggregation, and dysregulated autophagy, collectively contribute to the understanding of the disease pathophysiology and may pave the way for novel therapeutic approaches.

Future research directions should focus on further characterizing the impact of SPN1 mutations on cellular homeostasis, with particular emphasis on autophagy, mitophagy, and mitochondrial dynamics. Investigating how these disruptions influence mitochondrial function will be crucial in delineating the full spectrum of disease mechanisms. Additionally, the development of an *in vivo* disease model is essential to better understand the systemic consequences of SPN1 deficiency and to serve as a platform for testing potential therapeutic interventions. Furthermore, elucidating the precise functional interplay between SPN1 and SMN may provide valuable insights into spinal muscular atrophy (SMA), one of the most prevalent genetic neuromuscular disorders in children, potentially revealing novel therapeutic targets that extend beyond the context of *SNUPN*-related muscular dystrophy.

Bibliography

Ahmad, K., Shaikh, S., Ahmad, S. S., Lee, E. J., & Choi, I. (2020). Cross-Talk Between Extracellular Matrix and Skeletal Muscle: Implications for Myopathies. *Front Pharmacol, 11*, 142. doi:10.3389/fphar.2020.00142

Alazami, A. M., Patel, N., Shamseldin, H. E., Anazi, S., Al-Dosari, M. S., Alzahrani, F., . . . Alkuraya, F. S. (2015). Accelerating novel candidate gene discovery in neurogenetic disorders via whole-exome sequencing of prescreened multiplex consanguineous families. *Cell Rep, 10*(2), 148-161. doi:10.1016/j.celrep.2014.12.015

Ashrafi, G., & Schwarz, T. L. (2013). The pathways of mitophagy for quality control and clearance of mitochondria. *Cell Death Differ, 20*(1), 31-42. doi:10.1038/cdd.2012.81

Barad, M., Csukasi, F., Bosakova, M., Martin, J. H., Zhang, W., Paige Taylor, S., . . . Duran, I. (2020). Biallelic mutations in LAMA5 disrupts a skeletal noncanonical focal adhesion pathway and produces a distinct bent bone dysplasia. *EBioMedicine, 62*, 103075. doi:10.1016/j.ebiom.2020.103075

Barton, E. R., Pacak, C. A., Stoppel, W. L., & Kang, P. B. (2020). The ties that bind: functional clusters in limb-girdle muscular dystrophy. *Skelet Muscle, 10*(1), 22. doi:10.1186/s13395-020-00240-7

Battle, D. J., Kasim, M., Yong, J., Lotti, F., Lau, C. K., Mouaikel, J., . . . Dreyfuss, G. (2006). The SMN complex: an assembly machine for RNPs. *Cold Spring Harb Symp Quant Biol, 71*, 313-320. doi:10.1101/sqb.2006.71.001

Benarroch, L., Bonne, G., Rivier, F., & Hamroun, D. (2023). The 2023 version of the gene table of neuromuscular disorders (nuclear genome). *Neuromuscul Disord, 33*(1), 76-117. doi:10.1016/j.nmd.2022.12.002

Ber, Y., Shiloh, R., Gilad, Y., Degani, N., Bialik, S., & Kimchi, A. (2015). DAPK2 is a novel regulator of mTORC1 activity and autophagy. *Cell Death Differ, 22*(3), 465-475. doi:10.1038/cdd.2014.177

Bernardi, P., & Bonaldo, P. (2013). Mitochondrial dysfunction and defective autophagy in the pathogenesis of collagen VI muscular dystrophies. *Cold Spring Harb Perspect Biol, 5*(5), a011387. doi:10.1101/cshperspect.a011387

Bhardwaj, A., & Cingolani, G. (2010). Conformational selection in the recognition of the snurportin importin beta binding domain by importin beta. *Biochemistry, 49*(24), 5042-5047. doi:10.1021/bi100292y

Bonnans, C., Chou, J., & Werb, Z. (2014). Remodelling the extracellular matrix in development and disease. *Nat Rev Mol Cell Biol, 15*(12), 786-801. doi:10.1038/nrm3904

Briguet, A., Courdier-Fruh, I., Foster, M., Meier, T., & Magyar, J. P. (2004). Histological parameters for the quantitative assessment of muscular dystrophy in the mdx-mouse. *Neuromuscul Disord, 14*(10), 675-682. doi:10.1016/j.nmd.2004.06.008

Bucelli, R. C., Arhzaouy, K., Pestronk, A., Pittman, S. K., Rojas, L., Sue, C. M., . . . Weihl, C. C. (2015). SQSTM1 splice site mutation in distal myopathy with rimmed vacuoles. *Neurology, 85*(8), 665-674. doi:10.1212/WNL.0000000000001864

Buckingham, M. (2007). Skeletal muscle progenitor cells and the role of Pax genes. *C R Biol, 330*(6-7), 530-533. doi:10.1016/j.crvi.2007.03.015

Buckingham, M., Bajard, L., Chang, T., Daubas, P., Hadchouel, J., Meilhac, S., . . . Relaix, F. (2003). The formation of skeletal muscle: from somite to limb. *J Anat, 202*(1), 59-68. doi:10.1046/j.1469-7580.2003.00139.x

Calik, M. (2021). *The Muscle Structure and Function*. Switzerland: Springer Nature.

Carmignac, V., Svensson, M., Korner, Z., Elowsson, L., Matsumura, C., Gawlik, K. I., . . . Durbeej, M. (2011). Autophagy is increased in laminin alpha2 chain-deficient muscle and its inhibition improves muscle morphology in a mouse model of MDC1A. *Hum Mol Genet, 20*(24), 4891-4902. doi:10.1093/hmg/ddr427

Castagnaro, S., Pellegrini, C., Pellegrini, M., Chrisam, M., Sabatelli, P., Toni, S., . . . Merlini, L. (2016). Autophagy activation in COL6 myopathic patients by a low-protein-diet pilot trial. *Autophagy, 12*(12), 2484-2495. doi:10.1080/15548627.2016.1231279

Chen, Y., Xin, H., Peng, H., Shi, Q., Li, M., Yu, J., . . . Li, F. (2020). Hypomethylation-Linked Activation of PLCE1 Impedes Autophagy and Promotes Tumorigenesis through MDM2-Mediated Ubiquitination and Destabilization of p53. *Cancer Res, 80*(11), 2175-2189. doi:10.1158/0008-5472.CAN-19-1912

Chompoopong, P., & Milone, M. (2023). GDP-Mannose Pyrophosphorylase B (GMPPB)-Related Disorders. *Genes (Basel), 14*(2). doi:10.3390/genes14020372

Cohen, E., Bonne, G., Rivier, F., & Hamroun, D. (2021). The 2022 version of the gene table of neuromuscular disorders (nuclear genome). *Neuromuscul Disord, 31*(12), 1313-1357. doi:10.1016/j.nmd.2021.11.004

Collier, J. J., Guissart, C., Olahova, M., Sasorith, S., Piron-Prunier, F., Suomi, F., . . . Taylor, R. W. (2021). Developmental Consequences of Defective ATG7-Mediated Autophagy in Humans. *N Engl J Med, 384*(25), 2406-2417. doi:10.1056/NEJMoa1915722

Cox, T. R., & Erler, J. T. (2011). Remodeling and homeostasis of the extracellular matrix: implications for fibrotic diseases and cancer. *Dis Model Mech, 4*(2), 165-178. doi:10.1242/dmm.004077

Crone, M., & Mah, J. K. (2018). Current and Emerging Therapies for Duchenne Muscular Dystrophy. *Curr Treat Options Neurol, 20*(8), 31. doi:10.1007/s11940-018-0513-6

Csapo, R., Gumpenberger, M., & Wessner, B. (2020). Skeletal Muscle Extracellular Matrix - What Do We Know About Its Composition, Regulation, and Physiological Roles? A Narrative Review. *Front Physiol, 11*, 253. doi:10.3389/fphys.2020.00253

D. J. Lowrie, J. (2020). *Histology - An Essential Textbook*. New York, USA: Thieme.

De Mario, A., Gherardi, G., Rizzuto, R., & Mammucari, C. (2021). Skeletal muscle mitochondria in health and disease. *Cell Calcium, 94*, 102357. doi:10.1016/j.ceca.2021.102357

De Palma, C., Morisi, F., Cheli, S., Pambianco, S., Cappello, V., Vezzoli, M., . . . Clementi, E. (2014). Autophagy as a new therapeutic target in Duchenne muscular dystrophy. *Cell Death Dis, 5*(8), e1363. doi:10.1038/cddis.2014.312

De Palma, C., Perrotta, C., Pellegrino, P., Clementi, E., & Cervia, D. (2014). Skeletal muscle homeostasis in duchenne muscular dystrophy: modulating autophagy as a promising therapeutic strategy. *Front Aging Neurosci, 6*, 188. doi:10.3389/fnagi.2014.00188

Descamps, S., Arzouk, H., Bacou, F., Bernardi, H., Fedon, Y., Gay, S., . . . Levin, J. (2008). Inhibition of myoblast differentiation by Sfrp1 and Sfrp2. *Cell Tissue Res, 332*(2), 299-306. doi:10.1007/s00441-008-0574-z

Di Martino, A., Cescon, M., D'Agostino, C., Schilardi, F., Sabatelli, P., Merlini, L., & Faldini, C. (2023). Collagen VI in the Musculoskeletal System. *Int J Mol Sci, 24*(6). doi:10.3390/ijms24065095

Elsaid, M. F., Chalhoub, N., Ben-Omran, T., Kumar, P., Kamel, H., Ibrahim, K., . . . Aleem, A. A. (2017). Mutation in noncoding RNA RNU12 causes early onset cerebellar ataxia. *Ann Neurol, 81*(1), 68-78. doi:10.1002/ana.24826

Fiacco, E., Castagnetti, F., Bianconi, V., Madaro, L., De Bardi, M., Nazio, F., . . . Latella, L. (2016). Autophagy regulates satellite cell ability to regenerate normal and dystrophic muscles. *Cell Death Differ, 23*(11), 1839-1849. doi:10.1038/cdd.2016.70

Fischer, U., Englbrecht, C., & Chari, A. (2011). Biogenesis of spliceosomal small nuclear ribonucleoproteins. *Wiley Interdiscip Rev RNA, 2*(5), 718-731. doi:10.1002/wrna.87

Fornerod, M., Ohno, M., Yoshida, M., & Mattaj, I. W. (1997). CRM1 is an export receptor for leucine-rich nuclear export signals. *Cell, 90*(6), 1051-1060. doi:10.1016/s0092-8674(00)80371-2

Franekova, V., Storjord, H. I., Leivseth, G., & Nilssen, O. (2021). Protein homeostasis in LGMDR9 (LGMD2I) - The role of ubiquitin-proteasome and autophagy-lysosomal system. *Neuropathol Appl Neurobiol, 47*(4), 519-531. doi:10.1111/nan.12684

Frontera, W. R., & Ochala, J. (2015). Skeletal muscle: a brief review of structure and function. *Calcif Tissue Int, 96*(3), 183-195. doi:10.1007/s00223-014-9915-y

Fujioka, Y., Suzuki, S. W., Yamamoto, H., Kondo-Kakuta, C., Kimura, Y., Hirano, H., . . . Noda, N. N. (2014). Structural basis of starvation-induced assembly of the autophagy initiation complex. *Nat Struct Mol Biol, 21*(6), 513-521. doi:10.1038/nsmb.2822

Fujita, N., Hayashi-Nishino, M., Fukumoto, H., Omori, H., Yamamoto, A., Noda, T., & Yoshimori, T. (2008). An Atg4B mutant hampers the lipidation of LC3 paralogues and causes defects in autophagosome closure. *Mol Biol Cell, 19*(11), 4651-4659. doi:10.1091/mbc.e08-03-0312

Fukai, Y., Ohsawa, Y., Ohtsubo, H., Nishimatsu, S. I., Hagiwara, H., Noda, M., . . . Sunada, Y. (2017). Cleavage of beta-dystroglycan occurs in sarcoglycan-deficient skeletal muscle without MMP-2 and MMP-9. *Biochem Biophys Res Commun, 492*(2), 199-205. doi:10.1016/j.bbrc.2017.08.048

Garcia-Prat, L., Martinez-Vicente, M., Perdiguero, E., Ortet, L., Rodriguez-Ubreva, J., Rebollo, E., . . . Munoz-Canoves, P. (2016). Autophagy maintains stemness by preventing senescence. *Nature, 529*(7584), 37-42. doi:10.1038/nature16187

Georganopoulou, D. G., Moisiadis, V. G., Malik, F. A., Mohajer, A., Dashevsky, T. M., Wuu, S. T., & Hu, C. K. (2021). A Journey with LGMD: From Protein Abnormalities to Patient Impact. *Protein J, 40*(4), 466-488. doi:10.1007/s10930-021-10006-9

Geranmayeh, F., Clement, E., Feng, L. H., Sewry, C., Pagan, J., Mein, R., . . . Muntoni, F. (2010). Genotype-phenotype correlation in a large population of muscular dystrophy patients with LAMA2 mutations. *Neuromuscul Disord, 20*(4), 241-250. doi:10.1016/j.nmd.2010.02.001

Goruppi, S., Procopio, M. G., Jo, S., Clocchiatti, A., Neel, V., & Dotto, G. P. (2017). The ULK3 Kinase Is Critical for Convergent Control of Cancer-Associated Fibroblast Activation by CSL and GLI. *Cell Rep, 20*(10), 2468-2479. doi:10.1016/j.celrep.2017.08.048

Greene, A. W., Grenier, K., Aguileta, M. A., Muise, S., Farazifard, R., Haque, M. E., . . . Fon, E. A. (2012). Mitochondrial processing peptidase regulates PINK1 processing, import and Parkin recruitment. *EMBO Rep, 13*(4), 378-385. doi:10.1038/embor.2012.14

Griffin, C., & Saint-Jeannet, J. P. (2020). Spliceosomopathies: Diseases and mechanisms. *Dev Dyn, 249*(9), 1038-1046. doi:10.1002/dvdy.214

Group, U. G. B. (2023). UCSC Genome Browser on Human (GRCh38/hg38) - SNUPN. Retrieved from https://genome.ucsc.edu/cgi-bin/hgTracks?db=hg38&lastVirtModeType=default&lastVirtModeExtraState=&virtMo

deType=default&virtMode=0&nonVirtPosition=&position=chr15%3A75598086%2D75625725&hgsid=1792429638_E8qx3lSDOqsPaktOav6iahuvdQiW

Grumati, P., & Bonaldo, P. (2012). Autophagy in skeletal muscle homeostasis and in muscular dystrophies. *Cells, 1*(3), 325-345. doi:10.3390/cells1030325

Grumati, P., Coletto, L., Sabatelli, P., Cescon, M., Angelin, A., Bertaggia, E., . . . Bonaldo, P. (2010). Autophagy is defective in collagen VI muscular dystrophies, and its reactivation rescues myofiber degeneration. *Nat Med, 16*(11), 1313-1320. doi:10.1038/nm.2247

Grumati, P., Coletto, L., Sandri, M., & Bonaldo, P. (2011). Autophagy induction rescues muscular dystrophy. *Autophagy, 7*(4), 426-428. doi:10.4161/auto.7.4.14392

Gruss, O. J., Meduri, R., Schilling, M., & Fischer, U. (2017). UsnRNP biogenesis: mechanisms and regulation. *Chromosoma, 126*(5), 577-593. doi:10.1007/s00412-017-0637-6

Gundesli, H., Talim, B., Korkusuz, P., Balci-Hayta, B., Cirak, S., Akarsu, N. A., . . . Dincer, P. (2010). Mutation in exon 1f of PLEC, leading to disruption of plectin isoform 1f, causes autosomal-recessive limb-girdle muscular dystrophy. *Am J Hum Genet, 87*(6), 834-841. doi:10.1016/j.ajhg.2010.10.017

Gupta, K., Wen, Y., Ninan, N. S., Raimer, A. C., Sharp, R., Spring, A. M., . . . Matera, A. G. (2021). Assembly of higher-order SMN oligomers is essential for metazoan viability and requires an exposed structural motif present in the YG zipper dimer. *Nucleic Acids Res, 49*(13), 7644-7664. doi:10.1093/nar/gkab508

Gustafsson, A. B., & Dorn, G. W., 2nd. (2019). Evolving and Expanding the Roles of Mitophagy as a Homeostatic and Pathogenic Process. *Physiol Rev, 99*(1), 853-892. doi:10.1152/physrev.00005.2018

Hara, Y., Balci-Hayta, B., Yoshida-Moriguchi, T., Kanagawa, M., Beltran-Valero de Bernabe, D., Gundesli, H., . . . Campbell, K. P. (2011). A dystroglycan mutation associated with limb-girdle muscular dystrophy. *N Engl J Med, 364*(10), 939-946. doi:10.1056/NEJMoa1006939

He, C., Bassik, M. C., Moresi, V., Sun, K., Wei, Y., Zou, Z., . . . Levine, B. (2012). Exercise-induced BCL2-regulated autophagy is required for muscle glucose homeostasis. *Nature, 481*(7382), 511-515. doi:10.1038/nature10758

He, C., Wang, S., Zhou, C., He, M., Wang, J., Ladds, M., . . . Karlsson, M. C. I. (2021). CD36 and LC3B initiated autophagy in B cells regulates the humoral immune response. *Autophagy, 17*(11), 3577-3591. doi:10.1080/15548627.2021.1885183

Heller, S. A., Shih, R., Kalra, R., & Kang, P. B. (2020). Emery-Dreifuss muscular dystrophy. *Muscle Nerve, 61*(4), 436-448. doi:10.1002/mus.26782

Heslop, L., Morgan, J. E., & Partridge, T. A. (2000). Evidence for a myogenic stem cell that is exhausted in dystrophic muscle. *J Cell Sci, 113 (Pt 12)*, 2299-2308. doi:10.1242/jcs.113.12.2299

Hindi, S. M., & Kumar, A. (2016). Toll-like receptor signalling in regenerative myogenesis: friend and foe. *J Pathol, 239*(2), 125-128. doi:10.1002/path.4714

Holt, K. H., Crosbie, R. H., Venzke, D. P., & Campbell, K. P. (2000). Biosynthesis of dystroglycan: processing of a precursor propeptide. *FEBS Lett, 468*(1), 79-83. doi:10.1016/s0014-5793(00)01195-9

Huang, D., Xu, B., Liu, L., Wu, L., Zhu, Y., Ghanbarpour, A., . . . Chen, X. W. (2021). TMEM41B acts as an ER scramblase required for lipoprotein biogenesis and lipid homeostasis. *Cell Metab, 33*(8), 1655-1670 e1658. doi:10.1016/j.cmet.2021.05.006

Huber, J., Cronshagen, U., Kadokura, M., Marshallsay, C., Wada, T., Sekine, M., & Luhrmann, R. (1998). Snurportin1, an m3G-cap-specific nuclear import receptor with a novel domain structure. *EMBO J, 17*(14), 4114-4126. doi:10.1093/emboj/17.14.4114

Huber, J., Dickmanns, A., & Luhrmann, R. (2002). The importin-beta binding domain of snurportin1 is responsible for the Ran- and energy-independent nuclear import of spliceosomal U snRNPs in vitro. *J Cell Biol, 156*(3), 467-479. doi:10.1083/jcb.200108114

Hynes, R. O., & Naba, A. (2012). Overview of the matrisome--an inventory of extracellular matrix constituents and functions. *Cold Spring Harb Perspect Biol, 4*(1), a004903. doi:10.1101/cshperspect.a004903

Iberite, F., Gruppioni, E., & Ricotti, L. (2022). Skeletal muscle differentiation of human iPSCs meets bioengineering strategies: perspectives and challenges. *NPJ Regen Med, 7*(1), 23. doi:10.1038/s41536-022-00216-9

Iruzubieta, P., Damborenea, A., Ioghen, M., Bajew, S., Fernandez-Torron, R., Topf, A., . . . Blazquez, L. (2024). Biallelic variants in SNUPN cause a limb girdle muscular dystrophy with myofibrillar-like features. *Brain, 147*(8), 2867-2883. doi:10.1093/brain/awae046

Jardin, F., Pujals, A., Pelletier, L., Bohers, E., Camus, V., Mareschal, S., . . . Leroy, K. (2016). Recurrent mutations of the exportin 1 gene (XPO1) and their impact on selective inhibitor of nuclear export compounds sensitivity in primary mediastinal B-cell lymphoma. *Am J Hematol, 91*(9), 923-930. doi:10.1002/ajh.24451

Jha, N. N., Kim, J. K., Her, Y. R., & Monani, U. R. (2023). Muscle: an independent contributor to the neuromuscular spinal muscular atrophy disease phenotype. *JCI Insight, 8*(18). doi:10.1172/jci.insight.171878

Johansen, T., & Lamark, T. (2020). Selective Autophagy: ATG8 Family Proteins, LIR Motifs and Cargo Receptors. *J Mol Biol, 432*(1), 80-103. doi:10.1016/j.jmb.2019.07.016

Johnson, N. E. (2019). Myotonic Muscular Dystrophies. *Continuum (Minneap Minn), 25*(6), 1682-1695. doi:10.1212/CON.0000000000000793

Jumper, J., Evans, R., Pritzel, A., Green, T., Figurnov, M., Ronneberger, O., . . . Hassabis, D. (2021). Highly accurate protein structure prediction with AlphaFold. *Nature, 596*(7873), 583-589. doi:10.1038/s41586-021-03819-2

Kane, L. A., Lazarou, M., Fogel, A. I., Li, Y., Yamano, K., Sarraf, S. A., . . . Youle, R. J. (2014). PINK1 phosphorylates ubiquitin to activate Parkin E3 ubiquitin ligase activity. *J Cell Biol, 205*(2), 143-153. doi:10.1083/jcb.201402104

Kang, C., Badr, M. A., Kyrychenko, V., Eskelinen, E. L., & Shirokova, N. (2018). Deficit in PINK1/PARKIN-mediated mitochondrial autophagy at late stages of dystrophic cardiomyopathy. *Cardiovasc Res, 114*(1), 90-102. doi:10.1093/cvr/cvx201

Kim, M., Sandford, E., Gatica, D., Qiu, Y., Liu, X., Zheng, Y., . . . Burmeister, M. (2016). Mutation in ATG5 reduces autophagy and leads to ataxia with developmental delay. *Elife, 5*. doi:10.7554/eLife.12245

Klionsky, D. J., Petroni, G., Amaravadi, R. K., Baehrecke, E. H., Ballabio, A., Boya, P., . . . Pietrocola, F. (2021). Autophagy in major human diseases. *EMBO J, 40*(19), e108863. doi:10.15252/embj.2021108863

Kour, S., Rajan, D. S., Fortuna, T. R., Anderson, E. N., Ward, C., Lee, Y., . . . Pandey, U. B. (2021). Loss of function mutations in GEMIN5 cause a neurodevelopmental disorder. *Nat Commun, 12*(1), 2558. doi:10.1038/s41467-021-22627-w

Krishna, L., Prashant, A., Kumar, Y. H., Paneyala, S., Patil, S. J., Ramachandra, S. C., & Vishwanath, P. (2024). Molecular and Biochemical Therapeutic Strategies for Duchenne Muscular Dystrophy. *Neurol Int, 16*(4), 731-760. doi:10.3390/neurolint16040055

Kuhn-Holsken, E., Lenz, C., Dickmanns, A., Hsiao, H. H., Richter, F. M., Kastner, B., . . . Urlaub, H. (2010). Mapping the binding site of snurportin 1 on native U1 snRNP by cross-linking and mass spectrometry. *Nucleic Acids Res, 38*(16), 5581-5593. doi:10.1093/nar/gkq272

Lamark, T., & Johansen, T. (2021). Mechanisms of Selective Autophagy. *Annu Rev Cell Dev Biol, 37*, 143-169. doi:10.1146/annurev-cellbio-120219-035530

Leduc-Gaudet, J. P., Hussain, S. N. A., Barreiro, E., & Gouspillou, G. (2021). Mitochondrial Dynamics and Mitophagy in Skeletal Muscle Health and Aging. *Int J Mol Sci, 22*(15). doi:10.3390/ijms22158179

Lemm, I., Girard, C., Kuhn, A. N., Watkins, N. J., Schneider, M., Bordonne, R., & Luhrmann, R. (2006). Ongoing U snRNP biogenesis is required for the integrity of Cajal bodies. *Mol Biol Cell, 17*(7), 3221-3231. doi:10.1091/mbc.e06-03-0247

Lemmers, R. J., Tawil, R., Petek, L. M., Balog, J., Block, G. J., Santen, G. W., . . . van der Maarel, S. M. (2012). Digenic inheritance of an SMCHD1 mutation and an FSHD-permissive D4Z4 allele causes facioscapulohumeral muscular dystrophy type 2. *Nat Genet, 44*(12), 1370-1374. doi:10.1038/ng.2454

Lim, K. R. Q., Nguyen, Q., & Yokota, T. (2020). Genotype-Phenotype Correlations in Duchenne and Becker Muscular Dystrophy Patients from the Canadian Neuromuscular Disease Registry. *J Pers Med, 10*(4). doi:10.3390/jpm10040241

Linares, J. F., Duran, A., Reina-Campos, M., Aza-Blanc, P., Campos, A., Moscat, J., & Diaz-Meco, M. T. (2015). Amino Acid Activation of mTORC1 by a PB1-Domain-Driven Kinase Complex Cascade. *Cell Rep, 12*(8), 1339-1352. doi:10.1016/j.celrep.2015.07.045

Lobrinus, J. A., Schorderet, D. F., Payot, M., Jeanrenaud, X., Bottani, A., Superti-Furga, A., . . . Jeannet, P. Y. (2005). Morphological, clinical and genetic aspects in a family with a novel LAMP-2 gene mutation (Danon disease). *Neuromuscul Disord, 15*(4), 293-298. doi:10.1016/j.nmd.2004.12.007

Logan, C. Y., & Nusse, R. (2004). The Wnt signaling pathway in development and disease. *Annu Rev Cell Dev Biol, 20*, 781-810. doi:10.1146/annurev.cellbio.20.010403.113126

Lopez, I., Mak, E. C., Ding, J., Hamm, H. E., & Lomasney, J. W. (2001). A novel bifunctional phospholipase c that is regulated by Galpha 12 and stimulates the Ras/mitogen-activated protein kinase pathway. *J Biol Chem, 276*(4), 2758-2765. doi:10.1074/jbc.M008119200

Lorson, C. L., Hahnen, E., Androphy, E. J., & Wirth, B. (1999). A single nucleotide in the SMN gene regulates splicing and is responsible for spinal muscular atrophy. *Proc Natl Acad Sci U S A, 96*(11), 6307-6311. doi:10.1073/pnas.96.11.6307

Lott, K., & Cingolani, G. (2011). The importin beta binding domain as a master regulator of nucleocytoplasmic transport. *Biochim Biophys Acta, 1813*(9), 1578-1592. doi:10.1016/j.bbamcr.2010.10.012

Lotti, F., Imlach, W. L., Saieva, L., Beck, E. S., Hao le, T., Li, D. K., . . . Pellizzoni, L. (2012). An SMN-dependent U12 splicing event essential for motor circuit function. *Cell, 151*(2), 440-454. doi:10.1016/j.cell.2012.09.012

Luther, P. K. (2009). The vertebrate muscle Z-disc: sarcomere anchor for structure and signalling. *J Muscle Res Cell Motil, 30*(5-6), 171-185. doi:10.1007/s10974-009-9189-6

Mao, Y. S., Zhang, B., & Spector, D. L. (2011). Biogenesis and function of nuclear bodies. *Trends Genet, 27*(8), 295-306. doi:10.1016/j.tig.2011.05.006

Marino, J. S., Tausch, B. J., Dearth, C. L., Manacci, M. V., McLoughlin, T. J., Rakyta, S. J., . . . Pizza, F. X. (2008). Beta2-integrins contribute to skeletal muscle hypertrophy in mice. *Am J Physiol Cell Physiol, 295*(4), C1026-1036. doi:10.1152/ajpcell.212.2008

Massenet, S., Pellizzoni, L., Paushkin, S., Mattaj, I. W., & Dreyfuss, G. (2002). The SMN complex is associated with snRNPs throughout their cytoplasmic assembly pathway. *Mol Cell Biol, 22*(18), 6533-6541. doi:10.1128/MCB.22.18.6533-6541.2002

Mastrapasqua, M., Rossi, R., De Cosmo, L., Resta, A., Errede, M., Bizzoca, A., . . . Girolamo, F. (2023). Autophagy increase in Merosin-Deficient Congenital Muscular Dystrophy type 1A. *Eur J Transl Myol, 33*(3). doi:10.4081/ejtm.2023.11501

Matera, A. G., & Wang, Z. (2014). A day in the life of the spliceosome. *Nat Rev Mol Cell Biol, 15*(2), 108-121. doi:10.1038/nrm3742

Matsumoto, G., Wada, K., Okuno, M., Kurosawa, M., & Nukina, N. (2011). Serine 403 phosphorylation of p62/SQSTM1 regulates selective autophagic clearance of ubiquitinated proteins. *Mol Cell, 44*(2), 279-289. doi:10.1016/j.molcel.2011.07.039

Mazzone, E., Vasco, G., Sormani, M. P., Torrente, Y., Berardinelli, A., Messina, S., . . . Mercuri, E. (2011). Functional changes in Duchenne muscular dystrophy: a 12-month longitudinal cohort study. *Neurology, 77*(3), 250-256. doi:10.1212/WNL.0b013e318225ab2e

Mejlvang, J., Olsvik, H., Svenning, S., Bruun, J. A., Abudu, Y. P., Larsen, K. B., . . . Johansen, T. (2018). Starvation induces rapid degradation of selective autophagy receptors by endosomal microautophagy. *J Cell Biol, 217*(10), 3640-3655. doi:10.1083/jcb.201711002

Mendoza-Londono, R., Lammer, E., Watson, R., Harper, J., Hatamochi, A., Hatamochi-Hayashi, S., . . . Lee, B. (2005). Characterization of a new syndrome that associates craniosynostosis, delayed fontanel closure, parietal foramina, imperforate anus, and skin eruption: CDAGS. *Am J Hum Genet, 77*(1), 161-168. doi:10.1086/431654

Mercuri, E., Bonnemann, C. G., & Muntoni, F. (2019). Muscular dystrophies. *Lancet, 394*(10213), 2025-2038. doi:10.1016/S0140-6736(19)32910-1

Mercuri, E., & Muntoni, F. (2013). Muscular dystrophies. *Lancet, 381*(9869), 845-860. doi:10.1016/S0140-6736(12)61897-2

Mercuri, E., Sumner, C. J., Muntoni, F., Darras, B. T., & Finkel, R. S. (2022). Spinal muscular atrophy. *Nat Rev Dis Primers, 8*(1), 52. doi:10.1038/s41572-022-00380-8

Miner, J. H., & Yurchenco, P. D. (2004). Laminin functions in tissue morphogenesis. *Annu Rev Cell Dev Biol, 20*, 255-284. doi:10.1146/annurev.cellbio.20.010403.094555

Mitrousis, G., Olia, A. S., Walker-Kopp, N., & Cingolani, G. (2008). Molecular basis for the recognition of snurportin 1 by importin beta. *J Biol Chem, 283*(12), 7877-7884. doi:10.1074/jbc.M709093200

Mizushima, N., & Komatsu, M. (2011). Autophagy: renovation of cells and tissues. *Cell, 147*(4), 728-741. doi:10.1016/j.cell.2011.10.026

Mizushima, N., & Levine, B. (2020). Autophagy in Human Diseases. *N Engl J Med, 383*(16), 1564-1576. doi:10.1056/NEJMra2022774

Mohassel, P., Foley, A. R., & Bonnemann, C. G. (2018). Extracellular matrix-driven congenital muscular dystrophies. *Matrix Biol, 71-72*, 188-204. doi:10.1016/j.matbio.2018.06.005

Monecke, T., Guttler, T., Neumann, P., Dickmanns, A., Gorlich, D., & Ficner, R. (2009). Crystal structure of the nuclear export receptor CRM1 in complex with Snurportin1 and RanGTP. *Science, 324*(5930), 1087-1091. doi:10.1126/science.1173388

Mukund, K., & Subramaniam, S. (2020). Skeletal muscle: A review of molecular structure and function, in health and disease. *Wiley Interdiscip Rev Syst Biol Med, 12*(1), e1462. doi:10.1002/wsbm.1462

Muntoni, F., Torelli, S., & Brockington, M. (2008). Muscular dystrophies due to glycosylation defects. *Neurotherapeutics, 5*(4), 627-632. doi:10.1016/j.nurt.2008.08.005

Myers, C. (2024). Basic Structure of Skeletal Muscle. In C. Myers (Ed.), *Skeletal Muscle Physiology: An Update to Anatomy and Function* (pp. 1-34). Cham: Springer Nature Switzerland.

Narayanan, U., Ospina, J. K., Frey, M. R., Hebert, M. D., & Matera, A. G. (2002). SMN, the spinal muscular atrophy protein, forms a pre-import snRNP complex with snurportin1 and importin beta. *Hum Mol Genet, 11*(15), 1785-1795. doi:10.1093/hmg/11.15.1785

Narendra, D. P., Jin, S. M., Tanaka, A., Suen, D. F., Gautier, C. A., Shen, J., . . . Youle, R. J. (2010). PINK1 is selectively stabilized on impaired mitochondria to activate Parkin. *PLoS Biol, 8*(1), e1000298. doi:10.1371/journal.pbio.1000298

Nashabat, M., Nabavizadeh, N., Saracoglu, H. P., Saribas, B., Avci, S., Borklu, E., . . . Escande-Beillard, N. (2024). SNUPN deficiency causes a recessive muscular dystrophy due to RNA mis-splicing and ECM dysregulation. *Nat Commun, 15*(1), 1758. doi:10.1038/s41467-024-45933-5

Neel, B. A., Lin, Y., & Pessin, J. E. (2013). Skeletal muscle autophagy: a new metabolic regulator. *Trends Endocrinol Metab, 24*(12), 635-643. doi:10.1016/j.tem.2013.09.004

Nilsen, T. W., & Graveley, B. R. (2010). Expansion of the eukaryotic proteome by alternative splicing. *Nature, 463*(7280), 457-463. doi:10.1038/nature08909

O'Grady, G. L., Lek, M., Lamande, S. R., Waddell, L., Oates, E. C., Punetha, J., . . . North, K. (2016). Diagnosis and etiology of congenital muscular dystrophy: We are halfway there. *Ann Neurol, 80*(1), 101-111. doi:10.1002/ana.24687

Okubo, M., Ogawa, M., Eura, N., Inoue, Y. U., Dewa, K.-i., Owa, T., . . . Noguchi, S. (2024). Genetic *SNUPN* variants cause spinocerebellar atrophy by disrupting global splicing in Purkinje cells. 2024.2007.2011.24310169. doi:10.1101/2024.07.11.24310169 medRxiv

Ospina, J. K., Gonsalvez, G. B., Bednenko, J., Darzynkiewicz, E., Gerace, L., & Matera, A. G. (2005). Cross-talk between snurportin1 subdomains. *Mol Biol Cell, 16*(10), 4660-4671. doi:10.1091/mbc.e05-04-0316

Paraskeva, E., Izaurralde, E., Bischoff, F. R., Huber, J., Kutay, U., Hartmann, E., . . . Gorlich, D. (1999). CRM1-mediated recycling of snurportin 1 to the cytoplasm. *J Cell Biol, 145*(2), 255-264. doi:10.1083/jcb.145.2.255

Pernas, L., & Scorrano, L. (2016). Mito-Morphosis: Mitochondrial Fusion, Fission, and Cristae Remodeling as Key Mediators of Cellular Function. *Annu Rev Physiol, 78*, 505-531. doi:10.1146/annurev-physiol-021115-105011

Piecyk, K., Niedzwiecka, A., Ferenc-Mrozek, A., Lukaszewicz, M., Darzynkiewicz, E., & Jankowska-Anyszka, M. (2015). How to find the optimal partner--studies of snurportin 1 interactions with U snRNA 5' TMG-cap analogues containing modified 2-amino group of 7-methylguanosine. *Bioorg Med Chem, 23*(15), 4660-4668. doi:10.1016/j.bmc.2015.05.054

Pistoni, M., Ghigna, C., & Gabellini, D. (2010). Alternative splicing and muscular dystrophy. *RNA Biol, 7*(4), 441-452. doi:10.4161/rna.7.4.12258

Prior, T. W., Leach, M. E., & Finanger, E. L. (1993). Spinal Muscular Atrophy. In M. P. Adam, J. Feldman, G. M. Mirzaa, R. A. Pagon, S. E. Wallace, & A. Amemiya (Eds.), *GeneReviews((R))*. Seattle (WA).

Rashid, S., & Dimitriadi, M. (2023). Autophagy in spinal muscular atrophy: from pathogenic mechanisms to therapeutic approaches. *Front Cell Neurosci, 17*, 1307636. doi:10.3389/fncel.2023.1307636

Rayagiri, S. S., Ranaldi, D., Raven, A., Mohamad Azhar, N. I. F., Lefebvre, O., Zammit, P. S., & Borycki, A. G. (2018). Basal lamina remodeling at the skeletal muscle stem cell niche mediates stem cell self-renewal. *Nat Commun, 9*(1), 1075. doi:10.1038/s41467-018-03425-3

Reid, A. L., & Alexander, M. S. (2021). The Interplay of Mitophagy and Inflammation in Duchenne Muscular Dystrophy. *Life (Basel), 11*(7). doi:10.3390/life11070648

Richards, S., Aziz, N., Bale, S., Bick, D., Das, S., Gastier-Foster, J., . . . Committee, A. L. Q. A. (2015). Standards and guidelines for the interpretation of sequence variants: a

joint consensus recommendation of the American College of Medical Genetics and Genomics and the Association for Molecular Pathology. *Genet Med, 17*(5), 405-424. doi:10.1038/gim.2015.30

Riemersma, M., Mandel, H., van Beusekom, E., Gazzoli, I., Roscioli, T., Eran, A., . . . van Bokhoven, H. (2015). Absence of alpha- and beta-dystroglycan is associated with Walker-Warburg syndrome. *Neurology, 84*(21), 2177-2182. doi:10.1212/WNL.0000000000001615

Roos, J. C. P., Daniels, M. J., Morris, E., Hyry, H. I., & Cox, T. M. (2018). Heterogeneity in a large pedigree with Danon disease: Implications for pathogenesis and management. *Mol Genet Metab, 123*(2), 177-183. doi:10.1016/j.ymgme.2017.06.008

Sampaolo, S., Napolitano, F., Tirozzi, A., Reccia, M. G., Lombardi, L., Farina, O., . . . Esposito, T. (2017). Identification of the first dominant mutation of LAMA5 gene causing a complex multisystem syndrome due to dysfunction of the extracellular matrix. *J Med Genet, 54*(10), 710-720. doi:10.1136/jmedgenet-2017-104555

Sanchez-Martin, P., & Komatsu, M. (2018). p62/SQSTM1 - steering the cell through health and disease. *J Cell Sci, 131*(21). doi:10.1242/jcs.222836

Sanes, J. R. (2003). The basement membrane/basal lamina of skeletal muscle. *J Biol Chem, 278*(15), 12601-12604. doi:10.1074/jbc.R200027200

Sawa-Makarska, J., Baumann, V., Coudevylle, N., von Bulow, S., Nogellova, V., Abert, C., . . . Martens, S. (2020). Reconstitution of autophagosome nucleation defines Atg9 vesicles as seeds for membrane formation. *Science, 369*(6508). doi:10.1126/science.aaz7714

Schatzl, T., Kaiser, L., & Deigner, H. P. (2021). Facioscapulohumeral muscular dystrophy: genetics, gene activation and downstream signalling with regard to recent therapeutic approaches: an update. *Orphanet J Rare Dis, 16*(1), 129. doi:10.1186/s13023-021-01760-1

Schneider, M., Will, C. L., Anokhina, M., Tazi, J., Urlaub, H., & Luhrmann, R. (2010). Exon definition complexes contain the tri-snRNP and can be directly converted into B-like precatalytic splicing complexes. *Mol Cell, 38*(2), 223-235. doi:10.1016/j.molcel.2010.02.027

Schot, R., Ferraro, F., Geeven, G., Diderich, K. E. M., & Barakat, T. S. (2024). Re-analysis of whole genome sequencing ends a diagnostic odyssey: Case report of an RNU4-2 related neurodevelopmental disorder. *Clin Genet, 106*(4), 512-517. doi:10.1111/cge.14574

Schuck, S. (2020). Microautophagy - distinct molecular mechanisms handle cargoes of many sizes. *J Cell Sci, 133*(17). doi:10.1242/jcs.246322

Schuler, S. C., Liu, Y., Dumontier, S., Grandbois, M., Le Moal, E., Cornelison, D., & Bentzinger, C. F. (2022). Extracellular matrix: Brick and mortar in the skeletal muscle stem cell niche. *Front Cell Dev Biol, 10*, 1056523. doi:10.3389/fcell.2022.1056523

Scotti, M. M., & Swanson, M. S. (2016). RNA mis-splicing in disease. *Nat Rev Genet, 17*(1), 19-32. doi:10.1038/nrg.2015.3

Seidman, R. J. (2016). Skeletal Muscle Pathology. *eMedicine.* Retrieved from https://emedicine.medscape.com/article/1869808-overview#a5

Seidman, R. J. (2017). Skeletal Muscle - Structure and Histology. *eMedicine.* Retrieved from https://emedicine.medscape.com/article/1923188-overview#a3

Sheikh, O., & Yokota, T. (2021). Developing DMD therapeutics: a review of the effectiveness of small molecules, stop-codon readthrough, dystrophin gene replacement, and exon-skipping therapies. *Expert Opin Investig Drugs, 30*(2), 167-176. doi:10.1080/13543784.2021.1868434

Shimozawa, M., Anzai, S., Satow, R., & Fukami, K. (2017). Phospholipase C delta1 negatively regulates autophagy in colorectal cancer cells. *Biochem Biophys Res Commun, 488*(4), 578-583. doi:10.1016/j.bbrc.2017.05.098

Shin, J. Y., & Worman, H. J. (2022). Molecular Pathology of Laminopathies. *Annu Rev Pathol, 17*, 159-180. doi:10.1146/annurev-pathol-042220-034240

Sieck, G. C., Ferreira, L. F., Reid, M. B., & Mantilla, C. B. (2013). Mechanical properties of respiratory muscles. *Compr Physiol, 3*(4), 1553-1567. doi:10.1002/cphy.c130003

Singh, P., Carraher, C., & Schwarzbauer, J. E. (2010). Assembly of fibronectin extracellular matrix. *Annu Rev Cell Dev Biol, 26*, 397-419. doi:10.1146/annurev-cellbio-100109-104020

Singh, R. N., Howell, M. D., Ottesen, E. W., & Singh, N. N. (2017). Diverse role of survival motor neuron protein. *Biochim Biophys Acta Gene Regul Mech, 1860*(3), 299-315. doi:10.1016/j.bbagrm.2016.12.008

Sleboda, D. A., Stover, K. K., & Roberts, T. J. (2020). Diversity of extracellular matrix morphology in vertebrate skeletal muscle. *J Morphol, 281*(2), 160-169. doi:10.1002/jmor.21088

Smirnova, E., Griparic, L., Shurland, D. L., & van der Bliek, A. M. (2001). Dynamin-related protein Drp1 is required for mitochondrial division in mammalian cells. *Mol Biol Cell, 12*(8), 2245-2256. doi:10.1091/mbc.12.8.2245

Sou, Y. S., Waguri, S., Iwata, J., Ueno, T., Fujimura, T., Hara, T., . . . Komatsu, M. (2008). The Atg8 conjugation system is indispensable for proper development of autophagic isolation membranes in mice. *Mol Biol Cell, 19*(11), 4762-4775. doi:10.1091/mbc.e08-03-0309

Strasser, A., Dickmanns, A., Luhrmann, R., & Ficner, R. (2005). Structural basis for m3G-cap-mediated nuclear import of spliceosomal UsnRNPs by snurportin1. *EMBO J, 24*(13), 2235-2243. doi:10.1038/sj.emboj.7600701

Tan, D., Liu, Y., Luo, H., Shen, Q., Long, X., Xu, L., . . . Xiong, H. (2025). A Novel Mouse Model for *LAMA2*-Related Muscular Dystrophy: Analysis of Molecular Pathogenesis and Clinical Phenotype. 2024.2001.2006.574440. doi:10.1101/2024.01.06.574440 %J bioRxiv

Tang, A. H., & Rando, T. A. (2014). Induction of autophagy supports the bioenergetic demands of quiescent muscle stem cell activation. *EMBO J, 33*(23), 2782-2797. doi:10.15252/embj.201488278

Theocharis, A. D., Skandalis, S. S., Gialeli, C., & Karamanos, N. K. (2016). Extracellular matrix structure. *Adv Drug Deliv Rev, 97*, 4-27. doi:10.1016/j.addr.2015.11.001

Thorsteinsdottir, S., Deries, M., Cachaco, A. S., & Bajanca, F. (2011). The extracellular matrix dimension of skeletal muscle development. *Dev Biol, 354*(2), 191-207. doi:10.1016/j.ydbio.2011.03.015

Trabelsi, M., Kavian, N., Daoud, F., Commere, V., Deburgrave, N., Beugnet, C., . . . Chelly, J. (2008). Revised spectrum of mutations in sarcoglycanopathies. *Eur J Hum Genet, 16*(7), 793-803. doi:10.1038/ejhg.2008.9

Tran, S., Fairlie, W. D., & Lee, E. F. (2021). BECLIN1: Protein Structure, Function and Regulation. *Cells, 10*(6). doi:10.3390/cells10061522

Turco, E., Witt, M., Abert, C., Bock-Bierbaum, T., Su, M. Y., Trapannone, R., . . . Martens, S. (2019). FIP200 Claw Domain Binding to p62 Promotes Autophagosome Formation at Ubiquitin Condensates. *Mol Cell, 74*(2), 330-346 e311. doi:10.1016/j.molcel.2019.01.035

Uggenti, C., Lepelley, A., Depp, M., Badrock, A. P., Rodero, M. P., El-Daher, M. T., . . . Crow, Y. J. (2020). cGAS-mediated induction of type I interferon due to inborn errors of histone pre-mRNA processing. *Nat Genet, 52*(12), 1364-1372. doi:10.1038/s41588-020-00737-3

Vainzof, M., Souza, L. S., Gurgel-Giannetti, J., & Zatz, M. (2021). Sarcoglycanopathies: an update. *Neuromuscul Disord, 31*(10), 1021-1027. doi:10.1016/j.nmd.2021.07.014

Verma, B., Akinyi, M. V., Norppa, A. J., & Frilander, M. J. (2018). Minor spliceosome and disease. *Semin Cell Dev Biol, 79*, 103-112. doi:10.1016/j.semcdb.2017.09.036

Wang, E. T., Sandberg, R., Luo, S., Khrebtukova, I., Zhang, L., Mayr, C., . . . Burge, C. B. (2008). Alternative isoform regulation in human tissue transcriptomes. *Nature, 456*(7221), 470-476. doi:10.1038/nature07509

Wilkinson, M. E., Charenton, C., & Nagai, K. (2020). RNA Splicing by the Spliceosome. *Annu Rev Biochem, 89*, 359-388. doi:10.1146/annurev-biochem-091719-064225

Will, C. L., & Luhrmann, R. (2011). Spliceosome structure and function. *Cold Spring Harb Perspect Biol, 3*(7). doi:10.1101/cshperspect.a003707

Wing, C. E., Fung, H. Y. J., & Chook, Y. M. (2022). Karyopherin-mediated nucleocytoplasmic transport. *Nat Rev Mol Cell Biol, 23*(5), 307-328. doi:10.1038/s41580-021-00446-7

Wolfe, R. R. (2006). The underappreciated role of muscle in health and disease. *Am J Clin Nutr, 84*(3), 475-482. doi:10.1093/ajcn/84.3.475

Yamamoto, H., Fujioka, Y., Suzuki, S. W., Noshiro, D., Suzuki, H., Kondo-Kakuta, C., . . . Ohsumi, Y. (2016). The Intrinsically Disordered Protein Atg13 Mediates Supramolecular Assembly of Autophagy Initiation Complexes. *Dev Cell, 38*(1), 86-99. doi:10.1016/j.devcel.2016.06.015

Yamamoto, H., Zhang, S., & Mizushima, N. (2023). Autophagy genes in biology and disease. *Nat Rev Genet, 24*(6), 382-400. doi:10.1038/s41576-022-00562-w

Yoon, J. H., Her, S., Kim, M., Jang, I. S., & Park, J. (2012). The expression of damage-regulated autophagy modulator 2 (DRAM2) contributes to autophagy induction. *Mol Biol Rep, 39*(2), 1087-1093. doi:10.1007/s11033-011-0835-x

Zambon, A. A., & Muntoni, F. (2021). Congenital muscular dystrophies: What is new? *Neuromuscul Disord, 31*(10), 931-942. doi:10.1016/j.nmd.2021.07.009

Zhang, C., Gao, J., Li, M., Deng, Y., & Jiang, C. (2018). p38delta MAPK regulates aggresome biogenesis by phosphorylating SQSTM1 in response to proteasomal stress. *J Cell Sci, 131*(14). doi:10.1242/jcs.216671

Zhang, W., Liu, Y., & Zhang, H. (2021). Extracellular matrix: an important regulator of cell functions and skeletal muscle development. *Cell Biosci, 11*(1), 65. doi:10.1186/s13578-021-00579-4

Zhang, Y. (2008). I-TASSER server for protein 3D structure prediction. *BMC Bioinformatics, 9*, 40. doi:10.1186/1471-2105-9-40

Zhao, Y. G., & Zhang, H. (2019). Autophagosome maturation: An epic journey from the ER to lysosomes. *J Cell Biol, 218*(3), 757-770. doi:10.1083/jcb.201810099

Zhong, W., Zhu, H., Sheng, F., Tian, Y., Zhou, J., Chen, Y., . . . Lin, J. (2014). Activation of the MAPK11/12/13/14 (p38 MAPK) pathway regulates the transcription of autophagy genes in response to oxidative stress induced by a novel copper complex in HeLa cells. *Autophagy, 10*(7), 1285-1300. doi:10.4161/auto.28789